

Appendix C: Central Sands Lakes Study

Technical Report: Modeling Documentation

Michael N. Fiene, Megan J. Haserodt, Andrew T. Leaf, and Stephen M. Westenbroek
U.S. Geological Survey Upper Midwest Water Science Center, Middleton, Wisconsin.

Introduction.....	1
Purpose and Scope	2
Study Area Description and Hydrogeologic Setting.....	3
Conceptualization of Groundwater Flow in the Central Sands Region	4
Regional Groundwater Flow System	4
Hydrologic Budget	5
Aquifer Properties	7
Local-scale Groundwater Flow Systems	7
Plainfield Tunnel Channel Lakes	7
Pleasant Lake	8
Numerical Models	9
Soil Water Balance (SWB).....	10
Regional Model.....	13
Domain	13
Model Grid and Layering	14
Boundary Conditions	14
Aquifer Properties	16
History Matching Approach and Results	18
Regional Model Results	23
Focus Area Inset Models	23
Inset model domains and horizontal discretization	24
Inset model layering	25
Time discretization	25
Boundary conditions.....	26
Perimeter boundaries.....	26
Recharge.....	26

Streams.....	27
Lakes.....	27
Water use.....	28
Aquifer properties.....	28
Parameter Estimation and uncertainty analysis.....	29
The iterative ensemble smoother method and uncertainty quantification.....	29
Observation data.....	30
Parameterization.....	32
History Matching Results.....	36
Focus Area Inset Model Results.....	45
Parameter estimates.....	45
Groundwater Flow and Boundary Condition Fluxes for Mean (2012 -2015) Conditions .	46
Groundwater Flow and Boundary Condition Fluxes for Transient (2012-2018) Conditions	47
.....	47
Lake Ecosystem Response Assessment (LERA).....	48
Assumptions and Limitations.....	54
Disclaimer.....	56
References.....	57

Figures

Figure 1: Location map showing Central Sands study area extent, moraines, streams, study lakes and boundaries of all GW models.	3
Figure 2: Annual precipitation for the Central Sands study area, 2012-2018.	6
Figure 3 – Mean 2012 – 2018 annual net infiltration estimated by SWB.....	13
Figure 4 – Map of model boundary conditions for the regional model.	14
Figure 5 – Horizontal hydraulic conductivity values after history matching for each of the four model layers.	18
Figure 6 – Vertical hydraulic conductivity values after history matching for each of the four model layers.	18
Figure 7 – Specific yield values after history matching for each of the four model layers.....	18
Figure 8 – Specific storage values after history matching for each of the four model layers.	18
Figure 9 – One-to-one plot of measured and simulated groundwater elevations for the steady-state and transient head targets.	20
Figure 10 – One-to-one plot of measured and simulated streamflow under base-flow conditions for the transient streamflow targets.	20
Figure 11 – Map of steady-state hydraulic head target residuals displayed by calibration group.	21

Figure 12 – Map of steady-state streamflow residuals and gaining and losing stream reaches. .21

Figure 13 – Transient groundwater elevations at select wells with long-term records (well locations shown in Figure 11; site number is from National Water Information System (<https://doi.org/10.5066/F7P55KJN>)). Elevations are shown in meters and feet above North American Vertical Datum of 1988 (NAVD88).21

Figure 14 – Transient streamflow at select streams locations near the study lakes and with longer-term record (stream locations shown in Figure 12; site number is from National Water Information System (<https://doi.org/10.5066/F7P55KJN>)).....21

Figure 15 – Pilot points and multiplier zones for each of the four model layers. Note, pilot points extend past the zone boundaries in layer 2 to allow for kriging but the aquifer properties in the New Rome Member and pinched areas are not influenced by pilot point multipliers.22

Figure 16 – Map of the simulated water table and streamflow for the regional model during the steady-state stress period representing mean conditions from 2012 – 2018.....23

Figure 17 – Regional model groundwater budget showing the major model inflows and outflows for each stress period. Inflows and outflows are named using the MODFLOW List file convention.....23

Figure 18 – Plainfield Tunnel Channel Lakes model boundary conditions with local-grid refinement extent.24

Figure 19 – Pleasant Lake model boundary conditions with local-grid refinement extent.....24

Figure 20 – Inset model cross sections showing inset and parent layer surfaces. Gaps in the cross sections indicate the extent of the refined areas within the inset models. Cross-section locations are shown in Figure 18 and Figure 19.25

Figure 21 Locations of observations that were assigned observation weight greater than zero for the Pleasant Lake inset model.32

Figure 22 Locations of observations that were assigned observation weight greater than zero for the Plainfield Tunnel Channel Lakes inset model.32

Figure 23 Summary of ensemble (black lines) and base (blue line) objective function progress by iES iteration for Pleasant Lake inset model.35

Figure 24 Summary of ensemble (black lines) and base (blue line) objective function progress by iES iteration for Plainfield Tunnel Channel Lakes inset model.35

Figure 25 Rejection sampling for the Pleasant Lake inset model. A subjective decision is made to only retain ensemble members at or below a selected cutoff value. For Pleasant Lake, this cutoff was 5,800.35

Figure 26 Rejection sampling for the Plainfield Tunnel Channel Lakes inset model. A subjective decision is made to only retain ensemble members at or below a selected cutoff value. For Plainfield Tunnel Channel Lakes, this cutoff was 2,400.....36

Figure 27 Fit between measured and simulated values at observation locations for observation groups nwis_dvs (panel A) and nwisdvflx_tr (panel B) for the Pleasant Lake inset model.37

Figure 28 Fit between measured and simulated values at observation locations for observation groups nwis_dvs_tr (panel A) and nwisdvflx_tr_tdiff (panel B) for the Pleasant Lake inset model.37

Figure 29 Fit between measured and simulated values at observation locations for observation groups usgs_stages (panel A) and usgs_stages_tr (panel B) for the Pleasant Lake inset model..37

Figure 30 Fit between measured and simulated values at observation locations for observation groups wdnr_lakes (panel A) and wdnr_lb (panel B) for the Pleasant Lake inset model.37

Figure 31 Fit between measured and simulated values at observation locations for observation groups wdnr_lb_sdiff (panel A) and wdnrflx_tr (panel B) for the Pleasant Lake inset model.37

Figure 32 Fit between measured and simulated values at observation locations for observation groups wdnrlks_ann_tr (panel A) and wdnrlks_mon_tr (panel B) for the Pleasant Lake inset model.37

Figure 33 Fit between measured and simulated values at observation locations for observation groups wdnrwells_tr (panel A) and wdnrwells_tr_sdiff (panel B) for the Pleasant Lake inset model.37

Figure 34 Fit between measured and simulated values at observation locations for observation group wdnrwells_tr_sdiff (panel A) for the Pleasant Lake inset model.37

Figure 35 Fit between measured and simulated values at observation locations for observation groups nwis_dvs (panel A) and nwisdvs_tr (panel B) for the Plainfield Tunnel Channel Lakes inset model.37

Figure 36 Fit between measured and simulated values at observation locations for observation groups nwisdvs_tr_tdiff (panel A) and usgs_stages (panel B) for the Plainfield Tunnel Channel Lakes inset model.37

Figure 37 Fit between measured and simulated values at observation locations for observation groups wdnrflx_tr (panel A) and wdnrlks_ann_tr (panel B) for the Plainfield Tunnel Channel Lakes inset model.37

Figure 38 Fit between measured and simulated values at observation locations for observation groups wdnrlks_mon_tr (panel A) and wdnrwells_tr (panel B) for the Plainfield Tunnel Channel Lakes inset model.37

Figure 39 Fit between measured and simulated values at observation locations for observation groups wdnrwells_tr_sdiff (panel A) and wdnrwells_tr_tdiff (panel B) for the Plainfield Tunnel Channel Lakes inset model.38

Figure 40 Spatial pattern of mean fit between measured and simulated observations for Pleasant Lake inset model38

Figure 41 Spatial pattern of mean fit between measured and simulated observations for Plainfield Tunnel Channel Lakes inset model38

Figure 42 Time series of measured and simulated results for lake level observations in the Pleasant Lake inset model. Panel A is observation group wdnrlks_mon_tr, Panel B is observation group wdnrlks_ann_tr, and Panel C is observation group usgs_stages_tr.....39

Figure 43 Time series of measured and simulated results for streamflow observations in Chaffee Creek sites 10039561 (panel A) and 04073240 (panel B) in the Pleasant Lake inset model.40

Figure 44 Time series of measured and simulated results for streamflow observations in Tagatz Creek sites 10029382 (panel A), 10039577 (panel B), and 10028958 (panel C) in the Pleasant Lake inset model.40

Figure 45 Time series of measured and simulated results over time for streamflow observations in South Branch Wedde Creek site 10039101 (panel A) and Mecan Creek site 10034799 (panel B).40

Figure 46 Time series of measured and simulated results for transient piezometers near Pleasant Lake in the group wdnrwells_tr, (part 1).40

Figure 47 Time series of measured and simulated results for transient piezometers near Pleasant Lake in the group wdnrwells_tr, (part 2).40

Figure 48 Time series of measured and simulated results for temporal differences in transient piezometers near Pleasant Lake in the group wdnrwells_tr_tdiff, (part 1).40

Figure 49 Time series of measured and simulated results for temporal differences in transient piezometers near Pleasant Lake in the group wdnrwells_tr_tdiff, (part 2).40

Figure 50 Time series of measured and simulated results for spatial differences in transient piezometers near Pleasant Lake in the group wdnrwells_tr_sdiff (part 1).41

Figure 51 Time series of measured and simulated results for spatial differences in transient piezometers near Pleasant Lake in the group wdnrwells_tr_sdiff (part 2).41

Figure 52 Time series of measured and simulated results for heads in wells with daily values in NWIS in the Pleasant Lake inset model in the group nwisdvs_tr (part 1).41

Figure 53 Time series of measured and simulated results for heads in wells with daily values in NWIS in the Pleasant Lake inset model in the group nwisdvs_tr (part 2).41

Figure 54 Time series of measured and simulated results for temporal difference of hydraulic heads in wells with daily values in NWIS in the Pleasant Lake inset model in the group nwisdvs_tr_tdiff (part 1).....41

Figure 55 Time series of measured and simulated results for temporal difference of hydraulic heads in wells with daily values in NWIS in the Pleasant Lake inset model in the group nwisdvs_tr_tdiff (part 2).....41

Figure 56 Time series of measured and simulated results for lake level observations in the Pleasant Lake inset model. Panel A is Plainfield Lake, observation group wdnrlks_mon_tr, Panel B is Plainfield Lake, observation group wdnrlks_ann_tr, Panel C is Long Lake, observation group wdnrlks_mon_tr, and Panel D is Long Lake, observation group wdnrlks_ann_tr.42

Figure 57 Time series of measured and simulated results for streamflow observations in North Branch Tenmile Creek site 10042017 (panel A) and Upper Pine River site 703070 (panel B) in the Plainfield Tunnel Channel Lakes inset model.42

Figure 58 Time series of measured and simulated results for transient piezometers near Long Lake in the group wdnrwells_tr (part 1).43

Figure 59 Time series of measured and simulated results for transient piezometers near Long Lake in the group wdnrwells_tr (part 2).43

Figure 60 Time series of measured and simulated results for transient piezometers near Plainfield Lake in the group wdnrwells_tr (part 1).43

Figure 61 Time series of measured and simulated results for transient piezometers near Plainfield Lake in the group wdnrwells_tr (part 2).43

Figure 62 Time series of measured and simulated results for temporal differences in transient piezometers near Long Lake in the group wdnrwells_tr_tdiff, (part 1).43

Figure 63 Time series of measured and simulated results for temporal differences in transient piezometers near Long Lake in the group wdnrwells_tr_tdiff, (part 2).43

Figure 64 Time series of measured and simulated results for temporal differences in transient piezometers near Plainfield Lake in the group wdnrwells_tr_tdiff, (part 1).43

Figure 65 Time series of measured and simulated results for temporal differences in transient piezometers near Plainfield Lake in the group wdnrwells_tr_tdiff, (part 2).43

Figure 66 Time series of measured and simulated results for spatial differences in transient piezometers near Long Lake in the group wdnrwwells_tr_sdiff, (part 1).44

Figure 67 Time series of measured and simulated results for spatial differences in transient piezometers near Long Lake in the group wdnrwwells_tr_sdiff, (part 2).44

Figure 68 Time series of measured and simulated results for spatial differences in transient piezometers near Plainfield Lake in the group wdnrwwells_tr_sdiff, (part 1).44

Figure 69 Time series of measured and simulated results for spatial differences in transient piezometers near Plainfield Lake in the group wdnrwwells_tr_sdiff, (part 2).44

Figure 70 Time series of measured and simulated results for hydraulic heads in wells with daily values in NWIS in the Plainfield Tunnel Channel Lakes inset model in the group nwisdvs_tr.44

Figure 71 Time series of measured and simulated results for temporal difference of hydraulic heads in wells with daily values in NWIS in the Plainfield Tunnel Channel Lakes inset model in the group nwisdvs_tr_tdiff.45

Figure 72 – Horizontal hydraulic conductivity (K_h) estimates for the Plainfield Tunnel Channel Lakes model. White areas indicate locations where a layer is absent in the model (idomain=0). Pilot point locations apply to all layers.45

Figure 73 – Vertical hydraulic conductivity (K_v) estimates for the Plainfield Tunnel Channel Lakes model. White areas indicate locations where a layer is absent in the model (idomain=0). Pilot point locations apply to all layers.45

Figure 74 – Specific yield (S_y) estimates for the Plainfield Tunnel Channel Lakes model. White areas indicate locations where a layer is absent in the model (idomain=0). Pilot point locations apply to all layers.46

Figure 75 – Specific storage (S_s) estimates for the Plainfield Tunnel Channel Lakes model. White areas indicate locations where a layer is absent in the model (idomain=0). Pilot point locations apply to all layers.46

Figure 76 – Horizontal hydraulic conductivity (K_h) estimates for the Pleasant Lake model. White areas indicate locations where a layer is absent in the model (idomain=0). Pilot point locations apply to all layers.46

Figure 77 – Vertical hydraulic conductivity (K_v) estimates for Pleasant Lake model. White areas indicate locations where a layer is absent in the model (idomain=0). Pilot point locations apply to all layers.46

Figure 78 – Specific yield (S_y) estimates for the Pleasant Lake model. White areas indicate locations where a layer is absent in the model (idomain=0). Pilot point locations apply to all layers.46

Figure 79 – Specific storage (S_s) estimates for the Pleasant Lake model. White areas indicate locations where a layer is absent in the model (idomain=0). Pilot point locations apply to all layers.46

Figure 80 – Recharge and well pumping multiplier estimates for the Plainfield Tunnel Channel Lakes inset model.46

Figure 81 – Lake package evaporation and rainfall multiplier estimates for Plainfield (A), Second (B), Sherman (C), and Long (D) Lakes in the Plainfield Tunnel Channel Lakes inset model.46

Figure 82 – Recharge and well pumping multiplier estimates for the Pleasant Lakes inset model.46

Figure 83 – Lake package evaporation and rainfall multiplier estimates for Pleasant Lake in the Pleasant Lake inset model.46

Figure 84 – Plainfield Tunnel Channel Lakes model steady-state water table and boundary fluxes.47

Figure 85 – Pleasant Lake model steady-state water table and boundary fluxes.47

Figure 86 – Plainfield Tunnel Channel Lakes inset model water budget. Inflows and outflows are named using the MODFLOW List file convention.....48

Figure 87 – Pleasant Lake inset model water budget. Inflows and outflows are named using the MODFLOW List file convention.48

Figure 88 – Plainfield Tunnel Channel Lakes LGR sub-model water budget. Inflows and outflows are named using the MODFLOW List file convention.48

Figure 89 – Pleasant Lake LGR sub-model water budget. Inflows and outflows are named using the MODFLOW List file convention.48

Figure 90 – Lake water budgets.48

Figure 91 Total acres of each major crop rotation in the regional model domain.....51

Figure 92 Spatial distribution of the major crop rotations in the regional model domain.51

Figure 93 Spatial distribution of alternative land use assumed for the no-irrigated-agriculture scenario in the regional model domain.....51

Figure 94 Spatial distribution of the major crop rotations (A) and the alternative land use assumed for the no-irrigated-agriculture scenario (B) in the Plainfield Tunnel Channel Lakes inset model.....51

Figure 95 Spatial distribution of the major crop rotations (A) and the alternative land use assumed for the no-irrigated-agriculture scenario (B) in the Pleasant Lake inset model51

Figure 96 Frequency of each land-use code/crop within the four crop rotations as a percent of area.....51

Figure 97 Lake stages for the three study lakes, Plainfield, Long, and Pleasant, in panels A, B, and C, respectively, over the Lake Ecosystem Response Assessment (LERA) representative climate. Blue lines indicate Monte Carlo ensemble members for the non-irrigation scenario, and orange lines indicate ensemble members for the current irrigation scenario.....52

Figure 98 Streamflow in selected streams in the Plainfield inset model respectively over the Lake Ecosystem Response Assessment (LERA) representative climate. Blue lines indicate Monte Carlo ensemble members for the non-irrigation scenario, and orange lines indicate ensemble members for the current irrigation scenario. Panel A is North Branch of Tenmile Creek, and panel B is Upper Pine River52

Figure 99 Streamflow in selected streams in the Pleasant inset model respectively over the Lake Ecosystem Response Assessment (LERA) representative climate. Blue lines indicate Monte Carlo ensemble members for the non-irrigation scenario, and orange lines indicate ensemble members for the current irrigation scenario. Panel A is Tagatz Creek, and panel B is Chaffee Creek52

Figure 100 Streamflow in selected streams in the Pleasant inset model respectively over the Lake Ecosystem Response Assessment (LERA) representative climate. Blue lines indicate Monte Carlo ensemble members for the non-irrigation scenario, and orange lines indicate ensemble members for the current irrigation scenario. Panel A is South Branch Wedde Creek, panel B is Carter Creek, and panel C is Mekan Creek52

Figure 101 Lake stages for the three study lakes, Plainfield, Long, and Pleasant, in panels A, B, and C, respectively, over the Lake Ecosystem Response Assessment (LERA) representative climate for the base SWB parameters. In each panel, the blue line depicts the no-irrigated-agriculture scenario, the orange line depicts the current-irrigated agriculture scenario, and the green line depicts the potential-irrigated-agriculture scenario.53

Figure 102 Group identification, based on distance from the center of Long Lake for irrigation wells in the Plainfield inset model and total pumping over the LERA simulation time. Orange 'x' indicates the center of Long Lake.....54

Figure 103 Stage changes in Long Lake resulting from each well group simulated as converted from current irrigation to no irrigation recharge and water use. Positive responses indicate an increase in lake stage due to the conversion.54

Tables

Table 1 Measured groundwater elevation and streamflow data sources used for history matching in the regional parent model.....20

Table 2 Observation data groups, values, and descriptions for Pleasant Lake inset model.....31

Table 3 Observation data groups, values, and descriptions for Plainfield Tunnel Channel Lakes inset model.....32

Table 4 Parameter groups, values, and descriptions for Pleasant Lake inset model34

Table 5 Parameter groups, values, and descriptions for Plainfield Tunnel Channel Lakes inset model35

Introduction

This report provides the necessary documentation of the numerical models developed for the Central Sands Lake study in central Wisconsin and will be included as a technical appendix in the report to the Wisconsin State Legislature by the Wisconsin Department of Natural Resources (WDNR) in response to 2017 Wisconsin Act 10. This legislation directed WDNR to determine whether existing and potential groundwater withdrawals are causing or are likely to cause significant reduction of mean seasonal water levels at Pleasant Lake, Long Lake, and Plainfield Lake (s. 281.34(7m)(2)(b), Wis. Stats.) in Waushara County, Wisconsin. To evaluate the potential hydrologic connection between groundwater withdrawals and the nearby study lakes, hydrologic models were created that focused on the lakes of interest and yet were large enough to cover a broad enough region to extend to the major hydrologic boundaries of the natural flow system. The areas near the lakes require finer-scale grid discretization (or spacing) to better represent the lakes and streams in the model, but also need to cover a large enough area to include the groundwater withdrawal locations that have the potential to cause reduction in water levels in the lakes. To accomplish these goals, three groundwater models were created: a regional model extending to major hydrologic boundaries; and two inset models, inheriting boundaries from the regional model but focused near the lakes. Each of the inset models, in turn, included a detailed area close to the lakes surrounded by an area at the same spatial scale as the regional model (Figure 1).

To support WDNR in evaluating the connection between groundwater withdrawals and lake levels, a representative time period was required over which to compare land use with and without irrigated agriculture and for WDNR to evaluate potential lake stage and flux changes related to irrigated agriculture. WDNR chose the climate period of 1981-2018 to be representative of a typical period and provided two land use scenarios—one with no irrigated agriculture and one with assumed crop rotations similar to current conditions—to simulate with groundwater models to, then, compare lake responses with. As a result, simulations over this climate record are not intended to recreate the history of 1981-2018 because land use changed over that time. These runs are, instead, intended to provide a basis on which to compare land use

with and without irrigation-related groundwater withdrawals based on the current arrangement of land use and a varied climatic record. Groundwater withdrawals focused on irrigated-agriculture-related water use because greater than 95% of groundwater withdrawal in the two inset models around the study lakes is for irrigated agriculture water use.

The period of 2012-2018 was used for parameter estimation (synonymously referred to as “history matching”) for the groundwater models. This time period was chosen because it includes the most complete water use records to simulate groundwater withdrawals. History matching was performed using groundwater elevations, lake stages, and streamflow observations over the 2012-2018 time period and processed observations derived from those raw data.

Climatic data were incorporated into the model using a soil-water balance approach.

A soil water balance model was constructed at the scale of the regional groundwater model to both calculate recharge based on land use and climate, and in the long-term climate-period runs, to estimate water use required by irrigated agriculture to apply as well boundary conditions in the groundwater model in the absence of reported water use values over that period.

Purpose and Scope

The purpose of this appendix is to document the various conceptual and numerical models created for the Central Sands Lake study by the U.S. Geological Survey in cooperation with the WDNR. Accompanying this discussion is background on the parameter estimation and uncertainty analysis used to estimate parameters for the models. Parameters are estimated to balance prior understanding of parameter values with correspondence between measured observations and collocated model outputs. Uncertainty analysis evaluates the confidence in the model outputs. Finally, the scenarios comparing different land uses over the representative climate period are documented.

The model construction and analysis were performed to address the main study question of whether agricultural-irrigation-related groundwater extraction significantly adversely affects lake hydrology. Conclusions about the impacts and potential policy recommendations are the subject of the main body of this report, which the U.S. Geological Survey did not formally contribute to

– this appendix is focused solely on the technical aspects of the model development, parameter estimation, and uncertainty analysis, as well as the land-use and representative long-term climate model scenarios.

Study Area Description and Hydrogeologic Setting

The Central Sands study area is defined as the contiguous area east of the Wisconsin River with surficial sand and gravel deposits greater than 50 feet thick (Bradbury and others, 2017). The regional groundwater model domain extends to major surface water features that serve as boundary conditions. This regional model, in turn, supplies boundaries for inset models focused on the study lakes. The regional model domain covers approximately the southern 75% of the Central Sands, extending from the Little Plover River Basin south to the border between Adams and Columbia Counties, and west to east from the Wisconsin River to the Tomorrow, Waupaca, Wolf, and Fox Rivers (Figure 1). Several terminal moraines of the Green Bay Lobe run north to south through the center of the study area. The moraines form the topographic high point between the Wisconsin River and the rivers that bound the study area to the east. The area around the moraines and the adjacent outwash plain to the west is characterized by a lack of surface water drainage and marks the hydrologic divide between the Great Lakes and Mississippi River Basins. The Plainfield Tunnel Channel Lakes are situated between the Hancock and Almond Moraines, which merge south of Plainfield, Wisconsin, to form a single moraine that continues south past the western edge of Pleasant Lake to the southern boundary of the regional model.

Figure 1: Location map showing Central Sands study area extent, moraines, streams, study lakes and boundaries of all GW models.

The area west of the moraines is characterized by flat topography and undisturbed outwash sediments at the surface. Beneath the outwash, fine-grained deposits of the Quaternary-aged New Rome Member of the Big Flats Formation (hereafter, New Rome Member), associated with Glacial Lake Wisconsin, thicken to the southwest. Near the Hancock Moraine and eastward, the New Rome Member is absent. The area between the Hancock and Almond Moraines consists of flat outwash plain broken by a series of tunnel channel features with surface expressions that are

1.5-9.1 meters (m) (5-30 feet (ft)) deep, east-west oriented linear depressions formed by glacial collapse. The subsurface between the two moraines is dominated by sand and gravel, but with more heterogeneity than west of the Hancock Moraine, including discontinuous patches of fine-grained sediments deposited by various pro, sub and supra-glacial processes. East of the Almond Moraine, the landscape is hummocky, underlain by collapsed sand and gravel outwash that is more heterogeneous than the outwash west of the moraines. Toward the eastern edge of the model, the coarser, sandy sediments transition to fine-grained deposits associated with Glacial Lake Oshkosh. More details on the geologic history and subsurface lithology of the study area are in Appendix A.

Conceptualization of Groundwater Flow in the Central Sands Region

The groundwater flow system was simulated and analyzed at two scales. The regional scale encompasses much of the Central Sands Region and was included to provide boundary conditions for the study lakes. The local-scale groundwater flow systems were focused around the Plainfield Tunnel Channel Lakes and Pleasant Lake.

Regional Groundwater Flow System

The study area is located at the groundwater divide between two major drainage basins. The groundwater flow system is fed almost entirely by terrestrial recharge, which creates high points in the water table between surface water features. Groundwater flows laterally away from these high points, until the water table meets the land surface, allowing it to discharge into wetlands and streams. Many streams on the outwash plain west of the moraines begin as drainage ditches that were installed to lower the water table for agriculture. East of the moraines, springs and local artesian conditions are common (Appendix A). Most groundwater flow occurs in the Quaternary-aged surficial aquifer made up of glacial lake, outwash, end moraine, till, stagnant ice, and stream from a wide variety of formations (hereafter, surficial aquifer). Hydraulic conductivity in the surficial aquifer is an order of magnitude greater than the Cambrian-aged sandstone bedrock of the Elk Mound and Tunnel City groups (hereafter, sandstone bedrock). The vast majority of groundwater discharge is to interior streams, which are almost all gaining.

Typically, most recharge to the groundwater system occurs in March through May, following the spring freshet, with little to no recharge occurring during the growing season followed by a pulse

of recharge in the fall after crops are harvested and negligible recharge in the winter when the ground is frozen. On the outwash plain west of the moraines, the water table is generally within a few meters of the land surface, and there is minimal lag between infiltration events and groundwater recharge arriving at the water table. Elsewhere, the depth of the water table varies with topography, but is generally greatest along the moraines, where it can locally exceed 33 m (100 ft). In areas of greater depth to water, the water-table response may lag infiltration events by a month or more (e.g. Hunt and others, 2008). During the period of spring recharge, there is a net gain in groundwater storage. With the onset of the growing season, recharge decreases dramatically, and the groundwater system transitions to a condition of net storage loss. In the summer months, groundwater abstraction can account for up to about half of the total groundwater discharge (wells_out in Figure 17). In the fall months, there is often some recharge, but typically a net loss of groundwater storage to streamflow is observed, maintaining a relatively stable supply of water to streams as base flow.

Hydrologic Budget

Much can be learned about a hydrologic system through analysis of the soil-water balance. Thornthwaite (1948) recognized the value of observing the “march of actual evapotranspiration” over the course of a year to quantify the periods of the growing season in which natural precipitation inputs are insufficient to balance evapotranspiration needs of crops and other vegetation. This study uses the components of the soil-water-balance to estimate net infiltration—the amount of soil moisture that passes through the root zone and into the unsaturated soil zone that lies beneath it in most places throughout the Central Sands. Given enough time, most of this net infiltration eventually finds its way to the water table, becoming groundwater recharge. Net infiltration estimates are fed directly into the groundwater flow models discussed throughout this report.

Net infiltration is one of the most challenging components of the hydrologic budget to estimate; few direct observations or measurements of net infiltration exist. The use of a soil-water-balance approach depends on properly defining the remaining components of the water budget; net infiltration may then be calculated as the difference between the inputs and outputs of water to

the root zone soil layer. A simplified description of the root zone soil-water balance is:
 $net\ infiltration = rainfall + snowmelt + irrigation - evapotranspiration - runoff - \Delta soil\ moisture$, where $\Delta soil\ moisture$ is the change in soil moisture from one day to the next.

Annual precipitation in the Central Sands study area ranges from less than 76.2 cm (30 inches) in 2012 to more than 114.3 cm (45 inches) in 2018 (Figure 2). For reference, the 30-year mean annual precipitation for the area (calculated for the years 1981 through 2010) ranges between 81.3 and 86.4 cm (32 and 34 inches, respectively) (PRISM Climate Group, 2020).

Figure 2: Annual precipitation for the Central Sands study area, 2012-2018.

The mean precipitation amount received over the Central Sands study area in recent years (2016-2018) has been well in excess of the 30-year long-term mean gross precipitation amounts.

Actual evapotranspiration (actual ET), the sum of bare soil evaporation and plant transpiration, varies widely with land use, crop or vegetative cover type, and the time of year. Actual ET over the model domain is generally low—less than 2.5 cm (1 inch)—for the months of January, February, and March (Reitz and others, 2017a). Actual ET increases steadily with springtime vegetation and crop growth, peaking in about July at about 12.7 cm (5 inches) per month. Actual ET continues to decrease through August, September, and October, and is generally less than 2.5 cm (1 inch) per month for November and December.

Runoff in the Central Sands is generally low but does play a role in the water budget. Annual mean runoff amounts for the study area range between 5 and 10 cm (2 and 4 inches, respectively; Reitz and others, 2017b); the years with larger runoff amounts are not surprisingly the same years for which gross precipitation is higher than the 30-year “normal” amounts.

Irrigation amounts, as estimated by means of the FAO-56 methodology (Allen and others, 1998), vary appreciably from year to year and from one crop type to another. Use of reported or metered irrigation amounts in the water budget calculations would be preferable to use of estimated values but reported values were only available for the history-matching period of 2012-2018. For the longer range of climatic conditions required for the Lake Ecosystem Response Assessment (LERA) scenarios (1981-2018) simulated in the lake study, irrigation amounts computed by

SWB (See Soil Water balance (SWB) subsection of the Numerical Models section for details) were used. Irrigation amounts represent between 0.8 and 1.3 cm (0.3 and 0.5 inch per year, respectively) of water when averaged over the entire study area for the time period 2012-2018.

Finally, the net annual infiltration amount can be estimated once all the other water budget components have been accounted for. Net infiltration averaged over the model domain ranges from 15.2 cm (6 inches) in 2012 to 33.0 cm (13 inches) in 2018. The months of April and October tend to see the highest estimated net infiltration amounts, with the lowest estimated amounts in June, July, and August.

Aquifer Properties

The surficial aquifer ranges in thickness from thin to absent near topographic high points in the bedrock surface, to more than 100 m (328 ft) thick along the Almond Moraine (Figure 1) east of Plainfield, Wisconsin. Horizontal hydraulic conductivity in the surficial aquifer ranges from less than 1 m (3.28 ft) per day locally to 150 m (492 ft) per day or more, with values of 10-80 m (32.8-262 ft) per day being common (Hart and others, 2021; Bradbury and others, 2017; Weeks and Stangland, 1971). Horizontal hydraulic conductivity is generally higher in the well-sorted, undisturbed outwash west of the moraines, especially in the northwest part of the study area. Vertical to horizontal anisotropy is commonly between 10 and 100. Specific yield ranges from about 0.12 to 0.33, with a mean of about 0.17 (Hart and others, 2021; Bradbury and others, 2017; Weeks and Stangland, 1971).

Local-scale Groundwater Flow Systems

To simulate the potential interactions between irrigated agricultural and the study lakes, two local-scale groundwater-flow systems were simulated and analyzed, inset into the regional Central Sands flow system. These two local-scale systems, Plainfield Tunnel Channel Lakes and Pleasant Lake (Figure 1), are discussed in the following to sections, respectively.

Plainfield Tunnel Channel Lakes

The Plainfield Tunnel Channel Lakes area is focused on two of the study lakes, Plainfield and Long Lakes. Both lakes are shallow (no more than a few meters deep) and were formed in a collapsed Tunnel Channel (e.g. Hart and others, 2021). The Tunnel Channel area hosts several

lakes in addition to the two explicitly considered in this study. Hydraulically, the Plainfield Tunnel Channel Lakes are situated near the groundwater divide, in an area with no streams. Regional groundwater flow in this area is from north to south, and towards the stream networks to the east and west (e.g. Central Sands model: Mechenich, 2012). The typical flow condition of the Plainfield Tunnel Channel Lakes is therefore one of through-flow, with groundwater discharge into the lake occurring on the north sides of the lakes, and leakage out of the lake into the aquifer occurring on the south sides. (See Figure 16 for water table contours from the regional model). However, the lack of streams in this area results in greater fluctuations in groundwater levels in response to changes in both recharge and pumping than in areas with more streams, where surface waters act as buffers to water-table fluctuations. This phenomenon is consistent with observations in seepage lakes in a similar glacial environment in Cape Cod, Massachusetts (McCobb and others, 1999) where the faster response of the surrounding groundwater system relative to the lake results in reversal of flow into or out of the lake depending on whether surrounding groundwater levels are rising or falling. In the spring of 2019, following an extended rise in the water table (Appendix A) a transition to nearly all groundwater discharge around the perimeter of Plainfield and Long Lakes was observed, making the lakes sinks to the groundwater system. At other times, when water levels are declining, the lakes may leak around their perimeters and act as sources of water to the groundwater system. Variable groundwater levels and shallow bathymetries make the Plainfield Tunnel Channel Lakes prone to large changes in exposed shoreline, volume and surface area, and even periodic drying.

Pleasant Lake

The third study lake—Pleasant Lake—is relatively deep (up to nearly 8 m (25 ft)) compared to the Plainfield Tunnel Channel Lakes and situated in a collapse feature just east of the moraine, near two headwater streams (Chaffee Creek and Tagatz Creek) (Figure 1). Regional groundwater flow in this area is to the east-southeast, away from the undrained area toward Chaffee Creek to the east, and Tagatz Creek to the south (Figure 16). The typical flow condition of Pleasant Lake is therefore one of groundwater discharge into the west and north sides, and leakage out to the groundwater system on the south and east sides. Hydraulic gradients around Pleasant Lake are relatively stable, due to the presence of nearby streams and it being downgradient from the groundwater divide. The steeper sides and greater depth of the Pleasant Lake basin also make the

shoreline area less sensitive to seasonal fluctuations in water levels. Unlike the Plainfield Tunnel Channel Lakes, where depth to bedrock is 50 m (164 ft) or more, bedrock depth around Pleasant Lake is much shallower, coming within 10 m (33 ft) of the land surface near the north and southeast edges of the lake, and cropping out in nearby areas south of the lake, as discussed further in Appendix A. The presence of shallow bedrock and steeper topography around Pleasant Lake results in more surface runoff than in the Plainfield Tunnel Channel Lakes. Shallow bedrock also decreases groundwater exchange with Pleasant Lake.

Numerical Models

The models developed for this study are intended as tools for simulating groundwater and surface water interactions in the Central Sands, focused in particular on the study lakes—Pleasant, Plainfield, and Long Lakes—and nearby streams. A Soil Water Balance (SWB) model partitions precipitation into rainfall and snowfall, and simulates the transformation of rainfall, snowmelt, and irrigation water into surface runoff, bare soil evaporation, plant transpiration, and net infiltration that can become groundwater recharge (Dripps and Bradbury, 2007; Westenbroek and others, 2010, 2018). Three groundwater models were developed for this study: (1) a regional model covering most of the Central Sands, (2) an inset model focus on the Plainfield Tunnel Channel Lakes, and (3) an inset model focused on Pleasant Lake. Figure 1 shows the locations of these model domains which are referred to throughout this appendix as the Regional Model, the Plainfield Tunnel Channel Lakes Inset Model, and the Pleasant Lake Inset Model, respectively.

The transmissive surficial aquifer and relative lack of streams, particularly in the Plainfield Tunnel Channel Lakes area, require a large model area to incorporate relevant surface-water boundaries and pumping wells that may affect the lakes of interest, thus posing a key challenge to detailed simulation of local-scale features. With a traditional regular grid, high resolution near the lakes must be carried throughout the model domain, resulting in a large number of cells and slow model runtimes. To overcome this challenge, a telescopic mesh refinement (TMR; e.g. Anderson and others, 2015) of a regional model was combined with local-grid refinement (LGR; e.g. Mehl and others, 2006, Langevin and others, 2017) in the vicinity of the lakes.

At the regional scale, a model was developed using the U.S. Geological Survey (USGS) code MODFLOW-NWT (Niswonger and others, 2011) to provide a connection to regional hydrologic boundary conditions including the Tomorrow and Waupaca Rivers to the east and the Wisconsin River to the west (Figure 1). The TMR inset models for the Plainfield Tunnel Channel Lakes and Pleasant Lake were then created within the Regional Model using the USGS code MODFLOW 6 (Langevin and others, 2017; 2020) with time-varying specified heads from the regional model solution around their perimeters. All these domains area shown in Figure 1. Within the inset models, local-grid refinement was used to provide a high level of detail around the lakes, with a minimum of extra cells. This approach leverages the capabilities of MODFLOW 6 to include multiple models that are solved simultaneously a single solution, reducing model runtimes by more than an order of magnitude compared to a regular grid, and using a formulation in MODFLOW 6 that allows for efficient, simultaneous execution of the two models. We initially intended to use the MODFLOW-NWT for all the models, but as the project progressed the LGR capabilities of MODFLOW 6 became apparent to be important for the multi-scale simulation of lakes within a large enough region to simulated representative land use. As a result, the two different codes were used in the same project.

History matching was performed to estimate model parameters that result in model outputs consistent with observations from the field. For the history matching period (2012-2018) the main stresses were provided as well pumping from reported water use from WDNR (<https://dnr.wisconsin.gov/topic/WaterUse/data.html>) and recharge from model runs with SWB. Long-term scenario model runs in support of the Lake Ecosystem Response Assessment (LERA) were performed using a representative set of hydrologic model parameters from the history matching process. For the stresses, however, estimated water use and recharge were provided from SWB model runs.

Soil Water Balance (SWB)

Soil-Water-Balance modeling is often used in support of groundwater flow modeling to provide estimates of the amount and timing of inputs of water to the groundwater table (Scanlon and others, 2002; Healy, 2010). The USGS Soil-Water-Balance (SWB) code was designed to provide groundwater models with gridded estimates of net infiltration, the water that has infiltrated the

soil and has migrated past the effective root zone of surface vegetation (Dripps and Bradbury, 2007; Westenbroek and others, 2010, 2018).

Net infiltration in the SWB approach is considered to occur when infiltration is added to soils that are already at field capacity. In order to assess when soil moisture conditions are near field capacity, SWB tracks daily soil moisture conditions within a single layer for each day in the simulation. Snowfall and snowmelt are simulated in order to provide more realistic additions of snowmelt to the soil layer. Interception by vegetation is accounted for with a simple bucket approach. Runoff is calculated by means of the venerable Soil Conservation Service Curve Number Approach (Cronshey, 1986). Bare soil evaporation and transpiration are simulated by application of FAO-56 methodology (Allen and others, 1998). The FAO-56 sub-model estimates crop water demand and plant transpiration by means of crop coefficient curves specific to each major crop type.

SWB has a short list of data requirements that includes several gridded datasets:

- Land use
- Hydrologic soil group
- Available water capacity
- Daily weather variables (precipitation, minimum and maximum air temperature).

In addition, a set of table values must be supplied defining parameter values for every combination of hydrologic soil group and land-use code contained in the grid files.

For the history matching simulation period (2012-2018), NRCS Cropland Data Layer files were supplied to SWB to define the spatial distribution of crop types (USDA National Agricultural Statistics Service, 2020). Soil available water capacity and hydrologic soil group grids were derived from the USDA's Gridded Soil Survey Geographic (gSSURGO) Database for the Conterminous United States (Soil Survey Staff, 2019). Any areas of missing data within the gSSURGO product were filled with data from the USDA's Digital General Soil Map of the United States (STATSGO2: Soil Survey Staff, 2018).

Gridded daily weather data were obtained from the PRISM Climate Group (2020); grids for the conterminous United States were obtained for 1981 through 2018 and were resampled and reprojected to Wisconsin Transverse Mercator (EPSG 3071: Wisconsin State Cartographer's Office, 2009).

The amount of water required for irrigation of crops is one of the most important components of the water budget for this project; the WDNR's Water Use database is especially useful for quantifying this amount. However, to apply SWB to hypothetical conditions involved in scenario testing it is useful to have another means to estimate irrigation water requirements. SWB uses the FAO-56 methodology (Allen and others, 1998) to estimate basic water requirements for crops. The FAO-56 parameters used for the baseline model run were taken from the values used in Bradbury and others (2017).

SWB tracks soil moisture on a daily basis for each model cell. Irrigation is "applied" by SWB whenever the simulated soil moisture deficit in a cell exceeds a predefined maximum allowable depletion value. "Maximum allowable depletion" is a parameter supplied to SWB in a lookup table; the value reflects the amount of soil-moisture deficit that might be tolerable before triggering an irrigation event. Maximum allowable depletion values used for the baseline run were generally taken from values published in Allen and others (1998).

Remote sensing of 'actual' evapotranspiration is commonly performed; one such product that was considered for use as direct input to SWB is based on the Moderate Resolution Imaging Spectroradiometer (MODIS) (Mu and others, 2013). The MODIS product provides an estimate of actual evapotranspiration approximately every 8 days; conditions between satellite passes are unknown. For use driving a continuous simulation model such as SWB, MODIS estimates pose several challenges: (1) evapotranspiration in and around urban areas cannot be estimated and is reported as zero; and (2) estimates are questionable during periods of snow cover. Another consideration is that similar to the irrigation water-use data, satellite-derived data may work well for more recent time periods but are unavailable for hypothetical conditions and drivers associated with scenario testing. Last, the experimental use of MODIS data as a direct input to SWB during initial model development introduced mass balance errors; MODIS estimates

sometimes estimated more moisture extracted from the soil moisture reservoirs than could be held within the root zone as parameterized within the SWB model. Based on these considerations, general correspondence between MODIS and SWB estimates was used as confirmatory, but MODIS was not used as a direct input.

The LERA simulations involve pre-satellite timeframes and weather drivers, so the MODIS data product was used as a verification of the SWB-generated actual evapotranspiration values. FAO-56 dual crop coefficient procedures for estimating soil-moisture depletion under ‘non-standard’ conditions were used. ‘Dual crop coefficient’ refers to the fact that the procedure accounts for bare soil evaporation separate from plant transpiration; this method is described as being best for irrigation scheduling software or other similar applications (Allen and others, 1998). ‘Non-standard’ indicates conditions that might be less than ideal (fully watered) for plant growth. Parameters used in the parameter estimation run were largely the same as those used in Bradbury and others (2017).

Figure 3 – Mean 2012 – 2018 annual net infiltration estimated by SWB.

Regional Model

A regional MODFLOW-NWT (Niswonger and others, 2011) model was developed to provide hydraulic head boundary conditions to the MODFLOW 6 lake models. The regional model was transient with monthly stress periods from 2012 to 2018 and began with a steady state stress period representing long-term mean conditions over the entire period of 2012-2018. Each transient stress period was subdivided into five time steps using a time-step multiplier of 1.5. Model files are provided in the model archive associated with this report (Fienen and others, 2021).

Domain

The regional model domain is shown in Figure 1. The active model extent was selected to include natural flow boundaries, where available, and all pumping stresses that may influence the hydraulic heads at the specified boundaries of the two lake inset models. Regional flow

boundaries included in the model are the Wisconsin and Plover Rivers to the west, the Tomorrow, Waupaca, and Wolf Rivers to the north, and the Fox River to the east. Areas beyond the regional boundaries were inactive in the model.

Model Grid and Layering

The regional model consists of a uniform grid of 572 rows and 533 columns of 200-m (656-ft) cells. The model has four layers to represent the hydrostratigraphic units discussed in the Conceptualization of Groundwater Flow in the Central Sands section and includes the following:

- Layer 1 – Upper glacial layer representing, unsorted glacial sediments to the east and more homogenous glacial sediments to the west.
- Layer 2 – Middle glacial layer representing glacial sediments in the moraines and collapsed outwash to the east, and the New Rome Member to the southwest. Areas west of the moraines where the New Rome Member is absent are pinched out in this layer.
- Layer 3 – Lower glacial layer representing glacial sediments to the east and more homogenous glacial sediments to the west.
- Layer 4 – Bedrock layer representing the sandstone bedrock.

The top of layer 1 is resampled from a 10-m digital elevation model (DEM) of the model domain (WDNR, 2019). The bottom elevations of layers 1 and 2 are defined by the bottom of the upper coarse layer and middle fine layer discussed in Appendix A. The bottom of layer 3 is the top of the sandstone bedrock unit and the bottom of the layer 4 is the top of the Precambrian bedrock. Additional information on the geologic layers is in Appendix A.

Boundary Conditions

Boundary conditions that control groundwater movement in the regional model included infiltration originating from precipitation and snowmelt, groundwater exchanges through the model perimeter and the stream network, and groundwater withdrawals through pumping. Figure 4 shows the boundary conditions used in the regional model.

Figure 4 – Map of model boundary conditions for the regional model.

Spatially averaged net infiltration (i.e. aquifer recharge) for the 2012–2018 period ranged from about 100 millimeters per year (mm/y) to 600 mm/y (3.9 inches per year (in/y) to 23.6 in/y) in the regional model domain. This net infiltration was specified using the MODFLOW Recharge (RCH) package (Harbaugh, 2005).

High-capacity pumping wells operating during any part of the 2012–2018 period were included in the regional model (Figure 4). Pumping was specified using the MODFLOW Well (WEL) package (Harbaugh, 2005). Well construction and reported monthly pumping information for high capacity wells was provided by the WDNR (<https://dnr.wisconsin.gov/topic/WaterUse/data.html>). Well locations were assigned to the model layer with highest transmissivity within the well open interval. Wells without open interval information were assigned to the highest transmissivity layer at their location.

Lateral flow boundaries were represented in the regional model using the MODFLOW General Head Boundary (GHB) package (Harbaugh, 2005). These flow boundaries included the Wisconsin and Plover Rivers to the west, the Tomorrow, Waupaca, and Wolf Rivers to the north, and the Fox River to the east. Groundwater exchanges with GHB cells are computed using the difference between the simulated hydraulic head in the aquifer and the assigned GHB elevation, and a conductance term. The elevation of the GHB cells was set to the minimum DEM elevation (WDNR, 2019) within the model cell area. The conductance term is a function of the cell area, the assumed thickness of the riverbed, and the vertical hydraulic conductivity of the riverbed material. GHB cells were assigned a conductance of 0.5 square meter per day (m^2/day) (1.6 square feet per day (ft^2/day)) which, assuming a 1-m (3.3-ft) thick riverbed, is equivalent to a 1.25×10^{-5} meter per day (m/day) (4.10×10^{-5} feet per day (ft/day)) vertical hydraulic conductivity. The conductance was adjusted during history matching to $3.9 \text{ m}^2/\text{day}$, which is equivalent to a $9.75 \times 10^{-5} \text{ m}/\text{day}$ ($3.20 \times 10^{-4} \text{ ft}/\text{day}$) vertical hydraulic conductivity. This value is similar to the calibrated vertical hydraulic conductivity of $4 \times 10^{-4} \text{ ft}/\text{day}$ for GHB cells representing Lake Superior in Leaf and others (2015).

Lateral flow boundaries form the perimeter of the active area of the regional model except along the southern boundary. The southern model boundary has no major river nearby and is located

far enough from the study lakes as to not affect groundwater flow in those areas. As a result, the southern model boundary was set as a no-flow boundary, consistent with a previous two-layer groundwater flow model (Mechenich, 2012) of the Central Sands region (referred to as the Mechenich Model), located perpendicular to the assumed groundwater flow direction east to the Fox River or west to the Wisconsin River.

Streams were represented in the model using the MODFLOW Streamflow Routing (SFR2) package (Niswonger and Prudic, 2005). SFR2 calculates exchanges between the aquifer and stream system while accounting for total streamflow in the channel. SFR2 input was developed from NHDPlus version 2 hydrography using the SFRmaker software (Leaf and others, 2021). NHDPlus flowline features were joined spatially to the model grids; with the resulting line/grid cell intersections and associated attributes forming the basis for SFR reaches. Streambed top elevations were sampled from the lidar-based DEM (WDNR, 2019) as the minimum elevation within a 100-m buffer around the line representing each SFR reach. Like GHB, SFR2 has a conductance term that represents the thickness of the streambed, the model cell area of the SFR cell, and the vertical hydraulic conductivity of the streambed. The vertical hydraulic conductivity of the streambed was estimated for each stream reach during history matching. Vertical hydraulic conductivity values of the streambed started at 1 m/day (3.28 ft/day) with final values ranging from 0.03–80.5 m/day (0.1–264.1 ft/day).

Aquifer Properties

Aquifer properties represented in the regional model include vertical and horizontal hydraulic conductivity, specific storage, and specific yield. Initial values were assigned based on literature values discussed below and then adjusted during history matching.

The initial hydraulic conductivity for the eastern half of the unconsolidated model layers (1-3) was estimated using the coarse/fine fractions from Appendix A and a power law approach similar to Feinstein and others (2010). The power law parameters were optimized so that the mean of the initial hydraulic conductivity values produced by the power law agreed with the mean values from the Mechenich Model. Hydraulic conductivity for the western half of the unconsolidated layers, west of the terminal moraine, where coarse/fine fraction estimates were

not made in Appendix A, used information from the upper layer, representing unconsolidated materials, of the two-layer Mechenich Model of the Central Sands region. The initial hydraulic conductivity of the sandstone (layer 4) came from layer 2, representing bedrock, in the existing Mechenich Model. Lakes across the model domain were included as high hydraulic conductivity zones in layer 1 with a horizontal hydraulic conductivity of 10,000 m/day.

Initial vertical hydraulic conductivity of the fine-grained New Rome Member in layer 2 was set to 0.01 m/day based on vertical hydraulic conductivity estimates for the New Rome Member of 0.2 and 8×10^{-5} m/day from Hart and others (2015). The initial horizontal hydraulic conductivity of the New Rome Member was set at 0.1 m/day, which is 10 times the vertical hydraulic conductivity. The specific yield for the New Rome Member was set to 0.20 based on a range of literature values for silt, clay, and fine sand specific yields of 0.06–0.33 (Duffield, 2019). The specific storage was set to 9.2×10^{-4} m⁻¹, slightly lower than the Hart (2015) estimate of 9.8×10^{-4} m⁻¹ for the transition zone of the New Rome and at the lowest end of the literature range of 9.2×10^{-4} - 2.0×10^{-2} m⁻¹ (2.8×10^{-4} - 6.2×10^{-3} ft⁻¹) for clays (Duffield, 2019). The aquifer properties of the New Rome Member after history matching were a horizontal hydraulic conductivity of 9.2×10^{-2} m/day (0.3 ft/day), vertical hydraulic conductivity of 2.0×10^{-3} m/day (0.007 ft/day), a specific yield of 0.2, and a specific storage of 9.2×10^{-4} m⁻¹ (2.8×10^{-4} ft⁻¹).

The aquifer properties of the regional model after history matching are shown in Figure 5 - Figure 8. Horizontal hydraulic conductivities ranged from 0.09–152 m/day (0.3–499 ft/day) in the three unconsolidated layers (Figure 5). The mean horizontal hydraulic conductivity was highest in layers 1 and 3 (46 m/day and 18 m/day; 151 ft/day and 59 ft/day) and lowest in layer 2 (13 m/day; 43 ft/day). This is consistent with layers 1 and 3 representing coarser glacial material and layer 2 representing finer material to the east and the New Rome Member to the west. The mean horizontal hydraulic conductivity was 9 m/day (30 ft/day) for the sandstone bedrock, represented by layer 4.

Vertical hydraulic conductivities of the three unconsolidated layers ranged from 0.002-2.93 m/day (0.007-9.61 ft/day) with a mean that was lowest in layer 2 (0.37 m/day; 1.21 ft /day) and

highest in layer 1 (1.01 m/day; 3.31 ft/day) (Figure 6). The vertical hydraulic conductivity of the sandstone had a mean of 0.13 m/day (0.43 ft/day).

The specific yield means for the three unconsolidated layers ranged from 0.19–0.37 and was 0.14 for the layer 4 sandstone (Figure 7). These values are within the literature ranges for till, clay, sand, and gravel specific yields of 0.06–0.33 and within the sandstone literature ranges of 0.06–0.27 (Duffield, 2019). The mean specific storage for the three unconsolidated layers ranged from about 3.3×10^{-4} – $4.8 \times 10^{-4} \text{ m}^{-1}$ (1.0×10^{-4} – $1.5 \times 10^{-4} \text{ ft}^{-1}$) (Figure 8). Model values for the unconsolidated material fell within the specific storage literature ranges (Duffield, 2019) for loose to dense sand and gravel (1.0×10^{-4} – $4.3 \times 10^{-4} \text{ m}^{-1}$; 3.1×10^{-5} – $1.3 \times 10^{-4} \text{ ft}^{-1}$) and clays (9.2×10^{-4} – $2.0 \times 10^{-2} \text{ m}^{-1}$; 2.8×10^{-4} – $6.2 \times 10^{-3} \text{ ft}^{-1}$) and close to the Hart and others (2015) estimate of specific storage in the sandy aquifer underlying the New Rome Member of $3.0 \times 10^{-4} \text{ ft}^{-1}$ ($9 \times 10^{-5} \text{ ft}^{-1}$). The specific storage was about $9.8 \times 10^{-5} \text{ m}^{-1}$ ($3.0 \times 10^{-5} \text{ m}^{-1}$) for the layer 4 sandstone and is just above the literature ranges (Duffield, 2019) for fissured rock 3.3×10^{-6} – $6.9 \times 10^{-5} \text{ m}^{-1}$ (1×10^{-6} – $2.1 \times 10^{-5} \text{ ft}^{-1}$).

Figure 5 – Horizontal hydraulic conductivity values after history matching for each of the four model layers.

Figure 6 – Vertical hydraulic conductivity values after history matching for each of the four model layers.

Figure 7 – Specific yield values after history matching for each of the four model layers.

Figure 8 – Specific storage values after history matching for each of the four model layers.

History Matching Approach and Results

We performed history matching (a process also referred to as “parameter estimation” and, sometimes, “model calibration,” although “calibration” implies a precise unique fit of the model to data and, as described below, that is not an accurate representation of this process) to systematically adjust parameter values in the model such that associated model outputs are consistent with historical observations including hydraulic head and base-flow values. The general history matching approach follows Bayes’ theorem (Tarantola, 2005) for parameter estimation. In this approach, we start with a prior estimate of both model parameters and their credible ranges (e.g. uncertainty). These prior parameter values and uncertainty are informed by

expert knowledge, literature values, and available direct measurements. Through a systematic conditioning step, the parameter values are updated to be consistent with observations that correspond with model outputs. This step is referred to as an “update” and results in a posterior set of parameter values (“posterior” meaning “after the update”). There are many algorithms that can be used to perform this conditioning. For the regional model, we used the PEST_HP (Doherty, 2020) software. The choice of software, in part, reflects rapid development of PEST-related tools throughout the modeling project timeframe. We used the iterative ensemble smoother (iES) in PEST++ (White and others, 2021) for the inset models. The history matching files are provided in Fienen and others (2021).

The measured values of groundwater hydraulic heads and streamflow used for history matching (referred as “targets”) came from several data sources that are summarized in Table 1. Data from a total of 177 streamflow and 464 well and lake elevation measurement locations were used during the history matching. Simulated groundwater elevations, lake elevations, and streamflow from the steady-state period at the start of the transient model were compared to targets of data averaged over the 2012–2018 period. Simulated groundwater elevations, lake elevations, and streamflow from the transient stress periods were compared with targets closest to the end of the month represented by each stress period, for whichever stress periods measured data were available.

A post-history-matching comparison between the measured and simulated values for lake and groundwater elevation targets are shown on Figure 9, and for the streamflow targets on Figure 10. The closer these values plot along the 1:1 line, the closer the match between the simulated and measured values. Groundwater elevation targets mostly plotted on or near the 1:1 line with some outliers scattered both above and below the line. The streamflow targets generally plotted on or near the 1:1 line for most of the data with a slight under-estimated bias (simulated lower than measured), particularly in comparison to the WDNR base-flow data (Figure 10).

Table 1 Measured groundwater elevation and streamflow data sources used for history matching in the regional parent model.

Group Name	Target Type	Description	Number of Locations	Data Source
hds_wgnhs_tr, heads_wgnhs	Hydraulic Head	Well construction report groundwater elevation measured after a well was drilled. Locations were determined by the WGNHS.	299	WGNHS data pulled from webservices.
nwis_dvs, nwisdvs_tr	Hydraulic Head	Groundwater elevations at locations with daily data that were collected by the USGS.	31	NWIS: https://doi.org/10.5066/F7P55KJN
nwis_fm, nwisfm_tr	Hydraulic Head	Groundwater elevations at locations with miscellaneous that were measured by the USGS.	23	NWIS: https://doi.org/10.5066/F7P55KJN
wdnr_wells	Hydraulic Head	Wells installed for this study and measured by WGNHS and WDNR.	36	WGNHS/WDNR data pulled from webservices.
wdnr_lakes, wdnr_lks_tr	Hydraulic Head	Lake elevations measured by the WDNR.	70	WDNR data pulled from web services.
usgs_stages	Hydraulic Head	Lake elevation measured by the USGS.	5	NWIS: https://waterdata.usgs.gov/nwis
nr_diff	Hydraulic Head difference (vertical)	Head difference measurement across the New Rome Member.	1	Hart and others (2015)
hd_diff	Hydraulic Head difference (temporal)	Calculated at the difference between two head measurements made at the same location for any head dataset where two or more measurements were made.	1573 differences; some locations have multiple differences if more than 2 groundwater elevations were collected.	All hydraulic head target datasets presented in this table.
nwis_dv_flx, nwisdvflx_tr	Streamflow	Streamflow measurements at USGS gaging stations with daily data. Data have been adjusted using base-flow separation techniques to reflect baseflow conditions.	6	NWIS: https://doi.org/10.5066/F7P55KJN
nwis_fm_flx, nwisfmflx_tr	Streamflow	Miscellaneous streamflow measurements collected by the USGS. Data have been adjusted to base-flow conditions using nearby gaging stations with daily data.	5	NWIS: https://doi.org/10.5066/F7P55KJN
wdnr_misflx, wdnrflx_tr	Streamflow	WDNR streamflow measurements made during base-flow conditions. No adjustments made.	166	WDNR data pulled from web services.

Figure 9 – One-to-one plot of measured and simulated groundwater elevations for the steady-state and transient head targets.

Figure 10 – One-to-one plot of measured and simulated streamflow under base-flow conditions for the transient streamflow targets.

The residuals (i.e. differences between simulated and measured) for the steady-state hydraulic head and streamflow targets are shown spatially in Figure 11 and Figure 12, respectively. Most hydraulic head targets are from well construction reports, with accurate locations limited to the central eastern part of the model domain, where location-corrected values were provided by WGNHS (Appendix A), focused close to the study lakes. Hydraulic head residuals were generally well distributed throughout the model domain with some locally biased over-estimated

values (simulated higher than measured) in the central portion of the domain. A comparison of flux (streamflow) target residuals show a general pattern of under-estimated streamflows, although the bias is less near the inset areas (e.g. Upper Pine River, Chaffee Creek, and Tagatz Creek; Figure 12).

Figure 11 – Map of steady-state hydraulic head target residuals displayed by calibration group.

Figure 12 – Map of steady-state streamflow residuals and gaining and losing stream reaches.

Transient hydraulic head and streamflow targets for a select subset of wells and streams are shown in Figure 13 and Figure 14, respectively. Well locations with data plotted in Figure 13 were selected to represent wells with longer-term records across the model domain and included a range of good to poorly matched simulated and measured water levels. Overall, the simulated transient hydraulic heads at most wells were in good agreement with long-term groundwater elevation data.

There were fewer stream locations with daily streamflow data in the model domain. Tenmile Creek has the most complete daily record for the history matching period, and the simulated fluxes generally were in good agreement with the trends and timing of peak flows for the period of record. The simulated fluxes generally were lower than the measured streamflow highs but were in good agreement with the mid- and lower base flows. Simulated fluxes in the headwater streams located near the focus area lakes reasonably matched the magnitude and trends measured in these streams, except for Tagatz Creek, where the simulated base flows in the headwaters were much lower than what was measured. This was, in part, due to bedrock anomalies in the area around Tagatz Creek, which were addressed in the inset models by adjusting the bedrock locally in near the creek to simulate incision of the stream.

Figure 13 – Transient groundwater elevations at select wells with long-term records (well locations shown in Figure 11; site number is from National Water Information System (<https://doi.org/10.5066/F7P55KJN>)). Elevations are shown in meters and feet above North American Vertical Datum of 1988 (NAVD88).

Figure 14 – Transient streamflow at select streams locations near the study lakes and with longer-term record (stream locations shown in Figure 12; site number is from National Water Information System (<https://doi.org/10.5066/F7P55KJN>)).

A total of 1,775 model parameters were adjusted during the history matching and included:

- the conductance of the GHB cells representing perimeter boundary conditions;
- the vertical hydraulic conductivity of each stream segment;
- a grid of pilot point multipliers across the aquifer property arrays representing the unconsolidated and sandstone units, except for the New Rome Member;
- a zone aquifer property multiplier for each array with pilot points;
- the aquifer properties of the New Rome Member;
- a 0.8–1.2 temporally variable multiplier on the SWB-estimated net infiltration for each monthly stress period; and
- a 0.75–1.25 multiplier on the reported pumping rates for all wells in each monthly stress period.

The aquifer properties included in the history matching were horizontal and vertical hydraulic conductivity, specific storage, and specific yield. These properties had initial values assigned as discussed in the Aquifer Properties section. These initial parameter arrays were then adjusted using a network of pilot points representing multipliers and zone multipliers for each layer.

Zones and pilot points are shown in Figure 15 for each of the four model layers, and include:

- a zone for each of the unconsolidated layers with a coarse/fine fraction assigned in Appendix A for materials on the eastern half of the model domain;
- a zone for the consolidated materials in the western half of layers 1 and 3;
- a zone for the sandstone unit represented by layer 4.

Figure 15 – Pilot points and multiplier zones for each of the four model layers. Note, pilot points extend past the zone boundaries in layer 2 to allow for kriging but the aquifer properties in the New Rome Member and pinched areas are not influenced by pilot point multipliers.

The aquifer properties after history matching are presented and discussed in the Aquifer Properties section and the GHB conductance is discussed in the Boundary Conditions section. The final multipliers on the SWB-estimated net infiltration ranged from 0.8–1.2 with a mean of 1.02, meaning that on average the adjustment to net infiltration was a 2% increase over what was estimated by SWB. The final multipliers on the reported well pumping rates ranged from 0.75

to 1.25 with a mean of 0.95, meaning that on average the adjustment to reported pumping rates was a 5% decrease in the reported rates.

Regional Model Results

The water table elevation contours and cumulative streamflow for the regional model are presented in Figure 16. The water table is mounded along the topographic high formed by the moraine that runs north-south through the center of the model domain. Groundwater flows from this water table high to the east and west towards the major rivers that form the major hydrologic boundaries in the region.

A simulated water budget of the major changes in inflows and outflows from 2012–2018 is shown in Figure 17. Water enters the groundwater system through recharge and stream leakage under losing flow conditions and exits through streams under gaining flow conditions, pumping from high capacity wells, and discharge to the major rivers at the lateral boundaries of this flow system. Excess inflows and outflows are balanced throughout the aquifer system by groundwater storage replenishment and depletion. During periods of high recharge (often in the spring) there is a gain in groundwater storage, which can be thought of as excess water leaves the aquifer system and goes into storage (STORAGE_OUT on Figure 17), whereas during the growing season periods when pumping is higher and recharge is lower, water is being removed from groundwater storage and goes into the aquifer system (STORAGE_IN on Figure 17).

Figure 16 – Map of the simulated water table and streamflow for the regional model during the steady-state stress period representing mean conditions from 2012 – 2018.

Figure 17 – Regional model groundwater budget showing the major model inflows and outflows for each stress period. Inflows and outflows are named using the MODFLOW List file convention.

Focus Area Inset Models

Two inset models were developed from the regional model, for the areas around the Plainfield Tunnel Channel Lakes (Plainfield Tunnel Channel Lakes model) and Pleasant Lake (Pleasant Lake model). The inset models were developed to simulate the study lakes and their competing sinks—streams and boundaries—at a level of detail sufficient for lake level simulation; a level of detail not possible with the regional-scale model. Base-case versions of each model were created

for history matching for the 2012 through 2018 period. Model parameters estimated from history matching were then applied to scenario-testing versions of the two models, which are described in the Lake Ecosystem Response Assessment (LERA) section. Model files are provided in the model archives associated with this report (Fienen and others, 2021 and Westenbroek and others, 2021).

Inset model domains and horizontal discretization

The inset model domains were designed to encompass the nearest headwater streams to the east and west of the study lakes, and the majority of high-capacity wells that might affect the lake water balances, while maintaining reasonable model execution times. A uniform grid with 20-m (65.62-ft) horizontal resolution of area surrounding the lakes was selected to adequately represent the detailed bathymetry and shoreline geometry of the lake basins. Initial testing of runtimes with the MODFLOW-NWT code and a 20-m grid spacing over the entire inset model domains resulted in unacceptably long runtimes (on the order of hours).

Therefore, a local-grid refinement (LGR) approach was adopted using the multiple model capabilities of MODFLOW 6 (Langevin and others, 2017). The models focused on the lakes each consist of two sub-models—the “inset” sub-model aligned with the regional model grid at the same 200-m (656.2-ft) resolution, and a locally refined “LGR” sub-model with a uniform 20-m resolution encompassing a rectangular area around the lake(s) of interest (Figure 18). For Pleasant Lake, this resulted in 100 rows and 100 columns for the Inset model and 100 rows and 120 columns for the LGR sub-model. The Plainfield Tunnel Channel Lakes Inset model has 90 rows and 110 columns and 120 rows and 250 columns for the LGR sub-model. Within MODFLOW 6, the two sub-models are coupled within the same solution matrix and solved simultaneously as a “simulation” (Langevin and others, 2017). This coupling greatly reduced the overall number of model cells, cutting the runtimes for the base-case simulation (2012-2018 period) to around 10 minutes.

Figure 18 – Plainfield Tunnel Channel Lakes model boundary conditions with local-grid refinement extent.

Figure 19 – Pleasant Lake model boundary conditions with local-grid refinement extent.

Inset model layering

Layering in the inset models was developed from the same data sources as the regional model, with the exceptions that layer 1 was typically split into two layers for the insets and was adjusted for lake bathymetry where the lakes are simulated. The model top (of layer 1) is based on mean elevations sampled for each model cell from a lidar-based DEM (WDNR, 2019), except within the basins of Plainfield, Long, and Pleasant Lakes, where bathymetry developed by WDNR (2020) was subtracted from the DEM elevations to develop the model top. The layer bottom surfaces in the inset models where lakes are not present are congruent with the regional model except that layers 1 and 2 are evenly subdivided from layer 1 in the regional model to better represent hydraulic gradients near surface water features.

Unlike MODFLOW-NWT, MODFLOW-6 allows for discontinuous layering, meaning cells can be removed from the model solution in places where a hydrogeologic unit is absent. In the Plainfield Tunnel Channel Lakes inset model, this feature was used to remove cells from layer 3 in areas west of the Hancock Moraine, where “layer 2” from Appendix A was not defined (Figure 20). Similarly, in the Pleasant Lake model, cells were removed from layer 3 in places where the New Rome Member or “layer 2” from Appendix A were absent. Cells were also removed from the models in places where the layer bottoms were within a meter of the land surface, for example, near high points in bedrock surface or along lake bottoms. Removing unneeded cells, which would otherwise need to be carried throughout the model at some minimum thickness (e.g. 1 m), can further increase the stability and speed of the model solution.

Figure 20 – Inset model cross sections showing inset and parent layer surfaces. Gaps in the cross sections indicate the extent of the refined areas within the inset models. Cross-section locations are shown in Figure 18 and Figure 19.

Time discretization

Time discretization for the base versions of the inset models is similar to the regional model with the exception that the initial steady-state period represents mean conditions for the period of 2012 through 2015. Subsequent transient monthly stress periods represent mean conditions for each month through 2018. Each transient stress period was subdivided into 5 time steps using a

time-step multiplier of 1.2. This time-step multiplier differs from the regional model multiplier of 1.5 because the lake package poses a greater challenge to model convergence and a smaller time-step multiplier can mitigate that.

Boundary conditions

Boundary conditions within the inset model domains include regional groundwater flow across the model perimeters, terrestrial recharge originating from precipitation, snowmelt and irrigation, and groundwater/surface water interactions with lakes and streams. The model perimeter boundaries were simulated as constant hydraulic head values from the regional model.

Perimeter boundaries

The inset models are connected to the regional model via specified head boundaries along their perimeters. Hydraulic head values were extracted from the regional model solution at each 200-m cell along the inset model perimeter (which corresponds one-to-one with a regional model cell), for each stress period. The difference in time-step length (due to the time-step multiplier) in the regional versus the inset model prevented closer linking at the time-step level, but linking at the stress period level matches the other stress definitions (e.g. pumping and recharge). The specified hydraulic head values were then simulated with the Constant Head (CHD) package in MODFLOW 6. Within the simulations for the inset models, the parent and inset sub-models are connected dynamically via the Groundwater Flow (GWF-GWF) Exchange package in MODFLOW 6 (Langevin and others, 2020).

Recharge

Recharge for the inset models was resampled from the net infiltration output of the SWB simulation to the model cell centers using a nearest-neighbor approach. This is mass-conservative because the subdivided inset model cells fall evenly within the parent cells. For the initial steady-state period, mean recharge for 2012 through 2015 was used. Monthly mean net infiltration was sampled from SWB for the subsequent monthly stress periods. Recharge was simulated in MODFLOW-6 using the Recharge (RCH) Package with array-based input (Langevin and others, 2020).

Streams

Streams were simulated with the SFR Package in MODFLOW-6 (Langevin and others, 2020). SFR input was developed using the same methods as the regional model (Leaf and others, 2021), except the NHDPlus flowlines were edited to more accurately represent the spring complexes at the headwaters of Chaffee and Tagatz Creeks and the Mekan River. In the Pleasant Lake model, Chaffee and Tagatz Creeks originate within the inset sub-model and flow out to the parent sub-model (Figure 19). These streams are linked between the two sub-models using the Water Mover (MVR) package at the simulation level (Langevin and others, 2020).

Lakes

The study lakes were represented in the LGR portion of the inset models using the Lake (LAK) package in MODFLOW-6, which couples a lake water balance and simulation of lake stage with the groundwater flow solution (Langevin and others, 2017). In the Plainfield Tunnel Channel Lakes model, this included Plainfield and Long Lakes, as well as Second Lake and Sherman Lake (Figure 18). In the Pleasant Lake model, only Pleasant Lake was simulated using the LAK package (Figure 19). All other lakes in the MODFLOW-6 inset models continue to be simulated using high hydraulic conductivity zones, as in the regional model.

Lake extents obtained from the WDNR 24k hydro dataset (WDNR 2015) were intersected with the model grid to develop the lake connections cells. Within the lake extents, the model top was set at the lake bottom, using bathymetric surfaces developed by the WDNR (Aaron Pruitt, WDNR, written communication, 2020), which are available in the accompanying model archive (Fienen and others, 2021). In areas where the lake bathymetry indicated lake bottoms incised deeper than the bottom of the regional model layer 1, those layer bottom elevations were also set to the lake bottom, resulting in zero thicknesses for those cells. The zero thickness cells were removed from the model (idomain set to -1) and vertical lake connections were made with the uppermost active cells beneath the lake footprints. Lakebed leakance was assigned to two zones—a littoral zone of approximately 1 cell (20-m) width around the lake perimeter, and profundal zone representing the interior of the lake basin. Within the Lake package solution, lake volumes were defined by the computed lake stage and the elevation of the lake bottom, as

defined by the model top (a separate bathymetry file defining the stage/area/volume relation was not used).

The Lake package water balance requires input of direct precipitation over the lakes and lake evaporation. Precipitation input was obtained for the lake locations from the PRISM dataset (PRISM Climate Group, 2019), which also includes daily mean air temperature estimates. Mean monthly open water evaporation rates were estimated from the air temperatures using the unmodified Hamon method (Harwell, 2012). Based on analysis by Pruitt (Appendix E) implementing the General Lake Model (Hipsey and others, 2019) for the study lakes, a systematic correction was made to decrease highest and increase lowest evaporation inputs by 25%. This correction is consistent with the Hamon method often calculating extreme values too far from the mean. For the initial steady-state period, precipitation and evaporation were averaged for the period of 2012 through 2015 resulting in a net influx of water to the lake from its surface.

Water use

High capacity wells operating during any part of the 2012 – 2018 period were represented with the Well (WEL) Package for MODFLOW 6 (Langevin and others, 2017). Figure 18 and Figure 19 show the locations of the pumping wells. Well package input was developed from reported pumping (<https://dnr.wisconsin.gov/topic/WaterUse/data.html>), with the same methods used for the regional model. Wells were assigned to the model layer with highest transmissivity within the well's open interval. Wells without open interval information were assigned to the highest transmissivity layer at their location.

Aquifer properties

Horizontal and vertical hydraulic conductivity were initially set at the values estimated for the regional model by history matching. To avoid having parameters adjusted to extreme values in the local-scale models history matching process, when applying multipliers to localized values that are already approaching extrema, specific storage (Ss) was initially set to $1 \times 10^{-6} \text{ m}^{-1}$ and specific yield (Sy) was initially set to 0.15 uniformly throughout the model domain; based on previous investigations for similar deposits.

Parameter Estimation and uncertainty analysis

The history matching approach used in this analysis is described in detail in Corson-Dosch and others (2021). Similar to what was done in the regional model, history matching was performed to refine parameter estimates for the inset and LGR models with the same observation data used for the regional model analysis, and additional observations in the area around the lakes. For the inset models, we used the iterative ensemble smoother (iES) implementation (White, 2018) of the Parameter ESTimation (PEST) software PEST++ (version 5.0.0; White, 2018; White and others, 2021). The goal of the iES is to both provide parameter estimates and to quantify the uncertainty of those estimates. This uncertainty is characterized by a range of estimated parameters that each reproduce simulated hydraulic heads and streamflows within an acceptable range of the measured values. Each observation is assigned an observation weight that, in principle, corresponds to the inverse of the standard deviation assuming a normal distribution of uncertainty around the measured observation value. As a result, in comparing the model output with measured values, the uncertainty of both the measured and simulated values should be considered and, ideally, they should overlap.

The iterative ensemble smoother method and uncertainty quantification

The iterative ensemble smoother (iES) is an ensemble method, meaning at every stage of analysis, an ensemble of parameter sets (or realizations) is generated consistent with their inherent uncertainty and the assumed uncertainty in the observations. Simulations are then made using each parameter set from this ensemble to produce a range of model output. The iES uses empirical correlations between parameter and observation ensembles to iteratively reduce the uncertainty and discrepancy between the simulated values and measured observations, providing a posterior parameter ensemble that reflects the inherent uncertainty in the parameters conditioned on the available data. A single “base-case” realization represents the minimum error variance solution and can be used when a single set of parameter values is required for model simulation. This base-case realization is the one used for the scenario testing documented in this appendix.

Observation data

Observation data were compiled for the inset models from the same dataset used for history matching in the regional model. Some additional observations focused around the study lakes were added for the inset models and some spatial water-level difference observations (measures of the horizontal hydraulic gradient between shallow piezometers installed near the lakes and the simulated lake elevations) were added along with the temporal difference observations.

Observation weights were initially assigned based on assumptions regarding a level of fit between model outputs and collocated measurements. These weights were adjusted to balance the objective function that drives the iES regression including assigning a weight of 0.0 to some classes of observations. These adjustments are all intended to steer the iES results toward a model design that is focused on the complex groundwater/surface water interactions in the study area, and in particular, matching observed lake elevations and streamflow values – a key objective of this analysis. Table 2 and Table 3 summarize the observations used, by observation group, and include values and observation weights for the Pleasant Lake and Plainfield Tunnel Channel Lakes inset models, respectively.

Water level and streamflow observations were assigned the values at the end of the month in which they were measured. In this way, intermediate results at a timescale shorter than the stress-periods are not considered. This is done to be consistent with the way stresses (including pumping and recharge) are implemented in the model. With monthly stress periods, all stresses that occur at any time in the month must be applied uniformly at the start of the stress period. As a result, observations at intermediate times within the month are not truly representative of their sub-monthly timescale location, so the end of the month is considered most representative. In the case of streamflow, total streamflow was used to assign observation value with the assumptions that there may be some stormflow in the observations that the models will not simulate as the models only simulate base flow. However, base flow is interpreted to dominate the streamflow in this area.

Figure 21 and Figure 22 show the locations of water level observations for the Pleasant Lake and Plainfield Tunnel Channel Lakes inset models, respectively. The labels correspond to observation names that were used in the PEST++ input files.

Table 2 Observation data groups, values, and descriptions for Pleasant Lake inset model

Group Name	Observed Values	Target Type	Description	Total number of Observations	Number of weighted observations	Number of zero-weighted observations	Weight	Weight-informed standard deviation	Data Source
hds_wgnhs_tr, heads_wgnhs	280.3 to 327.2	Hydraulic Head	Well construction report groundwater elevation measured after a well was drilled. Locations were determined by the WGNHS.	100	0	100	0	NA	WGNHS data pulled from webservices.
nwis_dvs	298.0 to 314.7	Hydraulic Head	Groundwater elevations at locations with daily data collected by USGS.	14	14	0	3.77936 to 7.12599	0.140331 to 0.264595	NWIS: https://doi.org/10.5066/F7P55KJN
nwis_fm	264.1 to 300.8	Hydraulic Head	Groundwater elevations at miscellaneous locations measured by USGS.	2	0	2	0	NA	NWIS: https://doi.org/10.5066/F7P55KJN
nwisdvs_tr	297.7 to 315.5	Hydraulic Head	Groundwater elevations at locations with daily data collected by USGS.	133	133	0	1.26021 to 2.04421	0.489187 to 0.79352	NWIS: https://doi.org/10.5066/F7P55KJN
nwisdvs_tr_tdiff	-0.3 to 0.5	Hydraulic Head Temporal Difference	Groundwater elevations at locations with daily data collected by USGS.	119	119	0	7.31772	0.136655	Lake elevations measured by WNDR
nwisfm_tr	263.1 to 300.8	Hydraulic Head	Groundwater elevations at miscellaneous locations measured by USGS.	5	0	5	0	NA	NWIS: https://doi.org/10.5066/F7P55KJN
nwisfm_tr_tdiff	0.1 to 0.6	Hydraulic Head Temporal Difference	Groundwater elevations at miscellaneous locations measured by USGS.	3	0	3	0	NA	Derived from data elsewhere in this table
usgs_stages	299.1	Lake Level	Lake elevations measured by USGS	1	1	0	63.6714	0.0157056	NWIS: https://doi.org/10.5066/F7P55KJN
usgs_stages_tr	298.9 to 299.3	Lake Level	Transient lake Elevations measured by USGS	8	8	0	50.4638	0.0198162	NWIS: https://doi.org/10.5066/F7P55KJN
nwisdvflx_tr	19,963 to 34,446	Streamflow	Streamflow at locations with daily data measured by USGS.	16	16	0	0.00124681 to 0.00215134	464.827 to 802.049	NWIS: https://doi.org/10.5066/F7P55KJN
wdnrflx_tr	0 to 14, 8776	Streamflow	WDNR streamflow measurements made during base-flow conditions. No adjustments made.	171	127	44	0 to 0.00404498	247.22 to 652.83	WDNR data pulled from web services.
wdnr_lakes	298.98	Lake Level	Lake elevations measured by WNDR	1	1	0	93.9908	0.0106393	WDNR data pulled from web services.
wdnr_lb	298.98 to 299.12	Lakebed Hydraulic Head	Lakebed piezometer groundwater elevation measured by WDNR	10	10	0	6.03941	0.165579	WDNR data pulled from web services.
wdnr_lb_sdiff	-0.1 to 0.05	Lakebed Hydraulic Head Spatial Difference	Lakebed piezometer groundwater elevation measured by WDNR	10	10	0	8.19499	0.122026	WDNR data pulled from web services.
wdnrllks_ann_tr	298.4 to 299.2	Lake Level	Lake Elevations measured by WNDR - long term	6	6	0	61.0192	0.0163883	WDNR data pulled from web services.
wdnrllks_mon_tr	298.9 to 299.2	Lake Level	Lake Elevations measured by WNDR - recent (2017-2018)	9	9	0	54.7467	0.0182659	WDNR data pulled from web services.
wdnrwells_tr	297.3 to 299.9	Hydraulic Head	Wells installed for this study and measured by WGNHS and WDNR.	68	68	0	1.25122 to 2.44875	0.408371 to 0.79922	WGNHS/WDNR data pulled from webservices.
wdnrwells_tr_sdiff	-0.6 to 1.8	Hydraulic Head Spatial Difference	Wells installed for this study and measured by WGNHS and WDNR.	56	56	0	2.30799 to 4.51695	0.221389 to 0.433278	Derived from data elsewhere in this table
wdnrwells_tr_tdiff	-0.06 to 0.3	Hydraulic Head Temporal Difference	Wells installed for this study and measured by WGNHS and WDNR.	56	56	0	12	0.0833333	Derived from data elsewhere in this table

Table 3 Observation data groups, values, and descriptions for Plainfield Tunnel Channel Lakes inset model

Group Name	Observed Values	Target Type	Description	Total number of Observations	Number of weighted observations	Number of zero-weighted observations	Weight	Weight-informed standard deviation	Data Source
hds_wgnhs_tr, heads_wgnhs	299.6 to 335.1	Hydraulic Head	Well construction report groundwater elevation measured after a well was drilled. Locations were determined by the WGNHS.	106	0	106	0	NA	WGNHS data pulled from webservices.
nwis_dvs	330.8 to 334.9	Hydraulic Head	Groundwater elevations at locations with daily data collected by USGS.	4	4	0	16.38 to 26.1616	0.0382239 to 0.0610501	NWIS: https://doi.org/10.5066/F7P55KJN
nwis_fm	310.8 to 327.1	Hydraulic Head	Groundwater elevations at miscellaneous locations measured by USGS.	2	0	2	0	NA	NWIS: https://doi.org/10.5066/F7P55KJN
nwisdvs_tr	329.9 to 335.4	Hydraulic Head	Groundwater elevations at locations with daily data collected by USGS.	82	82	0	2.3192 to 3.76202	0.265815 to 0.431184	NWIS: https://doi.org/10.5066/F7P55KJN
nwisdvs_tr_tdiff	-0.3 to 2.0	Hydraulic Head Temporal Difference	Groundwater elevations at locations with daily data collected by USGS.	78	78	0	0.791851 to 9.50221	0.105239 to 1.26286	Derived from data elsewhere in this table
nwisfm_tr	310.4 to 327.5	Hydraulic Head	Groundwater elevations at miscellaneous locations measured by USGS.	64	0	64	0	NA	NWIS: https://doi.org/10.5066/F7P55KJN
nwisfm_tr_tdiff	-0.6 to 0.8	Hydraulic Head Temporal Difference	Groundwater elevations at miscellaneous locations measured by USGS.	62	0	62	0	NA	Derived from data elsewhere in this table
usgs_stages	330.7 to 335.2	Lake Level	Lake elevations measured by USGS	3	3	0	17.7049	0.0564814	NWIS: https://doi.org/10.5066/F7P55KJN
wdnrflx_tr	0 to 14,434	Streamflow	WDNR streamflow measurements made during base-flow conditions. No adjustments made.	88	73	15	0 to 0.00808321	123.713 to 1149.53	WDNR data pulled from web services.
wdnrfls_ann_tr	333.65 to 334.97	Lake Level	Lake elevations measured by WDNR - long term	10	10	0	25.1506	0.0397605	WDNR data pulled from web services.
wdnrfls_mon_tr	334.74 to 335.47	Lake Level	Lake elevations measured by WDNR - recent (2017-2018)	16	16	0	16.6225	0.0601592	WDNR data pulled from web services.
wdnrwells_tr	334.8 to 335.6	Hydraulic Head	Wells installed for this study and measured by WGNHS and WDNR.	121	121	0	0.99777 to 1.95273	0.512104 to 1.00223	WGNHS/WDNR data pulled from webservices.
wdnrwells_tr_sdiff	-0.2 to 0.4	Hydraulic Head Spatial Difference	Wells installed for this study and measured by WGNHS and WDNR.	105	105	0	3.98557 to 7.80012	0.128203 to 0.250905	Derived from data elsewhere in this table
wdnrwells_tr_tdiff	-0.07 to 0.2	Hydraulic Head Temporal Difference	Wells installed for this study and measured by WGNHS and WDNR.	97	97	0	10.3183	0.0969153	Derived from data elsewhere in this table

Figure 21 Locations of observations that were assigned observation weight greater than zero for the Pleasant Lake inset model.

Figure 22 Locations of observations that were assigned observation weight greater than zero for the Plainfield Tunnel Channel Lakes inset model.

Parameterization

The parameterization strategy for the inset models was to use multipliers for most parameters in order to preserve, to the extent possible, the prior conceptualization of the regional model. In this approach, the initial parameter values used in the inset models resulted from the previous history matching in the regional model. The multipliers all were set to an initial value of 1.0 and were given narrow upper and lower bounds for adjustment. In this way, particularly with pilot points that apply to a relatively small spatial footprint in the property fields, only minor parameter adjustments are allowed. This approach avoids overfitting with iES. For specific storage and specific yield, however, a multi-scale approach to multipliers was employed following the techniques of McKenna and others (2019) and White and others (2020). In this approach, multipliers to entire zones (or, in this case, layers) can be combined with multipliers at a finer scale (in this case, pilot points). Streambed conductance and lakebed conductivity were both

parameterized using values in the properties' actual units rather than multipliers. Table 4 and Table 5 summarize the parameterization for the Pleasant Lake and Plainfield Tunnel Channel Lakes inset models, respectively. Pilot point locations for horizontal and vertical hydraulic conductivity, specific storage, and specific yield are shown in Figure 72 for the Plainfield Tunnel Channel Lakes inset model and in Figure 76 for the Pleasant Lake inset model.

Table 4 Parameter groups, values, and descriptions for Pleasant Lake inset model

Group name in the PEST files	Group Description	Transform	Count	Initial Value	Lower Bound	Upper Bound
_k33_pp_inset:0	Inset Vertical K pilot point multipliers: layer 1	log	99	1.00	0.01	10.00
_k33_pp_inset:1	Inset Vertical K pilot point multipliers: layer 2	log	99	1.00	0.01	10.00
_k33_pp_inset:2	Inset Vertical K pilot point multipliers: layer 3	log	99	1.00	0.01	10.00
_k33_pp_inset:3	Inset Vertical K pilot point multipliers: layer 4	log	99	1.00	0.01	10.00
_k33_pp_inset:4	Inset Vertical K pilot point multipliers: layer 5	log	99	1.00	0.01	10.00
_k33_pp_parent:0	Parent Vertical K pilot point multipliers: layer 1	log	81	1.00	0.01	10.00
_k33_pp_parent:1	Parent Vertical K pilot point multipliers: layer 2	log	81	1.00	0.01	10.00
_k33_pp_parent:2	Parent Vertical K pilot point multipliers: layer 3	log	81	1.00	0.01	10.00
_k33_pp_parent:3	Parent Vertical K pilot point multipliers: layer 4	log	81	1.00	0.01	10.00
_k33_pp_parent:4	Parent Vertical K pilot point multipliers: layer 5	log	81	1.00	0.01	10.00
_k_pp_inset:0	Inset Horizontal K pilot point multipliers: layer 1	log	99	1.00	0.01	10.00
_k_pp_inset:1	Inset Horizontal K pilot point multipliers: layer 2	log	99	1.00	0.01	10.00
_k_pp_inset:2	Inset Horizontal K pilot point multipliers: layer 3	log	99	1.00	0.01	10.00
_k_pp_inset:3	Inset Horizontal K pilot point multipliers: layer 4	log	99	1.00	0.01	10.00
_k_pp_inset:4	Inset Horizontal K pilot point multipliers: layer 5	log	99	1.00	0.01	10.00
_k_pp_parent:0	Parent Horizontal K pilot point multipliers: layer 1	log	81	1.00	0.01	10.00
_k_pp_parent:1	Parent Horizontal K pilot point multipliers: layer 2	log	81	1.00	0.01	10.00
_k_pp_parent:2	Parent Horizontal K pilot point multipliers: layer 3	log	81	1.00	0.01	10.00
_k_pp_parent:3	Parent Horizontal K pilot point multipliers: layer 4	log	81	1.00	0.01	10.00
_k_pp_parent:4	Parent Horizontal K pilot point multipliers: layer 5	log	81	1.00	0.01	10.00
_ss_con_inset__multiplier	Inset Specific Storage multipliers by layer	log	5	1.00	0.70	100.00
_ss_con_parent__multiplier	Parent Specific Storage multipliers by layer	log	5	1.00	0.70	100.00
_ss_pp_inset:0	Inset Specific Storage pilot point multipliers: layer 1	log	99	1.00	0.70	100.00
_ss_pp_inset:1	Inset Specific Storage pilot point multipliers: layer 2	log	99	1.00	0.70	100.00
_ss_pp_inset:2	Inset Specific Storage pilot point multipliers: layer 3	log	99	1.00	0.70	100.00
_ss_pp_inset:3	Inset Specific Storage pilot point multipliers: layer 4	log	99	1.00	0.70	100.00
_ss_pp_inset:4	Inset Specific Storage pilot point multipliers: layer 5	log	99	1.00	0.70	100.00
_ss_pp_parent:0	Parent Specific Storage pilot point multipliers: layer 1	log	81	1.00	0.70	100.00
_ss_pp_parent:1	Parent Specific Storage pilot point multipliers: layer 2	log	81	1.00	0.70	100.00
_ss_pp_parent:2	Parent Specific Storage pilot point multipliers: layer 3	log	81	1.00	0.70	100.00
_ss_pp_parent:3	Parent Specific Storage pilot point multipliers: layer 4	log	81	1.00	0.70	100.00
_ss_pp_parent:4	Parent Specific Storage pilot point multipliers: layer 5	log	81	1.00	0.70	100.00
_sy_con_inset__multiplier	Inset Specific Yield multipliers by layer	log	5	1.00	0.75	2.00
_sy_con_parent__multiplier	Parent Specific Yield multipliers by layer	log	5	1.00	0.75	2.00
_sy_pp_inset:0	Inset Specific Yield pilot point multipliers: layer 1	log	99	1.00	0.75	2.00
_sy_pp_inset:1	Inset Specific Yield pilot point multipliers: layer 2	log	99	1.00	0.75	2.00
_sy_pp_inset:2	Inset Specific Yield pilot point multipliers: layer 3	log	99	1.00	0.75	2.00
_sy_pp_inset:3	Inset Specific Yield pilot point multipliers: layer 4	log	99	1.00	0.75	2.00
_sy_pp_inset:4	Inset Specific Yield pilot point multipliers: layer 5	log	99	1.00	0.75	2.00
_sy_pp_parent:0	Parent Specific Yield pilot point multipliers: layer 1	log	81	1.00	0.75	2.00
_sy_pp_parent:1	Parent Specific Yield pilot point multipliers: layer 2	log	81	1.00	0.75	2.00
_sy_pp_parent:2	Parent Specific Yield pilot point multipliers: layer 3	log	81	1.00	0.75	2.00
_sy_pp_parent:3	Parent Specific Yield pilot point multipliers: layer 4	log	81	1.00	0.75	2.00
_sy_pp_parent:4	Parent Specific Yield pilot point multipliers: layer 5	log	81	1.00	0.75	2.00
lak_mults	Lake Evaporation/Precipitation multipliers by stress period	log	170	1.00	0.90	1.10
lakebedk	Lakebed Conductivity values by littoral or profundal zone	log	2	0.02 to 0.04	1.00e-04 to 1.00e-02	0.10 to 5.00
rch_child__multiplier	Inset Recharge multipliers by stress period	log	85	1.00	0.80	1.20
rch_parent__multiplier	Parent Recharge multipliers by stress period	log	85	1.00	0.80	1.20
sfrk	SFR Conductance values by reach	log	48	1.00	0.50	2.00
wel__parent_cnst	Well pumping multipliers by stress period	log	85	1.00	0.80	1.20

Table 5 Parameter groups, values, and descriptions for Plainfield Tunnel Channel Lakes inset model

Group name in the PEST files	Group Description	Transform	Count	Initial Value	Lower Bound	Upper Bound
_k33_pp_inset:0	Inset Vertical K pilot point multipliers: layer 1	log	264	1.00	0.01	10.00
_k33_pp_inset:1	Inset Vertical K pilot point multipliers: layer 2	log	264	1.00	0.01	10.00
_k33_pp_inset:2	Inset Vertical K pilot point multipliers: layer 3	log	264	1.00	0.01	10.00
_k33_pp_inset:3	Inset Vertical K pilot point multipliers: layer 4	log	264	1.00	0.01	10.00
_k33_pp_inset:4	Inset Vertical K pilot point multipliers: layer 5	log	264	1.00	0.01	10.00
_k33_pp_parent:0	Parent Vertical K pilot point multipliers: layer 1	log	80	1.00	0.01	10.00
_k33_pp_parent:1	Parent Vertical K pilot point multipliers: layer 2	log	80	1.00	0.01	10.00
_k33_pp_parent:2	Parent Vertical K pilot point multipliers: layer 3	log	80	1.00	0.01	10.00
_k33_pp_parent:3	Parent Vertical K pilot point multipliers: layer 4	log	80	1.00	0.01	10.00
_k33_pp_parent:4	Parent Vertical K pilot point multipliers: layer 5	log	80	1.00	0.01	10.00
_k_pp_inset:0	Inset Horizontal K pilot point multipliers: layer 1	log	264	1.00	0.01	10.00
_k_pp_inset:1	Inset Horizontal K pilot point multipliers: layer 2	log	264	1.00	0.01	10.00
_k_pp_inset:2	Inset Horizontal K pilot point multipliers: layer 3	log	264	1.00	0.01	10.00
_k_pp_inset:3	Inset Horizontal K pilot point multipliers: layer 4	log	264	1.00	0.01	10.00
_k_pp_inset:4	Inset Horizontal K pilot point multipliers: layer 5	log	264	1.00	0.01	10.00
_k_pp_parent:0	Parent Horizontal K pilot point multipliers: layer 1	log	80	1.00	0.01	10.00
_k_pp_parent:1	Parent Horizontal K pilot point multipliers: layer 2	log	80	1.00	0.01	10.00
_k_pp_parent:2	Parent Horizontal K pilot point multipliers: layer 3	log	80	1.00	0.01	10.00
_k_pp_parent:3	Parent Horizontal K pilot point multipliers: layer 4	log	80	1.00	0.01	10.00
_k_pp_parent:4	Parent Horizontal K pilot point multipliers: layer 5	log	80	1.00	0.01	10.00
_ss_con_inset__multiplier	Inset Specific Storage multipliers by layer	log	5	1.00	0.70	100.00
_ss_con_parent__multiplier	Parent Specific Storage multipliers by layer	log	5	1.00	0.70	100.00
_ss_pp_inset:0	Inset Specific Storage pilot point multipliers: layer 1	log	264	1.00	0.70	100.00
_ss_pp_inset:1	Inset Specific Storage pilot point multipliers: layer 2	log	264	1.00	0.70	100.00
_ss_pp_inset:2	Inset Specific Storage pilot point multipliers: layer 3	log	264	1.00	0.70	100.00
_ss_pp_inset:3	Inset Specific Storage pilot point multipliers: layer 4	log	264	1.00	0.70	100.00
_ss_pp_inset:4	Inset Specific Storage pilot point multipliers: layer 5	log	264	1.00	0.70	100.00
_ss_pp_parent:0	Parent Specific Storage pilot point multipliers: layer 1	log	80	1.00	0.70	100.00
_ss_pp_parent:1	Parent Specific Storage pilot point multipliers: layer 2	log	80	1.00	0.70	100.00
_ss_pp_parent:2	Parent Specific Storage pilot point multipliers: layer 3	log	80	1.00	0.70	100.00
_ss_pp_parent:3	Parent Specific Storage pilot point multipliers: layer 4	log	80	1.00	0.70	100.00
_ss_pp_parent:4	Parent Specific Storage pilot point multipliers: layer 5	log	80	1.00	0.70	100.00
_sy_con_inset__multiplier	Inset Specific Yield multipliers by layer	log	5	1.00	0.75	2.00
_sy_con_parent__multiplier	Parent Specific Yield multipliers by layer	log	5	1.00	0.75	2.00
_sy_pp_inset:0	Inset Specific Yield pilot point multipliers: layer 1	log	264	1.00	0.75	2.00
_sy_pp_inset:1	Inset Specific Yield pilot point multipliers: layer 2	log	264	1.00	0.75	2.00
_sy_pp_inset:2	Inset Specific Yield pilot point multipliers: layer 3	log	264	1.00	0.75	2.00
_sy_pp_inset:3	Inset Specific Yield pilot point multipliers: layer 4	log	264	1.00	0.75	2.00
_sy_pp_inset:4	Inset Specific Yield pilot point multipliers: layer 5	log	264	1.00	0.75	2.00
_sy_pp_parent:0	Parent Specific Yield pilot point multipliers: layer 1	log	80	1.00	0.75	2.00
_sy_pp_parent:1	Parent Specific Yield pilot point multipliers: layer 2	log	80	1.00	0.75	2.00
_sy_pp_parent:2	Parent Specific Yield pilot point multipliers: layer 3	log	80	1.00	0.75	2.00
_sy_pp_parent:3	Parent Specific Yield pilot point multipliers: layer 4	log	80	1.00	0.75	2.00
_sy_pp_parent:4	Parent Specific Yield pilot point multipliers: layer 5	log	80	1.00	0.75	2.00
lak_mults	Lake Evaporation/Precipitation multipliers by stress period	log	680	1.00	0.90	1.10
lakebedk	Lakebed Conductivity values by littoral or profundal zone	log	8	0.02 to 0.04	1.00e-04 to 1.00e-02	0.10 to 5.00
rch_child__multiplier	Inset Recharge multipliers by stress period	log	85	1.00	0.80	1.20
rch_parent__multiplier	Parent Recharge multipliers by stress period	log	85	1.00	0.80	1.20
sfrk	SFR Conductance values by reach	log	15	1.00	0.50	2.00
wel__parent_cnst	Well pumping multipliers by stress period	log	85	1.00	0.80	1.20
wel_inset_cnst	Well pumping multipliers by stress period	log	85	1.00	0.80	1.20

Figure 23 Summary of ensemble (black lines) and base (blue line) objective function progress by iES iteration for Pleasant Lake inset model.

Figure 24 Summary of ensemble (black lines) and base (blue line) objective function progress by iES iteration for Plainfield Tunnel Channel Lakes inset model.

Figure 25 Rejection sampling for the Pleasant Lake inset model. A subjective decision is made to only retain ensemble members at or below a selected cutoff value. For Pleasant Lake, this cutoff was 5,800.

Figure 26 Rejection sampling for the Plainfield Tunnel Channel Lakes inset model. A subjective decision is made to only retain ensemble members at or below a selected cutoff value. For Plainfield Tunnel Channel Lakes, this cutoff was 2,400.

History Matching Results

The ensemble approach in iES results in an ensemble of objective function values from iteration to iteration for the Pleasant Lake and Plainfield Tunnel Channel Lakes inset models, respectively (Figure 23 and Figure 24). In Figure 23 and Figure 24, the blue curve represents base ensemble member and the lighter gray lines indicate the trajectories of all the other ensemble members. As this technique explores a wide range of parameter combinations, some of those combinations results in MODFLOW-6 models that fail to run to completion. Others result in poor correspondence between model outputs and observations, expressed as high objective function values. As a result, two subjective steps are required to settle on a final posterior distribution of parameters and model outputs. First, an iteration is chosen from the objective function progress. This selection is made based on a heuristic balance between level of fit and variability in the ensemble. At later iterations, it is common to see overfitting and collapse of the ensemble, so typically an early iteration is chosen. In both inset models, iteration #3 was chosen as an acceptable level of fit. Second, a histogram of objective function values is evaluated at the chosen iteration and a cutoff of the objective function is chosen to remove outlier ensemble members that result in an unacceptably high objective function value—this process is referred to as “rejection sampling.” Figure 25 and Figure 26 show the histograms, cutoff objective function values, and effects on ensemble size for the Pleasant and Plainfield Tunnel Channel Lakes inset models, respectively.

Comparison of measured and simulated observations – by observation group

The match between model-calculated and measured observation values can be evaluated for each observation group both as a 1:1 line plot and as residuals. Residuals are calculated by subtracting the model-simulated value from the measured value for each observation. As described previously for the regional model, values plotting closer to the 1:1 line indicate a better match between model-simulated and measured values. The residuals plots provide a means to assess prediction bias in the history matching results over the entire range of observation values. The uncertainty of both the observation measurements and the ensembles of model outputs for those observations is depicted as $\pm 2 \times \sigma$ where σ is calculated as the inverse of the observation

weights and is calculated empirically from the ensembles for model outputs. This is a general metric of uncertainty both in how much information is expected to be provided by each observation and how variable the resulting parameter estimate ensembles are. Figure 27 through Figure 34 show fit and residuals plots for the Pleasant Lake inset model and Figure 35 through Figure 39 show fit and residual plots for the Plainfield Tunnel Channel Lakes inset model. The observation group names are defined in Table 2 and Table 3.

Figure 27 Fit between measured and simulated values at observation locations for observation groups nwis_dvs (panel A) and nwisdvflx_tr (panel B) for the Pleasant Lake inset model.

Figure 28 Fit between measured and simulated values at observation locations for observation groups nwis_dvs_tr (panel A) and nwisdvflx_tr_tdiff (panel B) for the Pleasant Lake inset model.

Figure 29 Fit between measured and simulated values at observation locations for observation groups usgs_stages (panel A) and usgs_stages_tr (panel B) for the Pleasant Lake inset model.

Figure 30 Fit between measured and simulated values at observation locations for observation groups wdnr_lakes (panel A) and wdnr_lb (panel B) for the Pleasant Lake inset model.

Figure 31 Fit between measured and simulated values at observation locations for observation groups wdnr_lb_sdiff (panel A) and wdnrflx_tr (panel B) for the Pleasant Lake inset model.

Figure 32 Fit between measured and simulated values at observation locations for observation groups wdnrlks_ann_tr (panel A) and wdnrlks_mon_tr (panel B) for the Pleasant Lake inset model.

Figure 33 Fit between measured and simulated values at observation locations for observation groups wdnrwwells_tr (panel A) and wdnrwwells_tr_sdiff (panel B) for the Pleasant Lake inset model.

Figure 34 Fit between measured and simulated values at observation locations for observation group wdnrwwells_tr_sdiff (panel A) for the Pleasant Lake inset model.

Figure 35 Fit between measured and simulated values at observation locations for observation groups nwis_dvs (panel A) and nwisdvs_tr (panel B) for the Plainfield Tunnel Channel Lakes inset model.

Figure 36 Fit between measured and simulated values at observation locations for observation groups nwisdvs_tr_tdiff (panel A) and usgs_stages (panel B) for the Plainfield Tunnel Channel Lakes inset model.

Figure 37 Fit between measured and simulated values at observation locations for observation groups wdnrflx_tr (panel A) and wdnrlks_ann_tr (panel B) for the Plainfield Tunnel Channel Lakes inset model.

Figure 38 Fit between measured and simulated values at observation locations for observation groups wdnrlks_mon_tr (panel A) and wdnrwwells_tr (panel B) for the Plainfield Tunnel Channel Lakes inset model.

Figure 39 Fit between measured and simulated values at observation locations for observation groups wdnr_wells_tr_sdiff (panel A) and wdnr_wells_tr_tdiff (panel B) for the Plainfield Tunnel Channel Lakes inset model.

Fit between measured and modeled observations – spatial distributions

Figure 40 and Figure 41 show the spatial patterns of weighted residuals for observations used for history matching in the Pleasant Lake and Plainfield Tunnel Channel Lakes inset models, respectively. These results were derived only from the base-case parameter set obtained from the iES ensembles, and therefore, do not reflect the range of simulation results available in the ensembles. Most of the observations are transient so the mean of the base realization over the entire simulation time is presented. These figures, therefore, provide only a partial understanding of the history matching process, but are useful for examining spatial patterns. Residuals showed spatial bias with water levels near the lake simulated higher than measured values, but the magnitude of misfit was small and simulated values greater than measured were near simulated values less than measured values. The streamflow measurements showed little spatial bias with a mix of simulated values greater and less than measurements. Subsequent sections explore individual locations as time series in more detail.

Figure 40 Spatial pattern of mean fit between measured and simulated observations for Pleasant Lake inset model

Figure 41 Spatial pattern of mean fit between measured and simulated observations for Plainfield Tunnel Channel Lakes inset model

Fit Between Measured and Simulated Observations – Time Series by Observation Location

Individual observation locations with transient data provide multiple targets for history matching, yet may result in multiple fit values for each location, spanning over simulation time. The uncertainty of the observed values, as informed to the iES process as the inverse of their observation weight, can be expressed as a 95% credible interval using bars that extend 2σ above and below the observed value at a given time. Unlike the 1:1 plots above, in Figure 42 through Figure 71, an accompanying bar for the simulated values is not presented. Instead, the time series for each ensemble member is displayed separately as a thin gray line. This shows not only the uncertainty of both observations and simulated values but also the continuity of values over time in each ensemble member.

Observation points labeled as “PDC” indicate observations that were under prior data conflict, meaning that in these cases, the initial ensemble evaluated by iES identifies observations where

simulated values are statistically distant from the measured values. Because iES evaluates a wide range of parameters in this initial run, it is unlikely that the history matching process will result in a reasonable set of parameters that will make the model fit at these observations close enough to be considered valid. In other words, the model is being used to flag observations that cannot be fit by the model and parameters. This is the result either of errors in the measurements or structural or parameters deficiencies in the model. In PEST++, these observations may be systematically assigned zero observation weight to prevent them from affecting the history matching process. Alternatively, prior data conflict can serve as a diagnostic tool to point out areas worthy of scrutiny either in the quality of the measurements or the representation of processes in the model. In this study, the latter approach was followed and PDC labels were assigned to observations in prior data conflict to indicate they were unlikely to result in low residuals, but they were retained with their initially assigned observation weight. In the remainder of this section results for time series in each of the two inset models is presented.

Pleasant Lake Inset Model

The general patterns of observed lake levels are reproduced in the Pleasant Lake inset model and at most times the simulated results from the model realizations overlap with the observed values (Figure 42). The bars indicating uncertainty of the observed values are not visible in these plots because the observation weight was assigned high enough to these important observations that the implied uncertainty is very small. The model results at the beginning of the simulation period may be affected by a need for a “spin-up” or “warm start” for the simulation of the lake level to reach a dynamic equilibrium with respect to changes in groundwater storage. To account for this potential misfit in simulated versus observed lake levels, recent observations were assigned higher observation weight than values for timesteps early in the model run that include data from early in the simulation period. The other period of large misfit occurs in the spring of 2018. This may indicate that the water level was anomalously high because of above-average surface runoff associated with the spring melt that year. Surface runoff is not simulated in this model so under-simulation of the lake level in the model under that condition is expected.

Figure 42 Time series of measured and simulated results for lake level observations in the Pleasant Lake inset model. Panel A is observation group wdnrlks_mon_tr, Panel B is observation group wdnrlks_ann_tr, and Panel C is observation group usgs_stages_tr

The patterns and magnitudes of simulated streamflow were generally similar to the measured values throughout the Pleasant Lake inset model (Figure 43 to Figure 46). Several observations are labeled as “PDC” indicating prior data conflict, as discussed above. These are typically locations where either the measured streamflow was already low and dropped to near zero or represented high flow due to runoff. While the streamflows generally are dominated by base flow, some storm events do occur and the SFR package in MODFLOW 6 does not include explicit consideration of that process.

Figure 43 Time series of measured and simulated results for streamflow observations in Chaffee Creek sites 10039561 (panel A) and 04073240 (panel B) in the Pleasant Lake inset model.

Figure 44 Time series of measured and simulated results for streamflow observations in Tagatz Creek sites 10029382 (panel A), 10039577 (panel B), and 10028958 (panel C) in the Pleasant Lake inset model.

Figure 45 Time series of measured and simulated results over time for streamflow observations in South Branch Wedde Creek site 10039101 (panel A) and Mecan Creek site 10034799 (panel B).

The time series results for the piezometers near Pleasant Lake in the wdnrwells_tr group—wells represent hydraulic head conditions around the lake perimeter—are shown in Figure 46 and Figure 47. These model results are nearly all within the 95% credible range for the observations.

Figure 46 Time series of measured and simulated results for transient piezometers near Pleasant Lake in the group wdnrwells_tr, (part 1).

Figure 47 Time series of measured and simulated results for transient piezometers near Pleasant Lake in the group wdnrwells_tr, (part 2).

The temporal differences for the piezometers near Pleasant Lake in the wdnrwells_tr_tdiff group are shown in Figure 48 and Figure 49. The differences are calculated as the difference in adjacent times and help inform storage conditions near the lakes. The patterns of differences are generally correct providing confidence in the temporal system response to stresses.

Figure 48 Time series of measured and simulated results for temporal differences in transient piezometers near Pleasant Lake in the group wdnrwells_tr_tdiff, (part 1).

Figure 49 Time series of measured and simulated results for temporal differences in transient piezometers near Pleasant Lake in the group wdnrwells_tr_tdiff, (part 2).

The spatial differences between the piezometers near Pleasant Lake and the simulated lake level in the wdnrwells_tr_sdiff group are shown in Figure 50 and Figure 51. The differences help inform the gradient between the lake and the surrounding aquifer. The general patterns of the

differences are correct over time although they express an underestimation of system dynamics that may, in part, be due to the averaging of monthly stresses or the influence of processes such as surface runoff not properly accounted for in the simulation.

Figure 50 Time series of measured and simulated results for spatial differences in transient piezometers near Pleasant Lake in the group wdnr wells_tr_sdiff (part 1).

Figure 51 Time series of measured and simulated results for spatial differences in transient piezometers near Pleasant Lake in the group wdnr wells_tr_sdiff (part 2).

The groundwater hydraulic head values in the wells of the nwisdvs_tr group for which daily values are available in the NWIS database are shown in Figure 52 and Figure 53. The wells reflect the overall pattern of groundwater levels in recent time. Where the greatest discrepancies are observed (particularly in Figure 53) the simulated values typically are too high rather than too low. This bias may be, at least in part, an unintended consequence caused by the assignment of high observation weight on streamflow and lake level observations that result in a parameter set yielding higher water levels in the aquifer to better match those observations. For streamflow, in particular, this could be compensating for water that enters the streams through processes not explicitly simulated in these models.

Figure 52 Time series of measured and simulated results for heads in wells with daily values in NWIS in the Pleasant Lake inset model in the group nwisdvs_tr (part 1).

Figure 53 Time series of measured and simulated results for heads in wells with daily values in NWIS in the Pleasant Lake inset model in the group nwisdvs_tr (part 2).

Temporal differences of hydraulic heads in wells of the nwisdvs_tr_tdiff group are shown in Figure 54 and Figure 55. Similar to the approach with the piezometers near the lake, temporal differences can help inform storage parameters in the model. The model results follow similar patterns to the measured values although in some cases the simulated differences are greater than the measured differences. This discrepancy is most pronounced in the wells (particularly in Figure 55) where the fit between measured and simulated hydraulic heads is poorest.

Figure 54 Time series of measured and simulated results for temporal difference of hydraulic heads in wells with daily values in NWIS in the Pleasant Lake inset model in the group nwisdvs_tr_tdiff (part 1).

Figure 55 Time series of measured and simulated results for temporal difference of hydraulic heads in wells with daily values in NWIS in the Pleasant Lake inset model in the group nwisdvs_tr_tdiff (part 2).

Plainfield Tunnel Channel Lakes Inset Model

The lake level time series for the Plainfield Tunnel Channel Lakes inset model are shown in Figure 56. Panels A and B show the recent and longer term patterns for Plainfield Lake, respectively and Panels C and D show the recent and longer term patterns for Long Lake, respectively. The general patterns of lake levels are reproduced and at most times the simulated realizations overlap with the observed values. Unlike Pleasant Lake, where some misfit likely resulted from spring runoff, in Plainfield and Long Lakes, the overall dynamics are captured as visible in the most recent monthly data in Panels A and C.

Figure 56 Time series of measured and simulated results for lake level observations in the Pleasant Lake inset model. Panel A is Plainfield Lake, observation group wdnrlks_mon_tr, Panel B is Plainfield Lake, observation group wdnrlks_ann_tr, Panel C is Long Lake, observation group wdnrlks_mon_tr, and Panel D is Long Lake, observation group wdnrlks_ann_tr.

The time series of streamflow in the two streams with history matching data in the Plainfield Tunnel Channel Lakes inset model are shown in Figure 57. The patterns and magnitudes of simulated streamflow were generally similar to the measured values. Nearly all ensemble simulated values fall within the 95% credible intervals for the streams. Streamflow in North Branch Tenmile Creek is simulated as higher than measured at the extremely low observed streamflow values between 2012 and 2015. Such low values are difficult to represent accurately with the model and difficult to quantify when measured in the field, as indicated by the relatively large credible interval around the observations. Similar to some of the observations in the Pleasant Lake model, at least one storm event in late 2017 simulated too low in both streams, likely due to runoff not being explicitly represented in the model. The simulated results in Upper Pine River are closer to measured values with the exception of the late 2017 storm.

Figure 57 Time series of measured and simulated results for streamflow observations in North Branch Tenmile Creek site 10042017 (panel A) and Upper Pine River site 703070 (panel B) in the Plainfield Tunnel Channel Lakes inset model.

The time series results for the piezometers near Long Lake in the wdnrwells_tr group are shown in Figure 58 and Figure 59 and the time series results for the piezometers near Plainfield Lake in the wdnrwells_tr group are shown in Figure 60 and Figure 61. These wells represent hydraulic head conditions around the lake perimeter and the simulated results are nearly all within the 95% credible range for the observations.

Figure 58 Time series of measured and simulated results for transient piezometers near Long Lake in the group wdnrwells_tr (part 1).

Figure 59 Time series of measured and simulated results for transient piezometers near Long Lake in the group wdnrwells_tr (part 2).

Figure 60 Time series of measured and simulated results for transient piezometers near Plainfield Lake in the group wdnrwells_tr (part 1).

Figure 61 Time series of measured and simulated results for transient piezometers near Plainfield Lake in the group wdnrwells_tr (part 2).

The time series results for temporal differences in the piezometers near Long Lake in the wdnrwells_tr_tdiff group are shown in Figure 62 and Figure 63 and the time series results for temporal differences in the piezometers near Plainfield Lake in the wdnrwells_tr_tdiff group are shown in Figure 64 and Figure 65. The differences are calculated as the difference in adjacent times and help inform storage conditions near the lakes. The patterns of simulated differences are generally consistent with the measured patterns, although the simulated differences are greater than those for the measured values for the simulation period. However, the overall agreement between the two provides confidence in the temporal system response to stresses.

Figure 62 Time series of measured and simulated results for temporal differences in transient piezometers near Long Lake in the group wdnrwells_tr_tdiff, (part 1).

Figure 63 Time series of measured and simulated results for temporal differences in transient piezometers near Long Lake in the group wdnrwells_tr_tdiff, (part 2).

Figure 64 Time series of measured and simulated results for temporal differences in transient piezometers near Plainfield Lake in the group wdnrwells_tr_tdiff, (part 1).

Figure 65 Time series of measured and simulated results for temporal differences in transient piezometers near Plainfield Lake in the group wdnrwells_tr_tdiff, (part 2).

The time series results for spatial differences in the piezometers near Long Lake in the wdnrwells_tr_sdiff group are shown in Figure 66 and Figure 67 and the time series results for spatial differences in the piezometers near Plainfield Lake in the wdnrwells_tr_sdiff group are shown in Figure 68 and Figure 69. As in the Pleasant Lake inset model, the spatial differences

are calculated as the difference between the hydraulic head in each piezometer relative to the simulated lake elevation. The differences help inform the gradient between the aquifer near the lake and the lake itself. In general, the simulated differences are a bit lower than the measured equivalents, although values typically fall within the 95% credible interval of the observation values. The poor fit of these observations highlights the challenge of matching all data in parameter estimation, as some data can be in conflict with other data. This group was included for completeness but because they are indirect observations relative to the main quantities of interest—lake levels and streamflows—they were assigned lower observation weight. As a result, conflicts between these data and more highly weighted observations favor the higher weighted observations.

Figure 66 Time series of measured and simulated results for spatial differences in transient piezometers near Long Lake in the group wdnrwells_tr_sdiff, (part 1).

Figure 67 Time series of measured and simulated results for spatial differences in transient piezometers near Long Lake in the group wdnrwells_tr_sdiff, (part 2).

Figure 68 Time series of measured and simulated results for spatial differences in transient piezometers near Plainfield Lake in the group wdnrwells_tr_sdiff, (part 1).

Figure 69 Time series of measured and simulated results for spatial differences in transient piezometers near Plainfield Lake in the group wdnrwells_tr_sdiff, (part 2).

Time series for groundwater hydraulic head values in the wells of the nwisdvs_tr group for which daily values are available in the USGS National Water Information System (NWIS) database are shown in Figure 70. Panel A shows site 1146089250301, which includes measurement from the beginning of the simulation. The wells in Panels B, C, and D are focused on recent time. Similar to the Pleasant Lake inset model, where the fit is poorest, simulated values are higher than measured. An exception is the winter of 2017-2018 where simulated values briefly decreased while measured values were increasing at site 1146089250301; however, the overall water-level response is similar in showing an increase in water elevations at the end of the simulation period.

Figure 70 Time series of measured and simulated results for hydraulic heads in wells with daily values in NWIS in the Plainfield Tunnel Channel Lakes inset model in the group nwisdvs_tr.

The temporal differences of hydraulic heads in wells of the `nwisdvs_tr_tdiff` group are shown in Figure 71. Similar to the approach with the piezometers near the lake, temporal differences can help inform storage parameters in the model. With the exception of the winter of 2017-2018 where the simulated differences are opposite from measured and overall the simulated hydraulic heads correspond the least with measured.

Figure 71 Time series of measured and simulated results for temporal difference of hydraulic heads in wells with daily values in NWIS in the Plainfield Tunnel Channel Lakes inset model in the group `nwisdvs_tr_tdiff`.

Focus Area Inset Model Results

Following history matching, both inset models were updated with the “base” parameter set from iES iteration #3, which represents the single best or “minimum error variance” estimate of parameter values (see the Parameter Estimation and uncertainty analysis section). The updated models were then run for the history matching time period of 2012 through 2018, and used for the scenarios described in the Lake Ecosystem Response Assessment (LERA) section. Results for the 2012 through 2018 history matching time period are shown below.

Parameter estimates

The base parameter set spatial distributions for the inset models, following history matching, are shown in Figure 72 to Figure 79. The use of multipliers against the parameter values estimated at the regional scale resulted in parameter fields similar to those in the regional model. In the Pleasant Lake model in particular, some greater changes in parameter values were estimated in the inset focused around the lake relative to the parent region. The high observation weight assigned to lake elevation observations and the presence of headwater streams that are highly sensitive to small changes in parameters make the parameters in the inset particularly important and subject to greater changes than the surrounding area.

Figure 72 – Horizontal hydraulic conductivity (K_h) estimates for the Plainfield Tunnel Channel Lakes model. White areas indicate locations where a layer is absent in the model (`idomain=0`). Pilot point locations apply to all layers.

Figure 73 – Vertical hydraulic conductivity (K_v) estimates for the Plainfield Tunnel Channel Lakes model. White areas indicate locations where a layer is absent in the model (`idomain=0`). Pilot point locations apply to all layers.

Figure 74 – Specific yield (S_y) estimates for the Plainfield Tunnel Channel Lakes model. White areas indicate locations where a layer is absent in the model ($idomain=0$). Pilot point locations apply to all layers.

Figure 75 – Specific storage (S_s) estimates for the Plainfield Tunnel Channel Lakes model. White areas indicate locations where a layer is absent in the model ($idomain=0$). Pilot point locations apply to all layers.

Figure 76 – Horizontal hydraulic conductivity (K_h) estimates for the Pleasant Lake model. White areas indicate locations where a layer is absent in the model ($idomain=0$). Pilot point locations apply to all layers.

Figure 77 – Vertical hydraulic conductivity (K_v) estimates for Pleasant Lake model. White areas indicate locations where a layer is absent in the model ($idomain=0$). Pilot point locations apply to all layers.

Figure 78 – Specific yield (S_y) estimates for the Pleasant Lake model. White areas indicate locations where a layer is absent in the model ($idomain=0$). Pilot point locations apply to all layers.

Figure 79 – Specific storage (S_s) estimates for the Pleasant Lake model. White areas indicate locations where a layer is absent in the model ($idomain=0$). Pilot point locations apply to all layers.

Transient multipliers that were applied to the Plainfield Tunnel Channel Lakes and Pleasant models, respectively, are shown in Figure 80 to Figure 83. In the Plainfield Tunnel Channel Lakes model, all four lakes simulated with the LAK package have separate multipliers applied to evaporation and rainfall. All of these multipliers are well within their bounds and depart from a value of 1.0 to a limited extent, indicating that the fine-tuning adjustments of these parameters did not exhibit substantial bias in either direction.

Figure 80 – Recharge and well pumping multiplier estimates for the Plainfield Tunnel Channel Lakes inset model.

Figure 81 – Lake package evaporation and rainfall multiplier estimates for Plainfield (A), Second (B), Sherman (C), and Long (D) Lakes in the Plainfield Tunnel Channel Lakes inset model.

Figure 82 – Recharge and well pumping multiplier estimates for the Pleasant Lakes inset model.

Figure 83 – Lake package evaporation and rainfall multiplier estimates for Pleasant Lake in the Pleasant Lake inset model.

Groundwater Flow and Boundary Condition Fluxes for Mean (2012 -2015) Conditions

Simulated steady-state water table elevations and boundary condition fluxes for both inset models, under mean conditions for the period of 2012-2015, are shown in Figure 84 and Figure 85. Discharge *from* the groundwater flow solution to streams, wells, or the specified head perimeter boundaries, is represented with a red color scale. Blue colors represent discharge *to* the groundwater flow solution from stream leakage or inflow through the specified head boundaries.

Note that for streams, this color scheme is opposite of that shown in Figure 12 for the regional model, where blue colors indicate groundwater discharge to streams (inflows from the perspective of the streams). Lake groundwater interactions are displayed separately from the perspective of the lakes, with blue indicating groundwater discharge to the lakes and red indicating lake leakage to groundwater.

The overall flow patterns indicated by the simulated water table elevation contours are consistent with the regional model (Figure 16). In both inset models, groundwater discharge along the perimeter is mostly simulated as leaving the model, a result of the models being located along the groundwater divide that runs through the stream-less portion of the study area. A minor amount of groundwater flow enters the domains from the north, consistent with regional flow patterns. Similarly, streams within the inset models are mostly gaining, with the exception of the Upper Pine River (Figure 12) and Tagatz Creek (Figure 85), which are both located in the hummocky collapsed terrain east of the moraines. Simulated groundwater discharge to and from the study lakes reflects the simulated water table gradients, with the lakes gaining on the upgradient side and losing on the downgradient side.

Figure 84 – Plainfield Tunnel Channel Lakes model steady-state water table and boundary fluxes.

Figure 85 – Pleasant Lake model steady-state water table and boundary fluxes.

Groundwater Flow and Boundary Condition Fluxes for Transient (2012-2018) Conditions

Because the local grid refinement for the inset models is implemented using linked models (within a MODFLOW 6 simulation), global budget results are reported separately for the parent (Figure 86 and Figure 87) and LGR (Figure 88 and Figure 89) sub-models within each inset. The parent sub-model budgets show seasonal trends that are similar to the regional model—a spring recharge period when water is added to storage, followed by a summer pumping period when water is removed from storage, and a less pronounced fall recharge period. In both inset models, there is a substantial increase in recharge in 2018, in response to above-normal precipitation that year. Flow out of the constant head boundaries is relatively steady in both models, although it does increase somewhat in 2018 in the Plainfield Tunnel Channel Lakes model, in response to the increase in recharge. A key difference between the two inset models is the greater amount of stream outflow in the Pleasant Lake model (approximately 20-40% of the water budget)

compared to the Plainfield Tunnel Channel Lakes model (where stream outflow is generally less than 10% of the total flow).

Figure 86 – Plainfield Tunnel Channel Lakes inset model water budget. Inflows and outflows are named using the MODFLOW List file convention.

Figure 87 – Pleasant Lake inset model water budget. Inflows and outflows are named using the MODFLOW List file convention.

Figure 88 – Plainfield Tunnel Channel Lakes LGR sub-model water budget. Inflows and outflows are named using the MODFLOW List file convention.

Figure 89 – Pleasant Lake LGR sub-model water budget. Inflows and outflows are named using the MODFLOW List file convention.

The inset sub-model budgets are dominated by flows exchanged with the parent sub-models (“FLOW-JA-FACE” term). This is acceptable because the two sub-models are fully coupled at the inner iteration level, meaning continuity in the groundwater flow solution is preserved throughout the inset model domain. Otherwise, the inset sub-model budgets show some of the same seasonal trends as the parent sub-model, and also illustrate the relatively small magnitude of flux through the lakes relative to other sources and sinks.

Figure 90 – Lake water budgets.

The water budgets for the Plainfield and Long Lakes (Figure 90) show a seasonal pattern of mostly net groundwater outflow in the fall and winter months, punctuated by net groundwater inflow in the spring, when groundwater levels are high. In both lakes, there is a trend towards predominantly gaining conditions later in the simulation, with net groundwater inflow for most of 2018, consistent with the field observations in Appendix A. In contrast Pleasant Lake has a relatively stationary seasonal cycle of predominantly net groundwater outflow, presumably due to the stabilizing effects of nearby Chaffee and Tagatz Creeks on the water table.

Lake Ecosystem Response Assessment (LERA)

The purpose of this project was to evaluate the potential local-scale effects of agricultural water and land use practices on lakes as well as on the regional groundwater flow system. To accomplish this goal, WDNR generated two potential land-use scenarios to be assessed with the

aforementioned models (see Appendix F for details). One land-use scenario, referred to as the “current-irrigated-agriculture” scenario, is based on current (2018) land use and irrigation practices (Figure 92). This can be considered a “control” or “business as usual” case which reflect the best estimate of hydrologic responses given current conditions. A second land-use scenario, referred to as the “no-irrigated-agriculture” scenario, is one in which existing irrigated agriculture areas are replaced with a land cover consistent with slope, soil-type, and other factors of the surrounding areas (Figure 93) (Appendix F). This alternative land use is meant to represent a land use pattern if irrigated agriculture had not been introduced to the region. As a result, unlike land use in irrigated agricultural fields, where crop type varies from year to year, the land use for this alternative no-irrigated-agriculture scenario is static over time. In areas of the model domain where irrigated agricultural land use is not simulated in 2018 conditions, the two scenarios are the same. The no irrigated agriculture is meant to provide a comparison point which, compared with the current irrigation scenario, helps identify potential effects from irrigated agriculture. These two land-use scenarios were run for a 38-year simulation time with the SWB code at the regional scale to provide recharge and water use values as needed for input into the regional model. The results from the regional model simulations then provided constant-head boundary conditions for the two focus lake inset models. The recharge and water use from the SWB simulations were also assigned to the two inset models to provide lake level and base-flow model outputs at the same locations as the history matching data. This analysis enabled a comparison of long-term responses in lakes and streams to land/water use with and without irrigated agriculture.

The 38-year period (climate years 1981-2018) is the timeframe for which daily PRISM precipitation and air temperature data were available, both of which are necessary inputs to SWB and the MODFLOW-6 LAK package. Furthermore, this period included multiple cycles of the typical range of weather variability seen in the region (See Appendix B for more discussion).

The land-use code for a given SWB model cell defines the kind of vegetation occurring in that parcel. This information controls how evapotranspiration is calculated in SWB. For the no-irrigated-agriculture scenario, the vegetation assemblage was assumed to remain static in each cell over the 38-year LERA simulations.

The current-irrigated-agriculture scenario is dynamic through time as most agriculture in the region and involves rotations of multiple crops. To account for this land cover variability in SWB, each parcel was assigned a crop rotation (Appendix F) based on several categories that describe prevailing agricultural practices. Figure 91 shows the distribution of the main crop rotations which include Potato/Vegetable, Cash Grain, Dairy, and Pasture/Hay. Non-agricultural land use is also quantified here as land that is owned by farms but not used for growing. Within each rotation, the current distribution (2018) of land-use code/crops was evaluated resulting in a discrete distribution of land-use codes for all parcels in the model domain assigned a rotation. In other words, the rotation determines which assemblage of crops are rotated through that location over time, and the discrete distributions within rotation are used to assign specific crops for each year. To assign land use in each climate year, the full complement of parcels assigned a rotation was filled in with a proportion of land-use codes corresponding to the current distributions as shown in Figure 96.

Figure 92 and Figure 93 show the spatial distributions of the crop rotations and the alternative no-irrigated-agriculture scenario land use assumed in the same parcels, respectively, for the regional model domain. Figure 94 and Figure 95 show the spatial distributions of crop rotations and the alternative no-irrigated-agriculture scenario land use assumed in the same parcels for the Plainfield Tunnel Channel Lakes and Pleasant Lake inset models, respectively. These figures show that the inter-morainal areas where the study lakes are located are areas where the Potato/Vegetable rotation is more prevalent relative to the other rotations found more commonly in the outlying parts of the study area (Figure 94 and Figure 95). For the no-irrigated-agriculture scenario, the alternate land use is assumed to be dominated by forest land use (Appendix F)

For the purpose of this analysis, special consideration was given to potatoes within the Potato/Vegetable rotation parcels because potatoes (land-use code 43) account for 25% of total land in the Potato/Vegetable rotation (Figure 96). To account for typical growing practices, a 4-year recurrence of potatoes was enforced such that every parcel in the Potato/Vegetable rotation was simulated as growing potatoes once every 4 years while still maintaining that 25% of all the Potato/Vegetable rotation be simulated as growing potatoes. After this requirement was met, the

remainder of parcels were randomly assigned crops following the distribution shown in Figure 96.

Figure 91 Total acres of each major crop rotation in the regional model domain.

Figure 92 Spatial distribution of the major crop rotations in the regional model domain.

Figure 93 Spatial distribution of alternative land use assumed for the no-irrigated-agriculture scenario in the regional model domain.

Figure 94 Spatial distribution of the major crop rotations (A) and the alternative land use assumed for the no-irrigated-agriculture scenario (B) in the Plainfield Tunnel Channel Lakes inset model

Figure 95 Spatial distribution of the major crop rotations (A) and the alternative land use assumed for the no-irrigated-agriculture scenario (B) in the Pleasant Lake inset model

Figure 96 Frequency of each land-use code/crop within the four crop rotations as a percent of area.

The land-use files for the “no-irrigated-agriculture” scenario and the “current-irrigated-agriculture” scenario were provided as input to SWB, along with representative climate data from PRISM resulting in grids of both agricultural demand and net infiltration, aggregated to monthly stress periods. Using parcel mapping from (Appendix F), water estimated by the agricultural demand was aggregated to existing permitted irrigation wells. The resulting recharge and well information was then conveyed to the regional model for simulation over the climate years to provide constant head boundary conditions for the inset models. The inset models were then run using both the boundaries supplied by the updated regional model and the recharge and well pumping from the SWB runs in addition to using evapotranspiration and precipitation for the LAK package, updated using the representative PRISM data. The other parameters for the three MODFLOW models were informed from history matching, using the optimal parameters for the regional model and the base realizations for the two inset models. To focus on differences between the noirrigated agriculture and current-irrigated-agriculture scenarios, the same constant head boundaries from the regional model (the no irrigated agriculture results) were used for all inset model LERA runs.

Three-hundred fifty SWB parameter sets were generated using a Monte Carlo approach in which parameters are assumed to vary about the values assigned during the base SWB run. The

parameters that were allowed to vary include many related to the FAO-56 calculations: irrigation starting and ending dates, planting dates, crop coefficient curve midpoint ($K_{cb_{mid}}$), along with the maximum allowable depletion (responsible for triggering virtual irrigation events) and the depletion fraction defining soil moisture conditions leading to plant stress. One other non-FAO-56 related parameter was also allowed to vary, specifically the rooting depth of the plant.

Each of these parameter sets was simulated with SWB, with the outputs then used as input to the inset models to explore the responses and associated uncertainties of lake levels and streamflows derived from varying SWB input parameters. Figure 97 shows the lake levels for all the study lakes. The boldest blue and orange lines indicate the results for the base run parameter set for the Monte Carlo SWB runs for the no irrigation and current irrigation scenarios, respectively. Lighter blue lines show the ensemble of results resulting from sampling the uncertainty of the SWB parameters. Note that, in panel B, short periods of time show the lake level simulated as at the bottom of the lake bathymetry for some realizations. Figure 98 shows similar plots for streamflow in two selected streams from the Plainfield Tunnel Channel Lakes inset model. Figure 99 and Figure 100 shows streamflow results for two sets of selected streams in the Pleasant Lake inset model.

Figure 97 Lake stages for the three study lakes, Plainfield, Long, and Pleasant, in panels A, B, and C, respectively, over the Lake Ecosystem Response Assessment (LERA) representative climate. Blue lines indicate Monte Carlo ensemble members for the non-irrigation scenario, and orange lines indicate ensemble members for the current irrigation scenario.

Figure 98 Streamflow in selected streams in the Plainfield inset model respectively over the Lake Ecosystem Response Assessment (LERA) representative climate. Blue lines indicate Monte Carlo ensemble members for the non-irrigation scenario, and orange lines indicate ensemble members for the current irrigation scenario. Panel A is North Branch of Tenmile Creek, and panel B is Upper Pine River

Figure 99 Streamflow in selected streams in the Pleasant inset model respectively over the Lake Ecosystem Response Assessment (LERA) representative climate. Blue lines indicate Monte Carlo ensemble members for the non-irrigation scenario, and orange lines indicate ensemble members for the current irrigation scenario. Panel A is Tagatz Creek, and panel B is Chaffee Creek

Figure 100 Streamflow in selected streams in the Pleasant inset model respectively over the Lake Ecosystem Response Assessment (LERA) representative climate. Blue lines indicate Monte Carlo ensemble members for the non-irrigation scenario, and orange lines indicate ensemble members for the current irrigation scenario. Panel A is South Branch Wedde Creek, panel B is Carter Creek, and panel C is Mekan Creek

Figure 101 Lake stages for the three study lakes, Plainfield, Long, and Pleasant, in panels A, B, and C, respectively, over the Lake Ecosystem Response Assessment (LERA) representative climate for the base SWB parameters. In each panel, the blue line depicts the no-irrigated-agriculture scenario, the orange line depicts the current-irrigated agriculture scenario, and the green line depicts the potential-irrigated-agriculture scenario.

A final LERA analysis run was a potential-irrigated-agriculture scenario in which a land-use scenario was generated (Appendix F) wherein all land considered suitable for irrigated agriculture was simulated as irrigated agriculture. The land-use patterns were assigned rotations and annual crop distributions following the same methodology as for the current-irrigation scenario discussed above. Only the base SWB parameters were simulated for this sensitivity run and Figure 101 shows the lake stages for the base SWB parameters for the no-irrigated-agriculture, current-irrigated-agriculture, and potential-irrigated-agriculture scenarios.

Two final evaluations following the same logic of the LERA runs were performed to more precisely evaluate the connection between irrigation and land use at individual parcels and the responses in lake stages. These were the “distance” scenario and the “lag-time” scenario, both of which were limited to Long Lake as a proof-of-concept. The distance from the geometric centroid of Long Lake to each permitted high capacity well was used to rank wells from 0 (closest) to 319 (farthest). Using this information, the two scenarios evaluated were (1) converting each well, cumulatively, from 0 to 319, in sequence, from current irrigated agriculture to no irrigated agriculture (the distance scenario) and (2) dividing the 320 wells into 20 groups of 16 wells and converting all wells in each group from current irrigated agriculture to no irrigated agriculture (the lag-time scenario). The distance scenario illustrates the cumulative effects of pumping on lake stages as a function of distance. The lag-time scenario illustrates the magnitude and timing of effects from smaller groups assigned based on similar distance on lake stages. The conversion from current irrigated agriculture to no irrigated agriculture was simulated for both scenarios by (1) removing the high capacity well(s) from the simulation and (2) substituting the recharge calculated for the no irrigated agriculture in place of the recharge calculated for the current-irrigated-agriculture scenario for the parcel(s) associated with the well(s). This is the same logic as the LERA runs above, but with subsets of wells selected to evaluate.

Figure 102 Group identification, based on distance from the center of Long Lake for irrigation wells in the Plainfield inset model and total pumping over the LERA simulation time. Orange 'x' indicates the center of Long Lake.

Figure 103 Stage changes in Long Lake resulting from each well group simulated as converted from current irrigation to no irrigation recharge and water use. Positive responses indicate an increase in lake stage due to the conversion.

Results of the distance scenario are presented and discussed further in Appendix B. For the lag-time scenario, Figure 102 shows the 20 groups of 16 wells each, grouped as quantiles of distance rank from the center of Long Lake. The color flood indicates the total amount of water simulated as pumped for irrigation in each group. Figure 103 shows the difference, over time, in Long Lake stage over the 38-year LERA simulation time, simulating the wells in each group using the no irrigated agriculture recharge and pumping relative to the current irrigated agriculture recharge and pumping. Positive values indicate higher stage in the no-irrigated-agriculture scenario relative to the current-irrigated-agriculture scenario.

Assumptions and Limitations

All models—including those in this analysis—are necessarily simplifications of the natural world and thus subject to limitations. Limitations include the spatial and temporal discretization of the region and hydrologic process simplification. These simplifications are necessary to balance computational expense with supporting information.

The spatial discretization is intended to capture as much hydrogeologic complexity as is practical, but, combined with inherent limitations to the ability to measure hydrogeologic properties, much actual detail in the hydrogeologic system is not represented at the spatial scales. Similarly, higher resolution (smaller model cells) was used to capture the greatest amount of detail around the study lakes, but these models are still simplifications.

The temporal discretization was monthly stress periods for the history matching and LERA models. This was limited by the availability of water use data from WDNR on a monthly timescale.

The SWB model represents the plant growth and infiltration processes within the rooting zone in a simplified manner. Rooting depth defines the size of the single soil-moisture reservoir used to track daily soil-moisture values. Although the rooting depth is allowed to vary and progress in a manner congruent with the crop coefficient curve, the representation is clearly simplified. The FAO-56 procedure is used worldwide as a way to implement irrigation scheduling (see for example Kebede and others, 2014; Pereira and others, 2015); however, the method relies on parameters that might not be widely transferable from one part of the country or world to another. The assumption that “net infiltration” occurs only after soil moisture conditions have reached field capacity is another simplification; in reality, gravity drainage of the root zone likely occurs before soil moisture values reach field capacity. The simplified treatment of root zone dynamics causes the timing of net infiltration estimates from the root zone to be less realistic; the aggregation of the SWB results to the monthly stress periods of the MODFLOW models mitigates this timing issue.

The MODFLOW-NWT and MODFLOW 6 models are derived and implemented from the perspective of the groundwater system. As a result, other aspects of the hydrologic cycle are simplified. Specifically, the streamflow routing package (SFR) simulated the groundwater component of streamflow (base flow) but not surface runoff. The streams in the model area are interpreted to be dominated by base flow, but some stormflow certainly occurs and is not simulated by the model explicitly. Recharge is provided by the SWB model for all the MODFLOW models, but in reality, the quantity calculated by SWB is deep drainage from the soil zone. MODFLOW-NWT and MODFLOW 6 both simulate this deep drainage as reaching the water table at the time it is applied without delay that, in reality, occurs due to moving downward through the unsaturated zone. Due to the necessity of using monthly stress periods, errors due to this delay are at least partially mitigated. An alternative would be to explicitly simulate the unsaturated zone using the UZF package. Experiments in early stages of the model development showed limited differences in model outputs using the UZF package but incurred a greater computational expense.

Specifically for the LGR approach in MODFLOW 6, the ghost node correction option was not used in linking the inset and parent models. Evaluation with and without this correction showed a small difference in lake stage (on the order of 3 cm in Pleasant Lake stage and on the order of 4 mm in the Plainfield Tunnel Channel Lakes stages) with and without the ghost node correction. As a result, some parameter compensation was likely incurred in other model parameters to result in the fit between measured and simulated results obtained during history matching. In future work, the ghost node correction may enhance stability of the modeling and obviate some minor parameter compensation. Also in the inset models, the spatially distributed parameters such as hydraulic conductivity and storage were not estimated continuously across the inset and parent model boundaries. This allows for some discontinuity in the properties at that artificial boundary. The results on the solution are not significant, but future development of methods for parameterization in such a case would benefit from enforcing continuity.

In the parameter estimation process, some of the limitations of the formulation are compensated for by estimated parameters responding to data that are in actuality, not related to them. This concept of parameter compensation is present in all parameter estimation efforts as discussed by Doherty and Welter (2010). Focusing on the dominant hydrologic processes limits this behavior as much as possible. This focus, on lake levels and streamflows, highlights the importance of considering potential parameter compensation if using the model for other purposes. Furthermore, for each of the inset LGR models, the two distinct models representing the two spatial discretization scales are parameterized separately without enforcing continuity across their boundaries. As a result, some discontinuities in the spatially distributed properties are inevitable. However, the use of multipliers helps mitigate the magnitude of this discontinuity and the impact on the model results is minimal.

Disclaimer

Any use of trade, firm, or product names is for descriptive purposes only and does not imply endorsement by the U.S. Government.

References

- Allen, R.G., Pereira, L.S., Raes, D., and Smith, M., 1998, Crop evapotranspiration-Guidelines for computing crop water requirements-FAO Irrigation and drainage paper 56: Food and Agriculture Organization of the United Nations, Rome.
- Anderson, M. P., W. W. Woessner, and R. J. Hunt 2015. Applied Groundwater Modeling (Second Edition). San Diego: Academic Press.
- Bradbury, K.R., Fienen, M.N., Kniffin, M.L., Krause, J.J., Westenbroek, S.M., Leaf, A.T., and Barlow, P.M., 2017, Groundwater flow model for the Little Plover River basin in Wisconsin's Central Sands: Wisconsin Geological and Natural History Survey Bulletin 111, 82 p.
- Corson-Dosch, N.T., Fienen, M.N., Finklestein, J.S., Leaf, A.T., White, J.T., Woda, J., and Williams, J.H. 2021. Areas contributing recharge to priority wells in valley-fill aquifers in the Neversink and Rondout Basins, New York. U.S. Geological Survey Scientific Investigations Report (in press).
- Cronshey, R., McCuen, R., Miller, N., Rawls, W., Robbins, S., and Woodward, D., 1986, Urban Hydrology for Small Watersheds – Technical release 55: U.S. Dept. of Agriculture, Soil Conservation Service, Engineering Division, accessed at http://www.nrcs.usda.gov/Internet/FSE_DOCUMENTS/16/stelprdb1044171.pdf.
- Doherty, J., 2020, PEST for highly parallelized computing environments: Brisbane, Australia, Watermark Numerical Computing, [88 p.] accessed April 28, 2020, at <http://www.pesthomepage.org/Downloads.php>.
- Doherty, J. and Welter, D., 2010, A short exploration of structural noise: Water Resources Research, v. 46, no. 5, W05525. <http://dx.doi.org/10.1029/2009wr008377>.

- Dripps, W.R., and Bradbury, K.R., 2007, A simple daily soil–water balance model for estimating the spatial and temporal distribution of groundwater recharge in temperate humid areas: *Hydrogeology Journal*, v. 15, no. 3, p. 433–444.
- Duffield, G.M., 2019, Representative values of hydraulic properties, accessed at http://www.aqtesolv.com/aquifer-tests/aquifer_properties.htm.
- Feinstein, D.T., Hunt, R.J., and Reeves, H.W., 2010, Regional groundwater-flow model of the Lake Michigan Basin in support of Great Lakes Basin water availability and use studies: U.S. Geological Survey Scientific Investigations Report 2010–5109, 379 p.
- Fienen, M.N., Haserodt, M.J., and Leaf, A.T., 2021, MODFLOW models used to simulate groundwater flow in the Wisconsin Central Sands Study Area, 2012–2018, U.S. Geological Survey Data Release, <https://doi.org/10.5066/P9BVFSGJ>
- Harbaugh, A.W., 2005, MODFLOW–2005, the U.S. Geological Survey modular ground-water model—the ground-water flow process: U.S. Geological Survey Techniques and Methods 6–A16, variously paginated.
- Hart, D., Bradbury, K., and Parsen, M., 2015, Using the New Rome Formation as a geologic weighing lysimeter for water management in Wisconsin’s sands plain, WDNR Project Report for Project Number 14-HDG-03, <https://www.wri.wisc.edu/research/using-the-new-rome-formation-as-a-geologic-weighing-lysimeter-for-water-management-in-wisconsins-sand-plain/>.
- Harwell, G.R., 2012, Estimation of evaporation from open water—A review of selected studies, summary of U.S. Army Corps of Engineers data collection and methods, and evaluation of two methods for estimation of evaporation from five reservoirs in Texas: U.S. Geological Survey Scientific Investigations Report 2012–5202, 96 p., <https://doi.org/10.3133/sir20125202>.

- Healy, R.W., 2010, Estimating groundwater recharge: Cambridge University Press, 245 p.
- Hipsey, M. R., Bruce, L. C., Boon, C., Busch, B., Carey, C. C., Hamilton, D. P., ... & Winslow, L. A. (2019). A General Lake Model (GLM 3.0) for linking with high-frequency sensor data from the Global Lake Ecological Observatory Network (GLEON). *Geoscientific Model Development*, 12(1), 473-523.
- Hunt, R.J, Prudic, D.E., Walker, J.F. and Anderson, M.P., 2008. Importance of Unsaturated Zone Flow for Simulating Recharge in a Humid Climate, *Groundwater* 46 (4): 551-560.
- Kebede, H., Fisher, D.K., Sui, R., and Reddy, K.N., 2014, Irrigation Methods and Scheduling in the Delta Region of Mississippi: Current Status and Strategies to Improve Irrigation Efficiency: *American Journal of Plant Sciences*, v. 05, no. 20, p. 2917–2928.
- Langevin, C.D., Hughes, J.D., Banta, E.R., Niswonger, R.G., Panday, Sorab, and Provost, A.M., 2017, Documentation for the MODFLOW 6 Groundwater Flow Model: U.S. Geological Survey Techniques and Methods, book 6, chap. A55, 197 p., <https://doi.org/10.3133/tm6A55>.
- Langevin, C.D., Hughes, J.D., Banta, E.R., Provost, A.M., Niswonger, R.G., and Panday, Sorab, 2020, MODFLOW 6 Modular Hydrologic Model version 6.2.0: U.S. Geological Survey Software Release, 22 October 2020, <https://doi.org/10.5066/F76Q1VQV>
- Leaf, A.T., Fienen, M.N., Hunt, R.J., and Buchwald, C.A., 2015, Groundwater/Surface-Water Interactions in the Bad River Watershed, Wisconsin: U.S. Geological Survey Scientific Investigations Report 2015–5162, 110 p., <https://doi.org/10.3133/sir20155162>.
- Leaf, A.T., Fienen, M.N. and Reeves, H.W., 2021. SFRmaker and Linesink-maker: Rapid construction of streamflow routing networks from hydrography data, *Groundwater*. <https://doi.org/10.1111/gwat.13095>.

- McKay, L., Bondelid, T., Dewald, T., Johnston, J., Moore, R., and Rea, A., 2012, NHDPlus Version 2—User guide, accessed November 15, 2014, at http://www.horizon-systems.com/NHDPlus/NHDPlusV2_documentation.php.
- McKenna, S. A., Akhriev, A., Ciaurri, D. E., and Zhuk, S. (2019). Efficient uncertainty quantification of reservoir properties for parameter estimation and production forecasting. *Mathematical Geosciences* 233–251. <https://10.1007/s11004-019-09810-y>.
- Mechenich, D. J. 2012. Extending the Wisconsin Central Sands Groundwater Flow Model. Appendix B in Kraft, G. J., D. J. Mechenich and J. Haucke. 2012. Information Support for Groundwater Management in the Wisconsin Central Sands, 2009-2011. A Report to the Wisconsin Department of Natural Resources in Completion of Project NMA00000253. Center for Watershed Science and Education, College of Natural Resources, University of Wisconsin – Stevens Point / Extension. Available at https://www.uwsp.edu/cnr-ap/watershed/Documents/kraft_centernalsands_2012.pdf.
- Mehl, S., Hill, M.C. and Leake, S.A. (2006), Comparison of Local Grid Refinement Methods for MODFLOW. *Groundwater*, 44: 792-796. <https://doi.org/10.1111/j.1745-6584.2006.00192.x>
- Miller, D.A., and White, R.A., 1998, A Conterminous United States Multilayer Soil Characteristics Dataset for Regional Climate and Hydrology Modeling: *Earth Interactions*, v. 2, no. 2, p. 1–26.
- McCobb, T.D., LeBlanc, D.R., and Hess, K.M. 1999, Determination of Temporal and Spatial Variability of Hydraulic Gradients in an Unconfined Aquifer Using Three-Point Triangulation, Cape Cod, Massachusetts in *U.S. Geological Survey Toxic Substances Hydrology Program: Proceedings of the Technical Meeting, Charleston, South Carolina, March 8-12, 1999*, Morganwalp, D.W., and Buxton, H.T., eds. v. 3, part C, p. 349-360. U.S. Geological Survey Water Resources Investigations Report 99-4018. <https://doi.org/10.3133/wri994018C>.

- Mu, Q., Zhao, M., and Running, S.W., 2013, MODIS Global Terrestrial Evaporation (ET) Product (NASA MOD16A2/A3), Algorithm Theoretical Basis Document: Numerical Terradynamic Simulation Group, University of Montana, 55 p., accessed February 5, 2021, at <https://modis-land.gsfc.nasa.gov/pdf/MOD16ATBD.pdf>.
- Niswonger, R.G. and Prudic, D.E., 2005, Documentation of the Streamflow-Routing (SFR2) Package to include unsaturated flow beneath streams—A modification to SFR1: U.S. Geological Survey Techniques and Methods book 6, chap. A13, 50 p.
- Niswonger, R.G., Panday, S., and Ibaraki, M., 2011, MODFLOW–NWT—A Newton formulation for MODFLOW–2005: U.S. Geological Survey Techniques and Methods, book 6, chap. A37, 44 p.
- Pereira, L.S., Allen, R.G., Smith, M., and Raes, D., 2015, Crop evapotranspiration estimation with FAO56: Past and future: Agricultural Water Management, v. 147, p. 4–20.
- PRISM Climate Group, Oregon State University, 2019. Time Series Values for Individual Locations, accessed at <https://prism.oregonstate.edu/explorer/> on December 10, 2019.
- PRISM Climate Group, 2020, Oregon State University PRISM Climate Data, accessed December 16, 2020, at <http://prism.oregonstate.edu/>.
- Reitz, M., Senay, G., and Sanford, W., 2017a, Combining Remote Sensing and Water-Balance Evapotranspiration Estimates for the Conterminous United States: Remote Sensing, v. 9, no. 12, p. 1181.
- Reitz, M., Sanford, W.E., Senay, G.B., and Cazenias, J., 2017b, Annual Estimates of Recharge, Quick-Flow Runoff, and Evapotranspiration for the Contiguous U.S. Using Empirical Regression Equations: JAWRA Journal of the American Water Resources Association, v. 53, no. 4, p. 961–983.

- Scanlon, B.R., Healy, R.W., and Cook, P.G., 2002, Choosing appropriate techniques for quantifying groundwater recharge: *Hydrogeology Journal*, v. 10, no. 1, p. 18–39.
- Soil Survey Staff, 2018, Web Soil Survey, Natural Resources Conservation Service, United States Department of Agriculture, accessed December, 2018 at <http://websoilsurvey.nrcs.usda.gov/>.
- Soil Survey Staff, 2019, Gridded Soil Survey Geographic (gSSURGO) Database for the Conterminous United States., at <https://gdg.sc.egov.usda.gov/>.
- Tarantola, Albert, 2005, *Inverse problem theory and methods for model parameter estimation*. Society for Industrial and Applied Mathematics, Society for Industrial and Applied Mathematics, Philadelphia, Pennsylvania, 354 p.
- Thornthwaite, C.W., 1948, An Approach toward a Rational Classification of Climate: *Geographical Review*, v. 38, no. 1, p. 55.
- USDA National Agricultural Statistics Service, Cropscape and Cropland Data Layer, accessed at https://www.nass.usda.gov/Research_and_Science/Cropland/SARS1a.php on December 16, 2020.
- Weeks, E.P. and Stangland, H.G., 1971, Effects of irrigation on streamflow in the Central Sand Plain of Wisconsin: U.S. Geological Survey Open-File Report 70-362, 113 p.
- Westenbroek, S.M., Kelson, V.A., Dripps, W.R., Hunt, R.J., and Bradbury, K.R., 2010, SWB—A modified Thornthwaite-Mather Soil-Water-Balance code for estimating groundwater recharge: U.S. Geological Survey Techniques and Methods 6-A31, 1–61 p.
- Westenbroek, S.M., Engott, J.A., Kelson, V.A., and Hunt, R.J., 2018, A Soil-Water-Balance code for estimating net infiltration and other water-budget components: U. S. Geological

Survey U.S. Geological Survey Techniques and Methods book 6, chap.A59, 118 p., accessed at <https://doi.org/10.3133/tm6A59>.

Westenbroek, S.M. and Fienen, M.N., 2021, MODEL ARCHIVE AND OUTPUT: Soil-Water-Balance model developed to simulate net infiltration, irrigation water requirements, and other water budget components in support of the Central Sands Lakes Study. U.S. Geological Survey Data Release. <https://doi.org/10.5066/P9SOJ01N>

White, J.T., 2018. A model-independent iterative ensemble smoother for efficient history-matching and uncertainty quantification in very high dimensions. *Environmental Modelling & Software*, 109, pp.191-201.

White, J.T., Hunt, R.J., Fienen, M.N., and Doherty, J.E., 2021, Approaches to Highly Parameterized Inversion: PEST++ Version 5, a Software Suite for Parameter Estimation, Uncertainty Analysis, Management Optimization and Sensitivity Analysis: U.S. Geological Survey Techniques and Methods 7C26, 52 p., <https://doi.org/10.3133/tm7C26>.

White, J.T., Foster, L.K., Fienen, M.N., Knowling, M.J., Hemmings, B. and Winterle, J.R., 2020. Toward Reproducible Environmental Modeling for Decision Support: A Worked Example. *Frontiers in Earth Science*, 8, p. 50.

Wisconsin Department of Natural Resources (WDNR), 2015, WDNR 24K Hydro Geodatabase, 1:24,000: accessed June 8, 2016, at <ftp://dnrftp01.wi.gov/geodata>.

Wisconsin Department of Natural Resources [WDNR], 2019, Digital Elevation Model (DEM) – 10 Meter, accessed at <https://data-wi-dnr.opendata.arcgis.com/search?q=DEM>.

Wisconsin State Cartographer's Office, 2009, Wisconsin Coordinate Reference Systems: Madison, Wisconsin, 112 p.

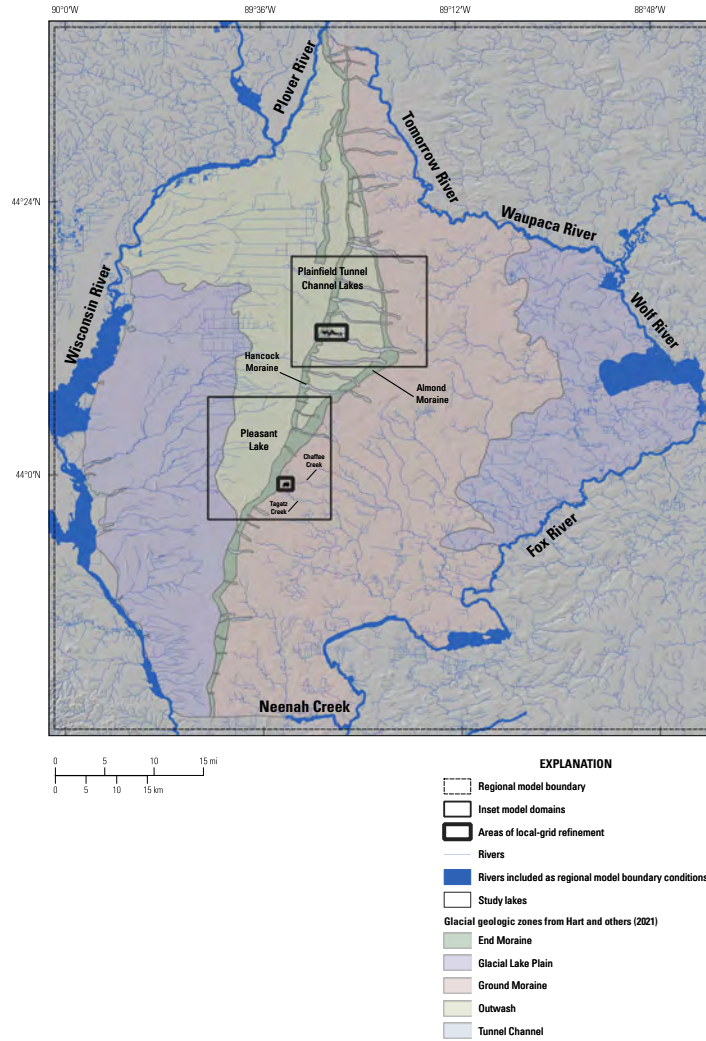


Figure 1: Location map showing Central Sands extent, moraines, streams, study lakes and boundaries of all GW models.

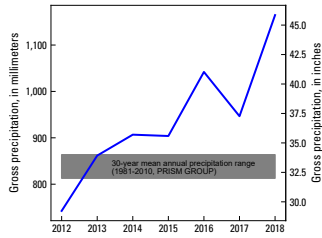


Figure 2: Annual precipitation for the Central Sands study area, 2012-2018.

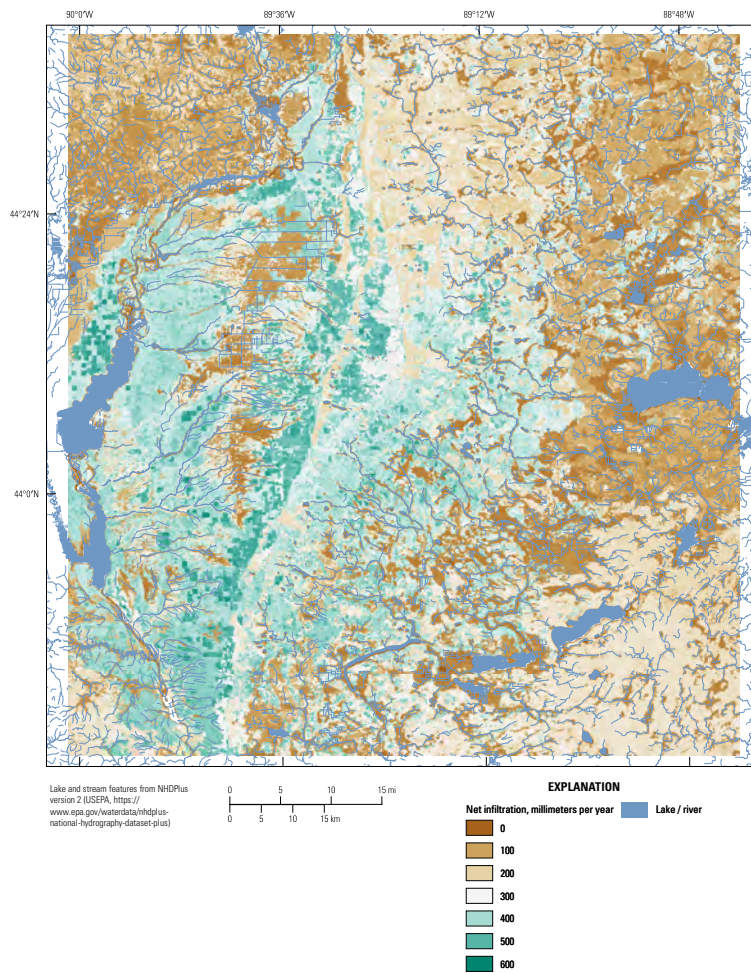


Figure 3: Average 2012 – 2018 annual net infiltration estimated by SWB.

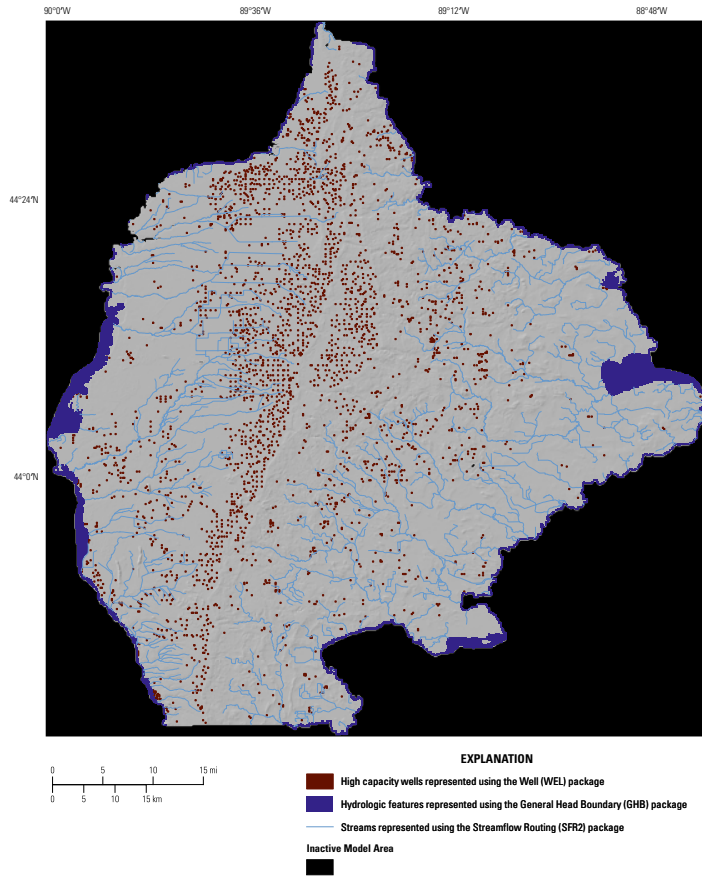


Figure 4: Map of model boundary conditions for the regional model.

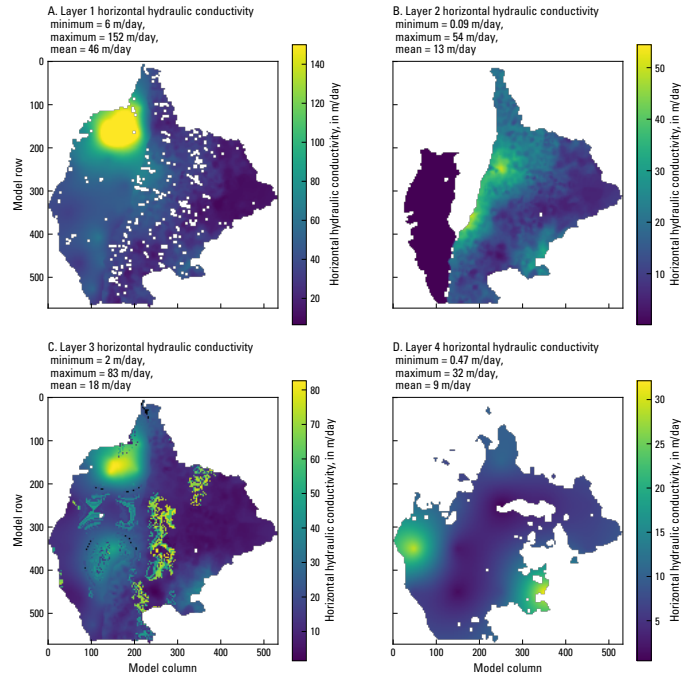


Figure 5: Horizontal hydraulic conductivity values after history matching for each of the four model layers.

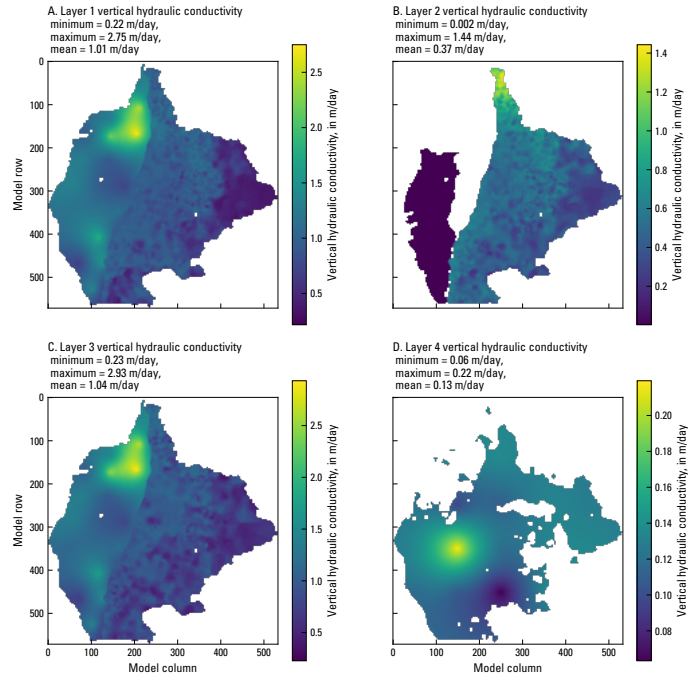


Figure 6: Vertical hydraulic conductivity values after history matching for each of the four model layers.

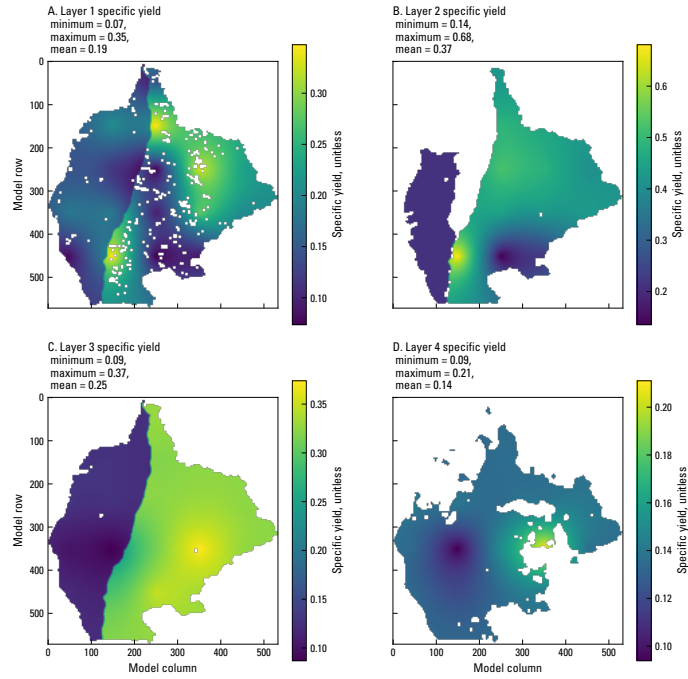


Figure 7: Specific yield values after history matching for each of the four model layers.

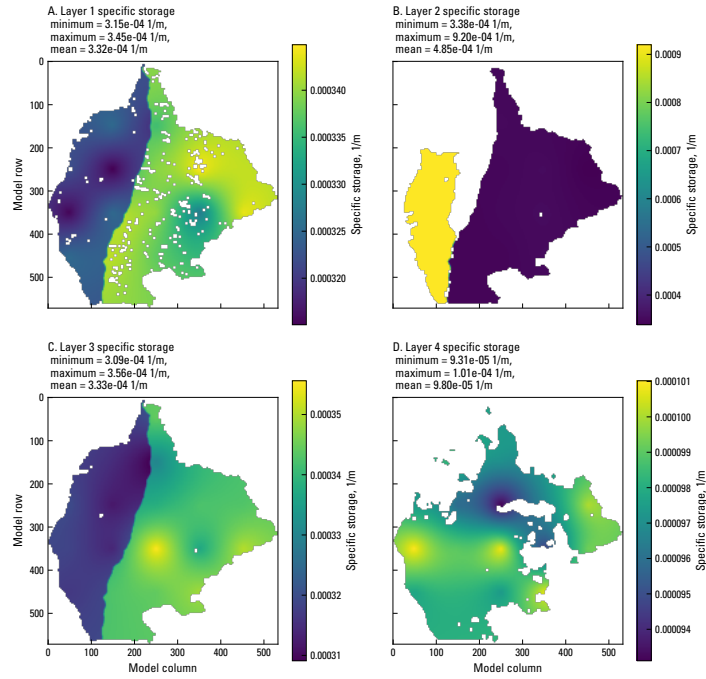


Figure 8: Specific storage values after history matching for each of the four model layers.

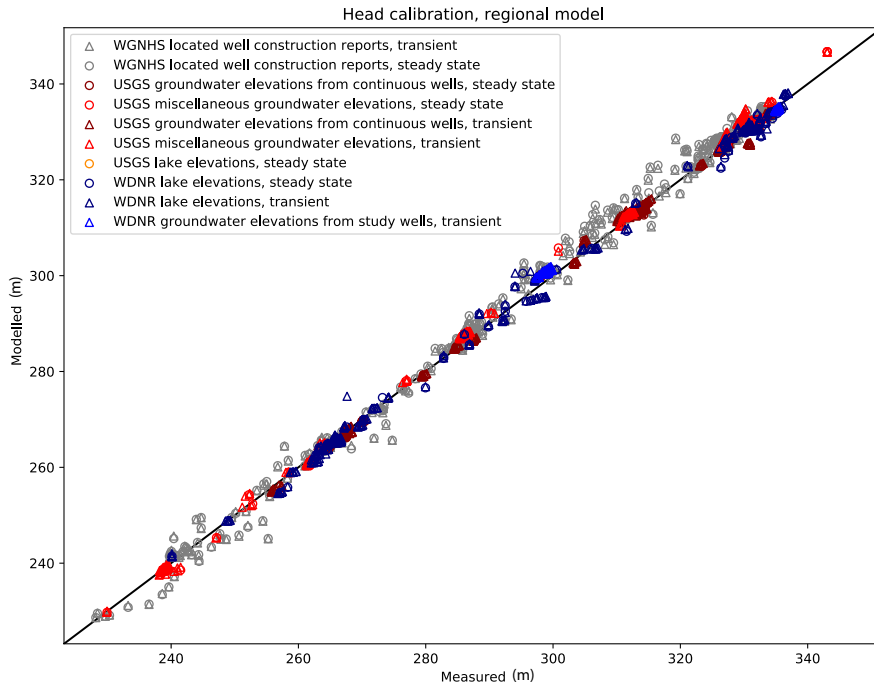


Figure 9: One-to-one plot of measured and modeled groundwater elevations for the steady-state and transient head targets.

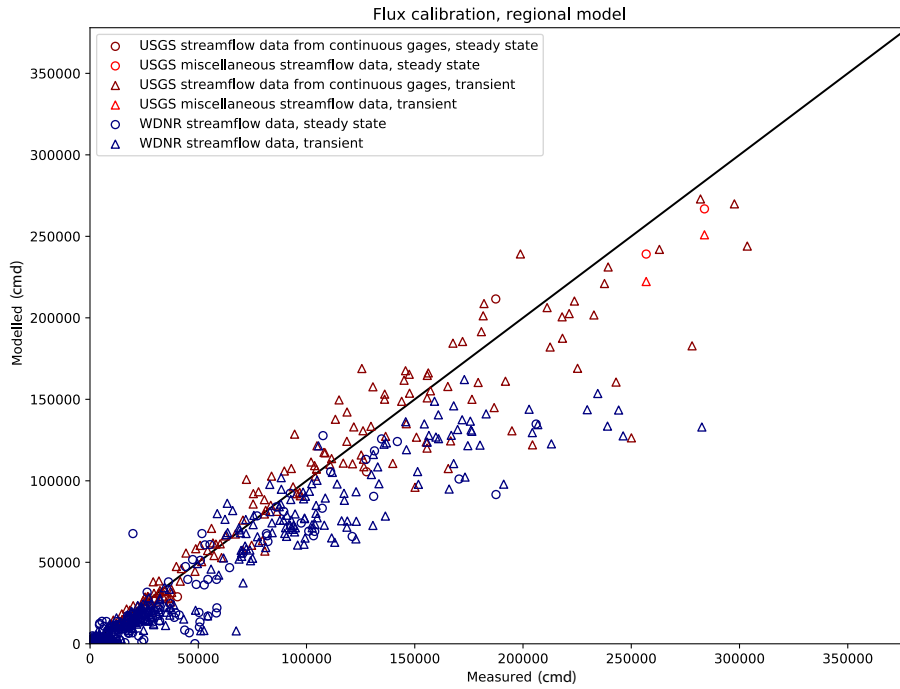


Figure 10: One-to-one plot of measured and modeled streamflow under baseflow conditions for the transient streamflow targets.

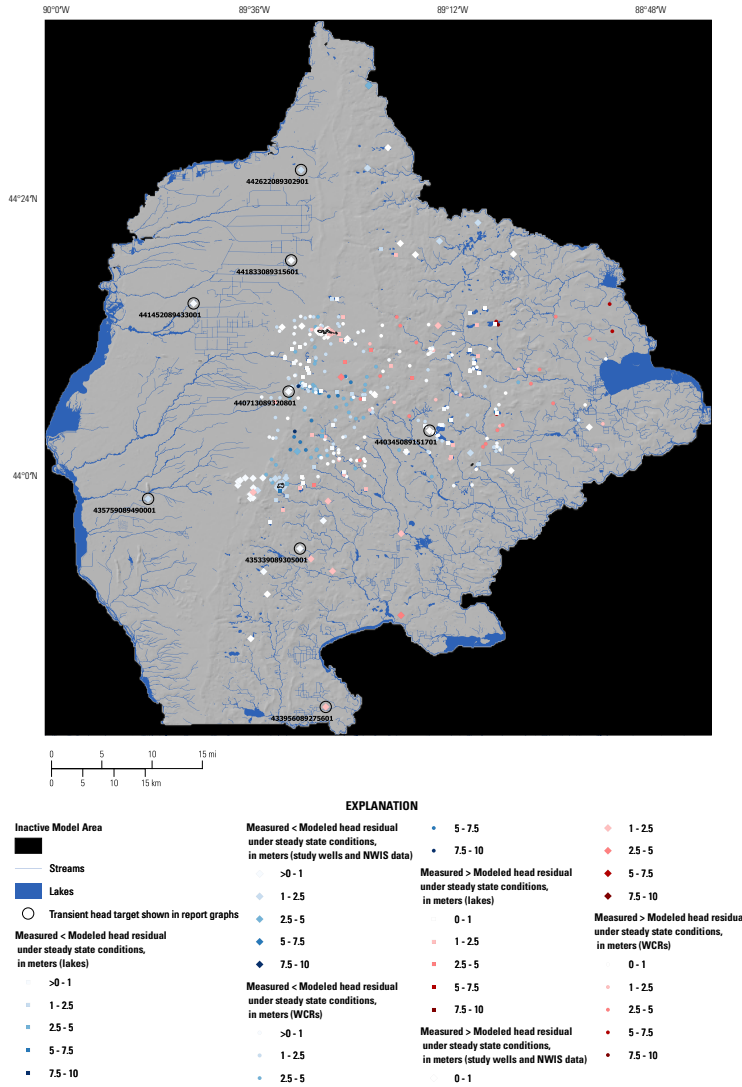


Figure 11: Map of steady-state head target residuals displayed by calibration group.

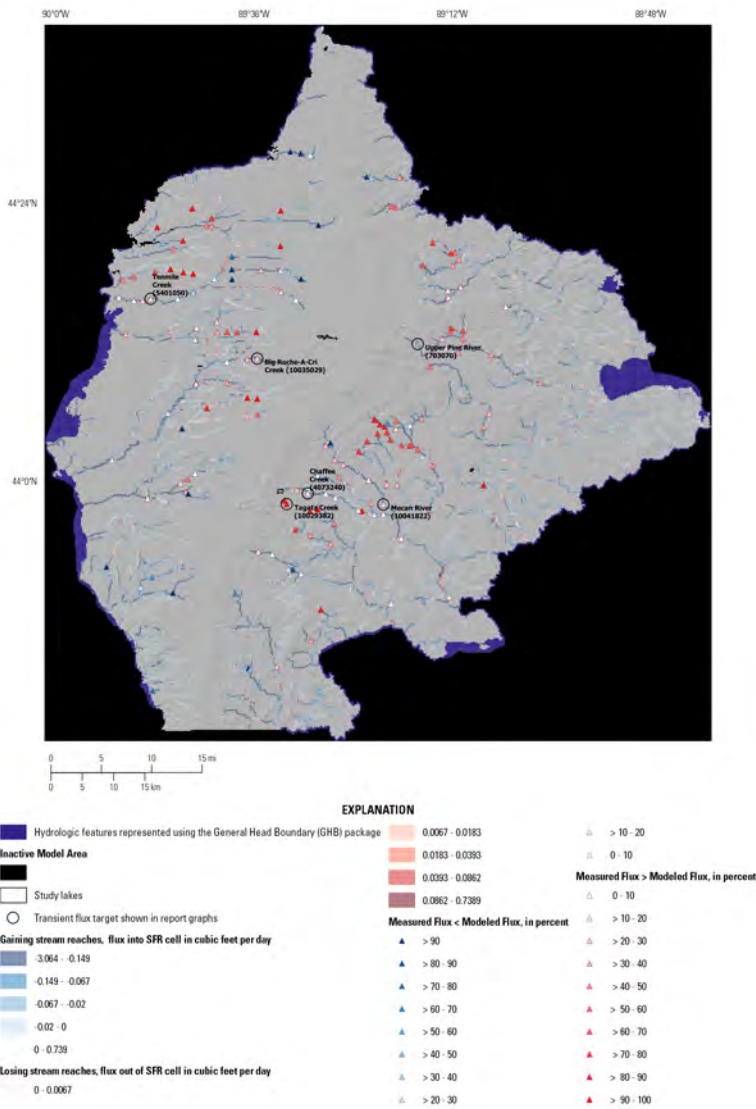


Figure 12: Map of steady-state streamflow residuals and gaining and losing stream reaches.

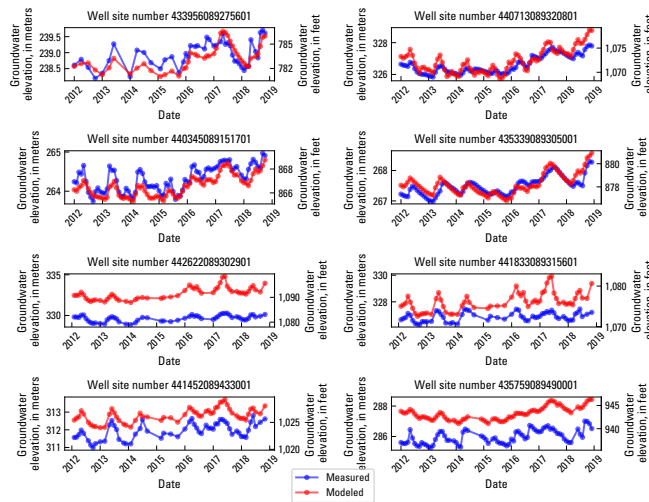


Figure 13: Transient groundwater elevations at select wells with long-term records (well locations shown in Figure 11). Elevations are shown in meters and feet above NAVD88.

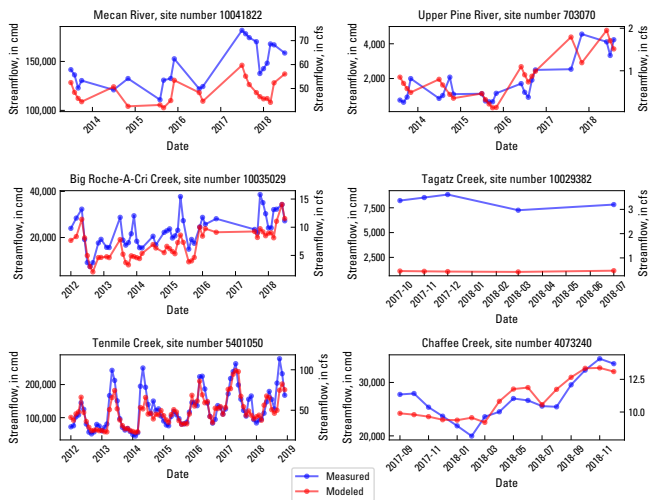


Figure 14: Transient streamflow at select streams locations near the study lakes and with longer-term record (stream locations shown in Figure 12).

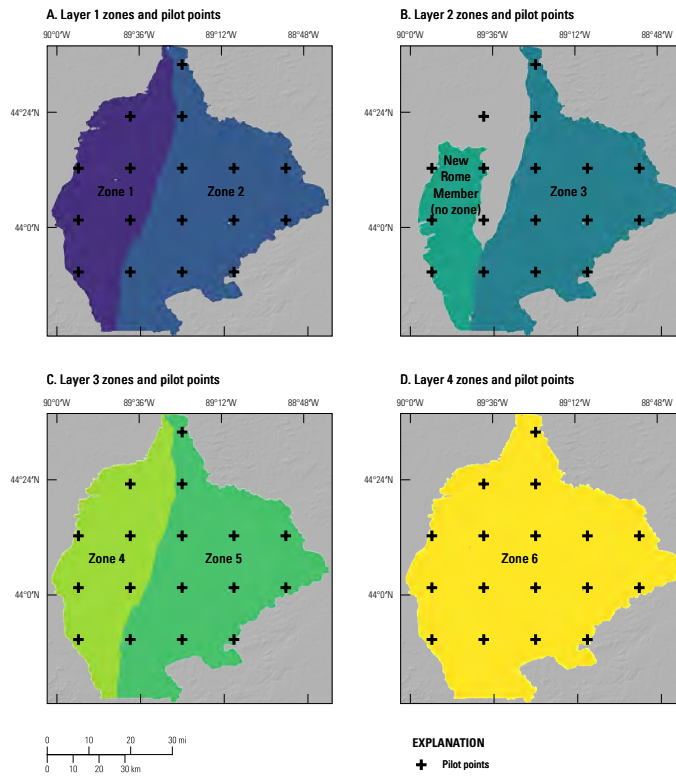


Figure 15: Pilot points and multiplier zones for each of the four model layers. Note, pilot points extend past the zone boundaries in layer 2 to allow for kriging but the aquifer properties in the New Rome and pinched areas are not influenced by pilot point multipliers.

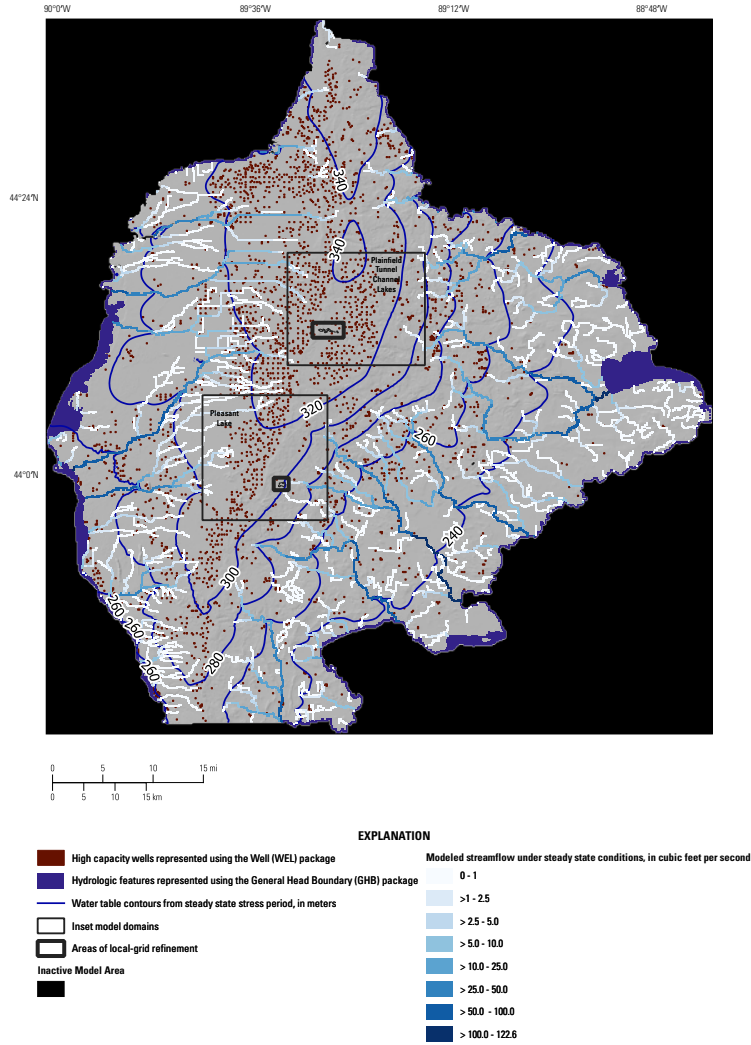


Figure 16: Map of the modeled water table and streamflow for the regional model during the steady-state stress period representing average conditions from 2012 – 2018.

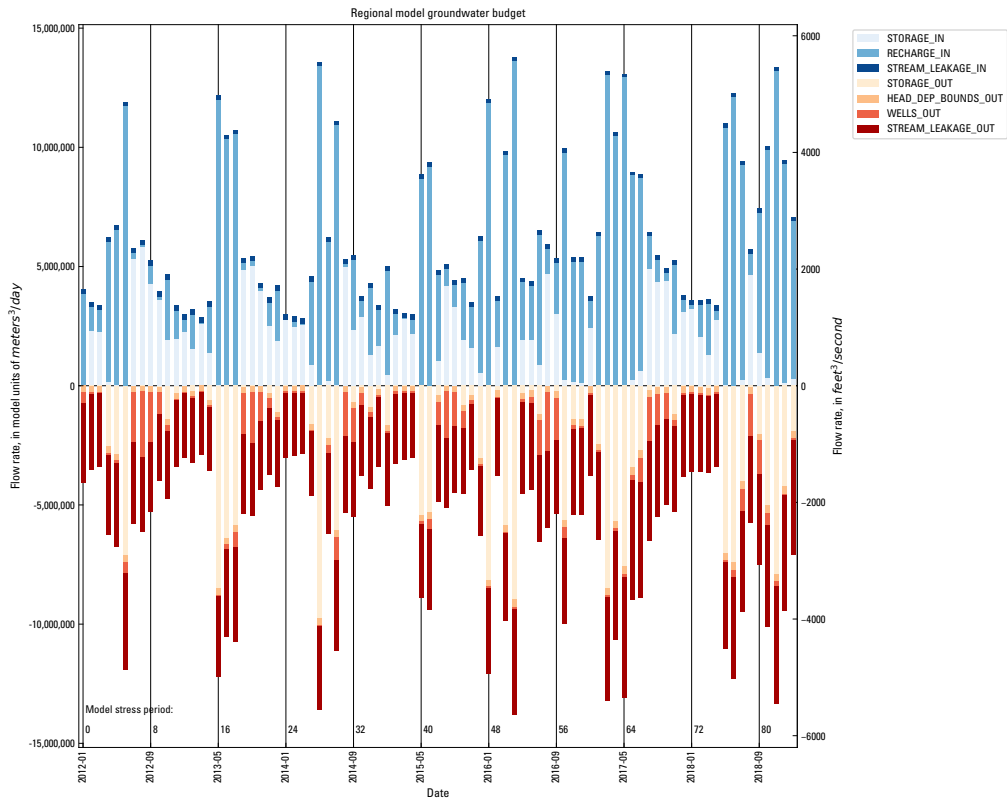


Figure 17: Regional model groundwater budget showing the major model inflows and outflows for each stress period. Inflows and outflows are named using the MODFLOW List file convention.

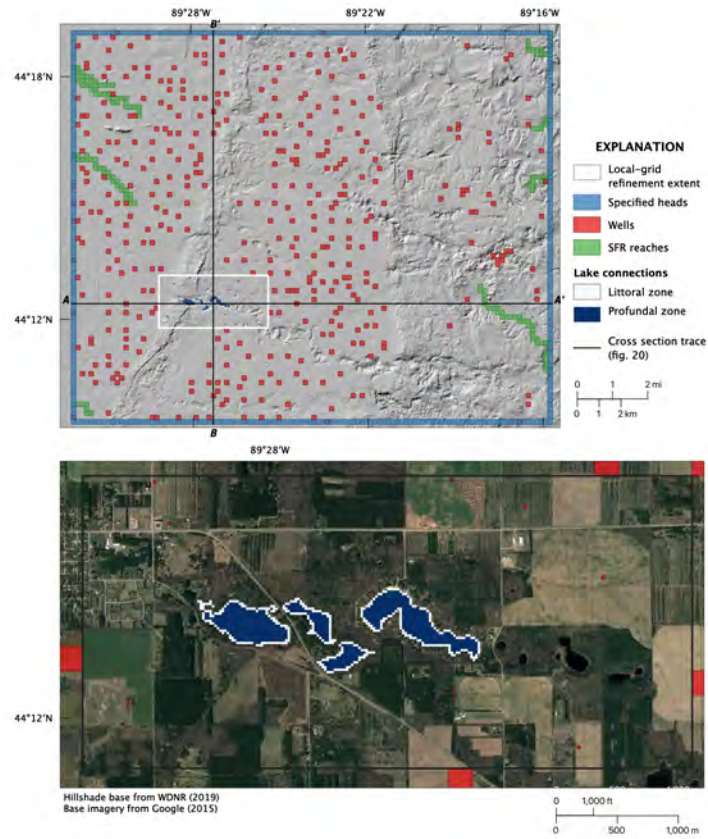


Figure 18: Plainfield Tunnel Channel Lakes model boundary conditions with local-grid refinement extent.

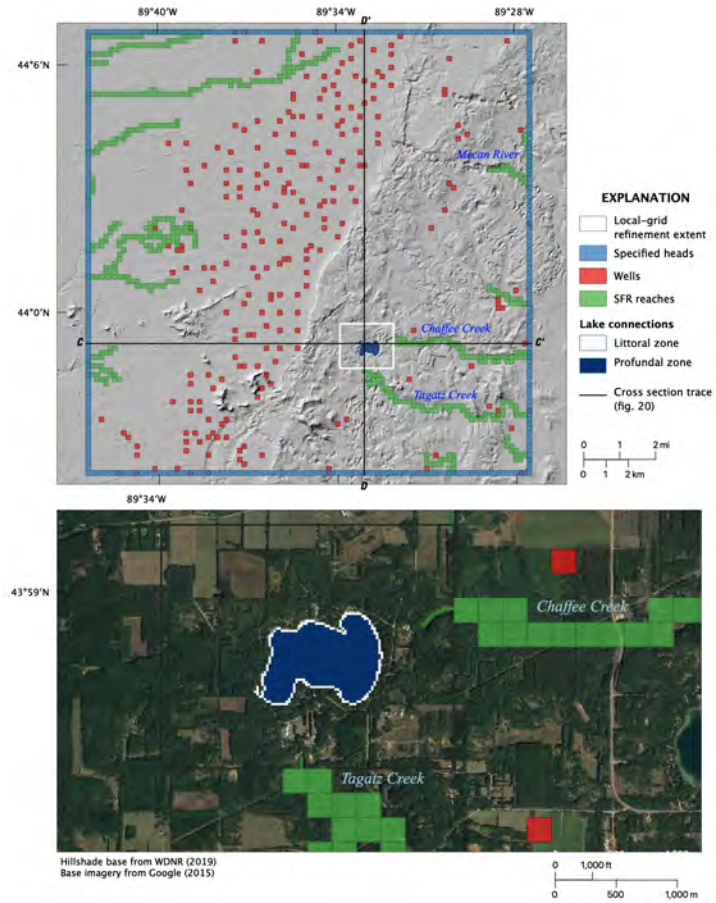


Figure 19: Pleasant Lake model boundary conditions with local-grid refinement extent.

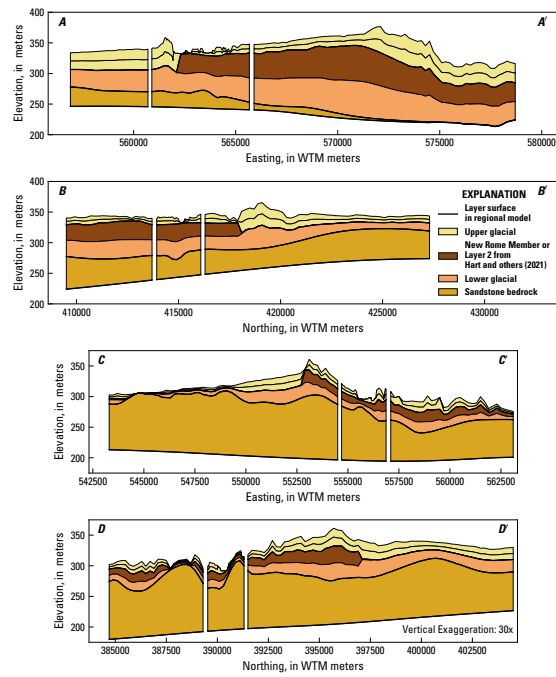


Figure 20: Inset model cross sections showing inset and parent layer surfaces. Gaps in the cross sections indicate the extent of the refined areas within the inset models. Cross section locations are shown in Figure 18 and Figure 19.

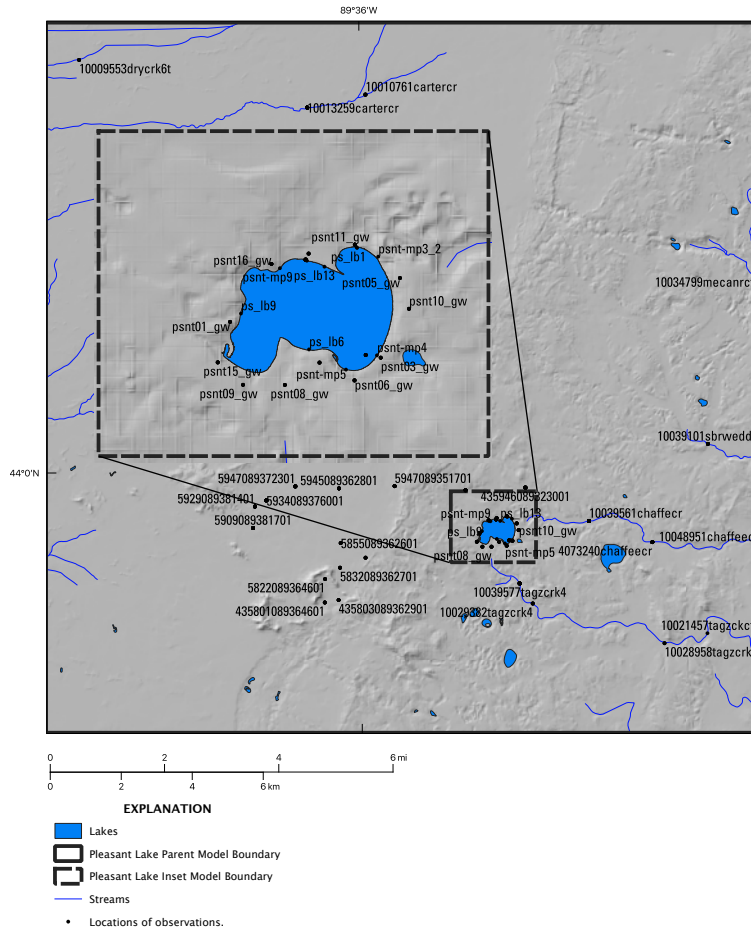


Figure 21: Locations of observations that were assigned observation weight greater than zero for the Pleasant Lake inset model.

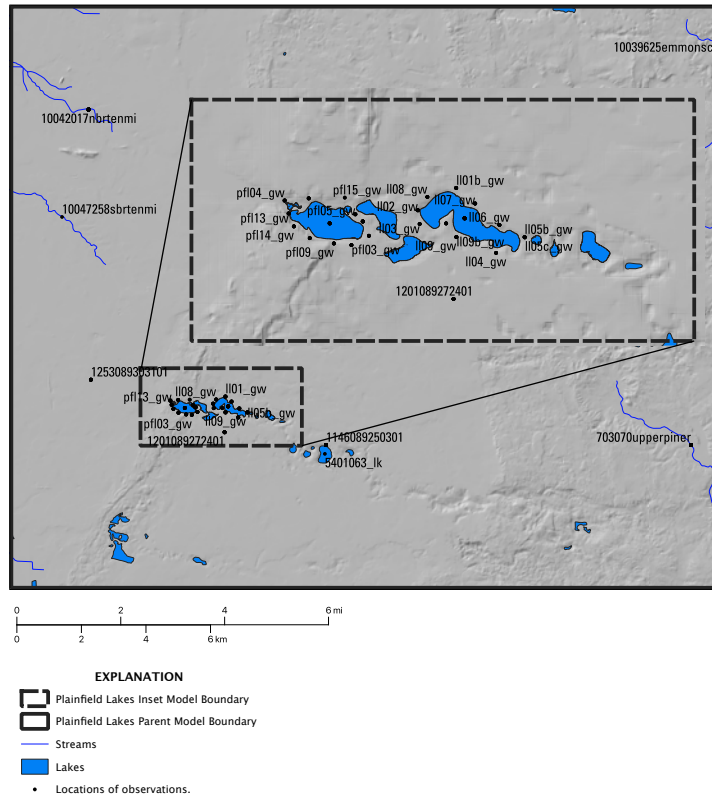


Figure 22: Locations of observations that were assigned observation weight greater than zero for the Plainfield Tunnel Channel Lakes inset model.

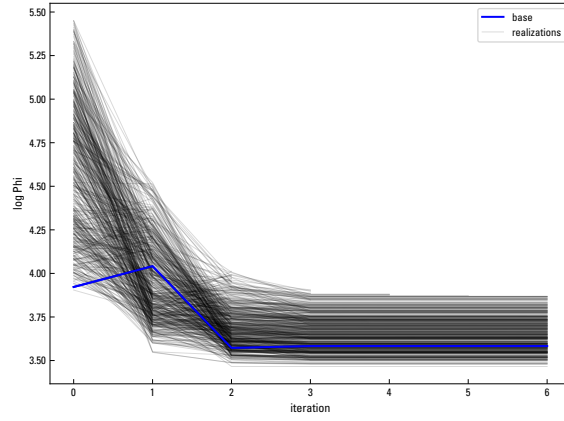


Figure 23: Summary of ensemble (black lines) and base (blue line) objective function progress by iES iteration for Pleasant Lake Inset model.

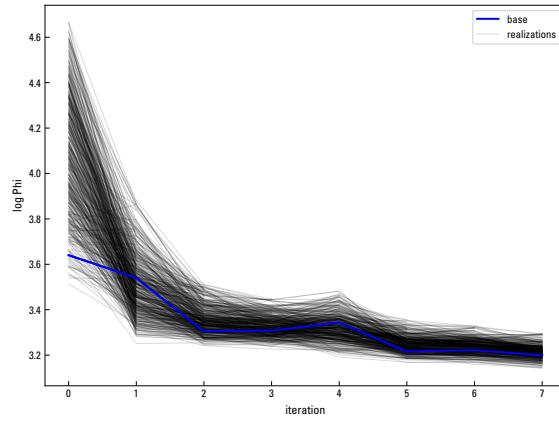


Figure 24: Summary of ensemble (black lines) and base (blue line) objective function progress by iES iteration for Plainfield Tunnel Channel Lakes Inset model.

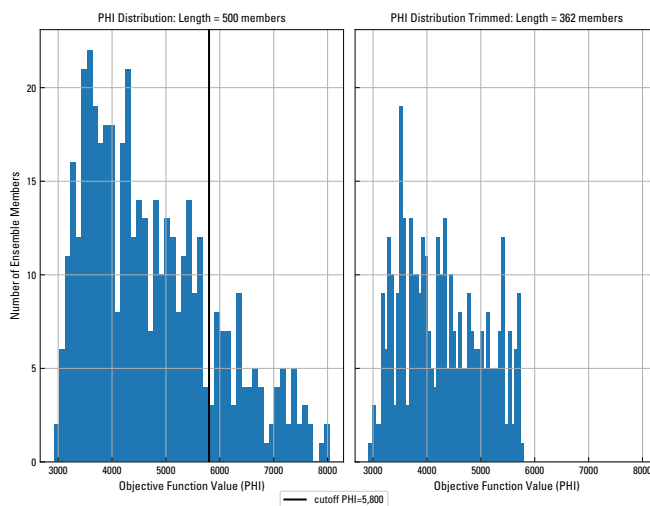


Figure 25: Rejection sampling for the Pleasant Lake model. A subjective decision is made to only retain ensemble members at or below a selected cutoff value. For Pleasant Lake, this cutoff was 5,800.

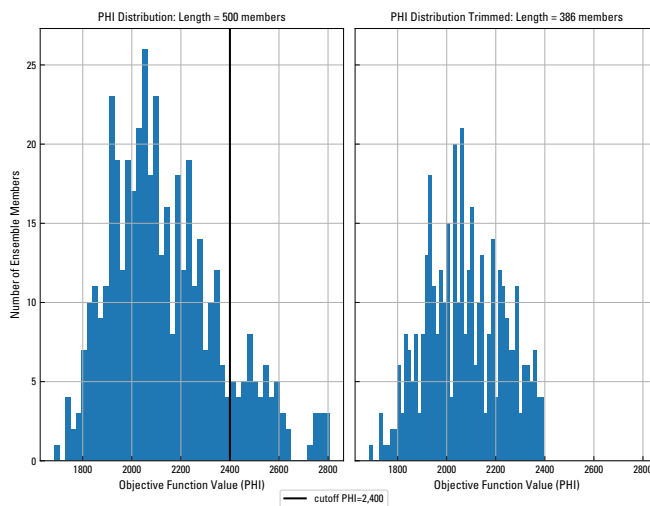


Figure 26: Rejection sampling for the Plainfield Tunnel Channel Lakes model. A subjective decision is made to only retain ensemble members at or below a selected cutoff value. For Plainfield Tunnel Channel Lakes, this cutoff was 2,400.

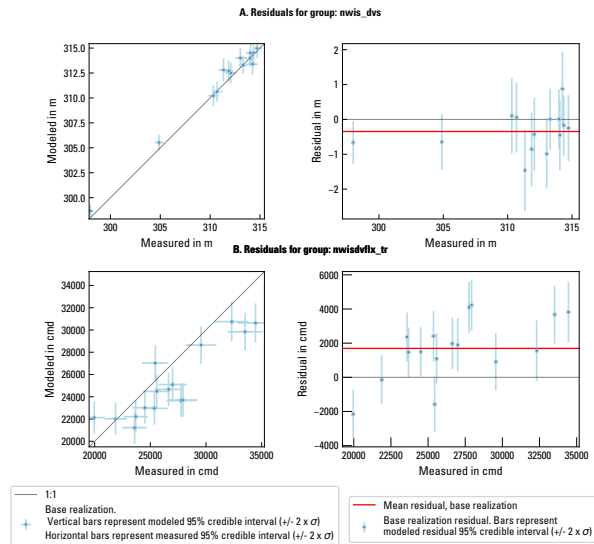


Figure 27: Fit between measured and modeled values at observation locations for observation groups nwis_dvs (panel A) and nwisdvflx_tr (panel B) for the Pleasant Lake model.

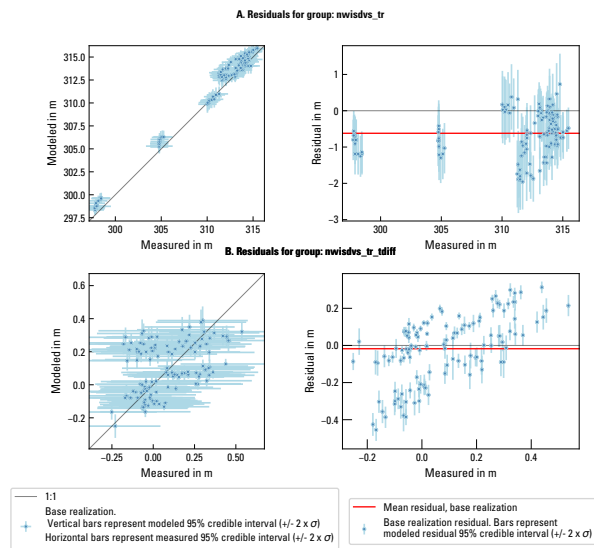


Figure 28: Fit between measured and modeled values at observation locations for observation groups nwis_dvs_tr (panel A) and nwisdvflx_tr_tdiff (panel B) for the Pleasant Lake model.

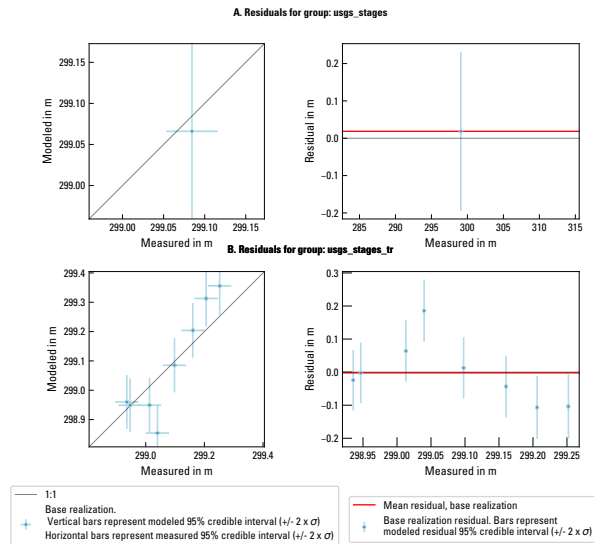


Figure 29: Fit between measured and modeled values at observation locations for observation groups usgs_stages (panel A) and usgs_stages_tr (panel B) for the Pleasant Lake model.

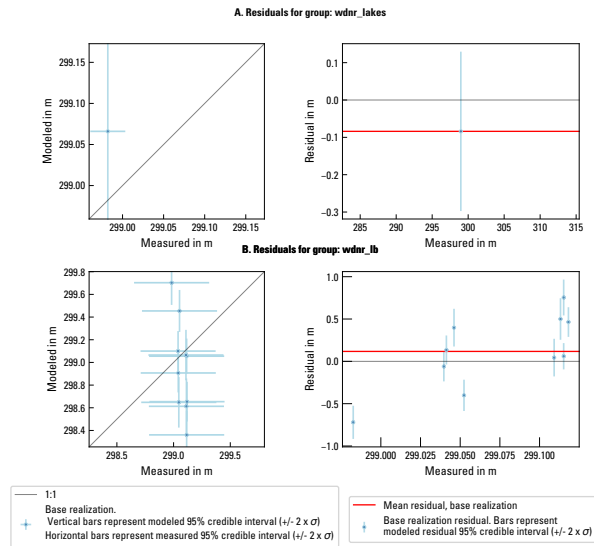


Figure 30: Fit between measured and modeled values at observation locations for observation groups wdnr_lakes (panel A) and wdnr_lb (panel B) for the Pleasant Lake model.

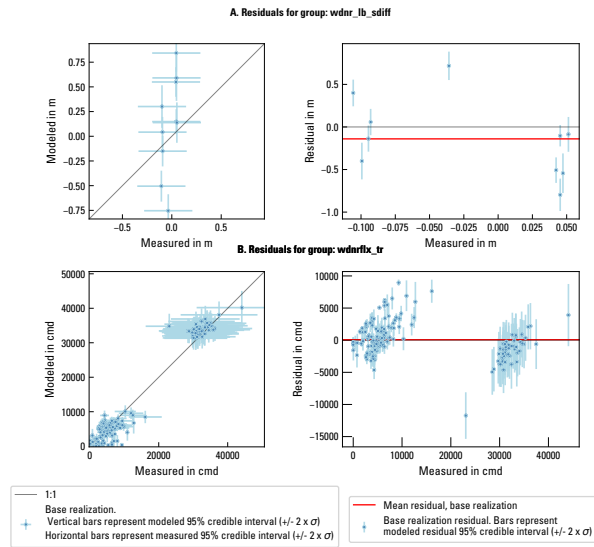


Figure 31: Fit between measured and modeled values at observation locations for observation groups wdnr_lb_sdifff (panel A) and wdnrflx_tr (panel B) for the Pleasant Lake model.

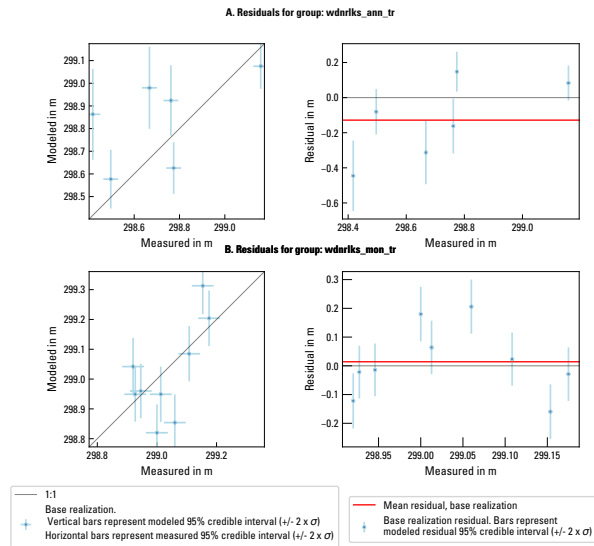


Figure 32: Fit between measured and modeled values at observation locations for observation groups wdnrlks_ann_tr (panel A) and wdnrlks_mon_tr (panel B) for the Pleasant Lake model.

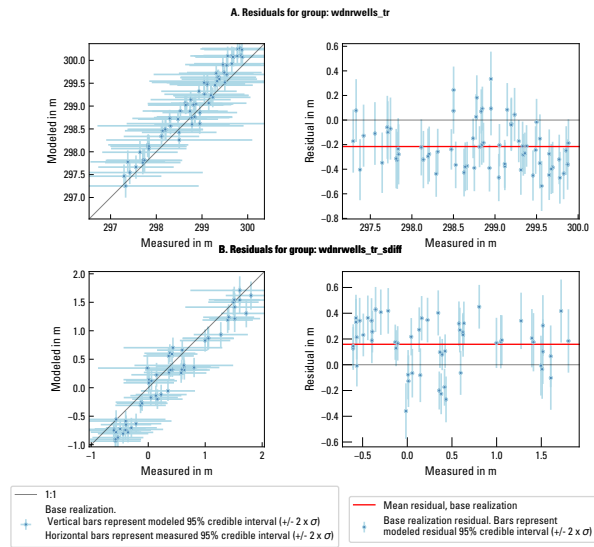


Figure 33: Fit between measured and modeled values at observation locations for observation groups wdnrwells_tr (panel A) and wdnrwells_tr_sdiff (panel B) for the Pleasant Lake model.

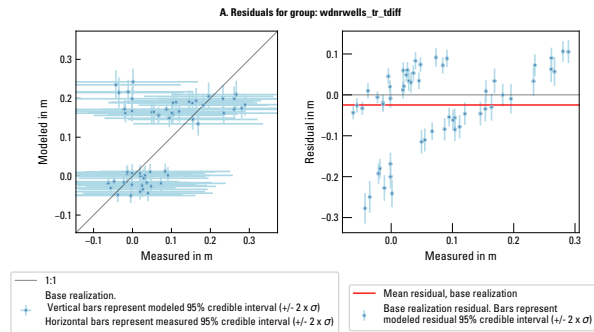


Figure 34: Fit between measured and modeled values at observation locations for observation group wdnrwells_tr_sdiff (panel A) for the Pleasant Lake model.

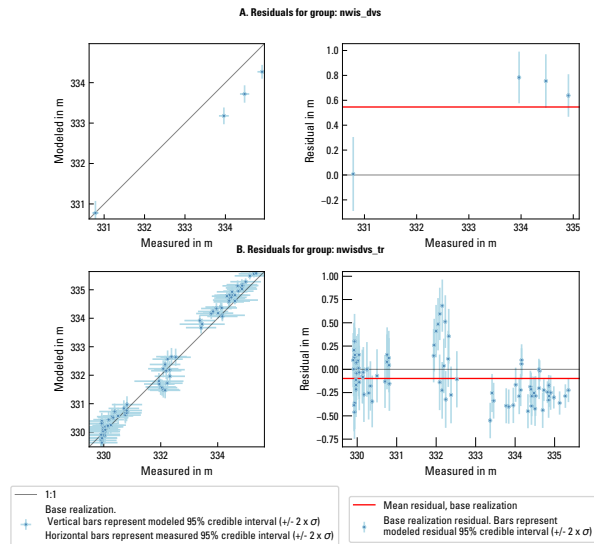


Figure 35: Fit between measured and modeled values at observation locations for observation groups nwis_dvs (panel A) and nwisdvs_tr (panel B) for the Plainfield Tunnel Channel Lakes model.

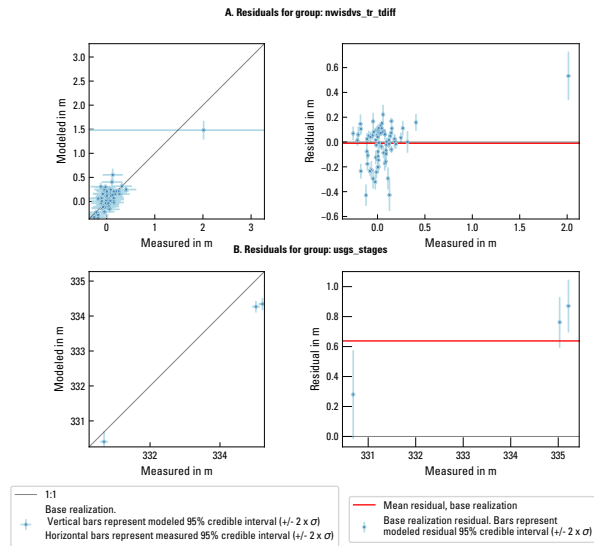


Figure 36: Fit between measured and modeled values at observation locations for observation groups nwisdvs_tr_tdiff (panel A) and usgs_stages (panel B) for the Plainfield Tunnel Channel Lakes model.

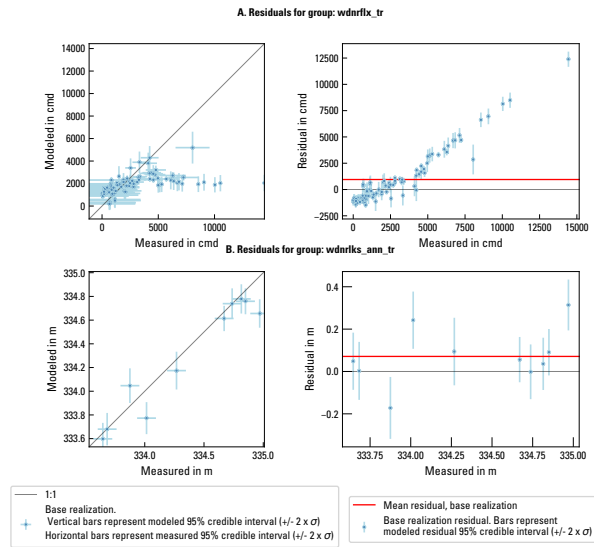


Figure 37: Fit between measured and modeled values at observation locations for observation groups wdnrflx_tr (panel A) and wdnrlks_ann_tr (panel B) for the Plainfield Tunnel Channel Lakes model.

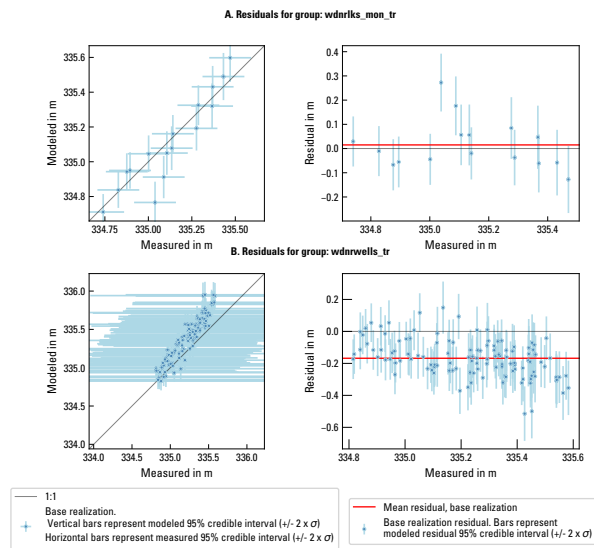


Figure 38: Fit between measured and modeled values at observation locations for observation groups wdnrlks_mon_tr (panel A) and wdnrwells_tr (panel B) for the Plainfield Tunnel Channel Lakes model.

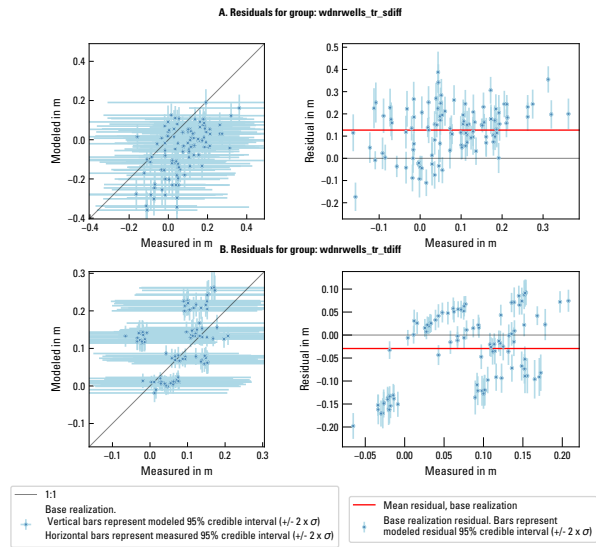


Figure 39: Fit between measured and modeled values at observation locations for observation groups wdnrwells_tr_sdiff (panel A) and wdnrwells_tr_tdiff (panel B) for the Plainfield Tunnel Channel Lakes model.

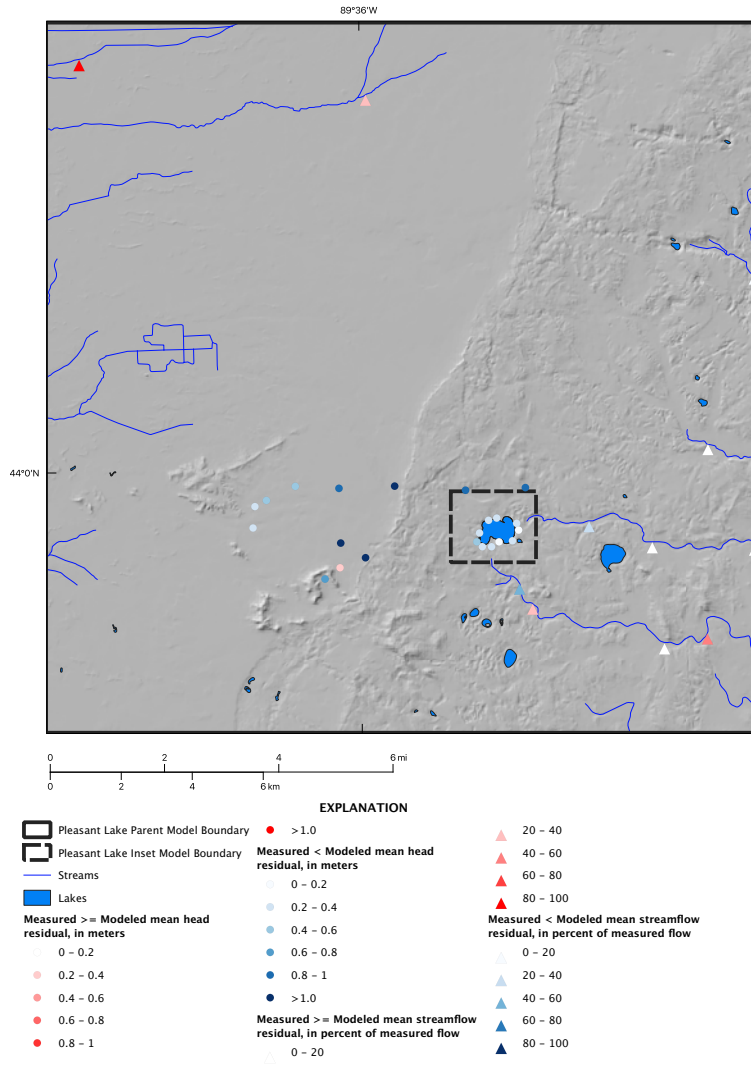


Figure 40: Spatial pattern of mean fit between measured and modeled observations for Pleasant Lake inset model.

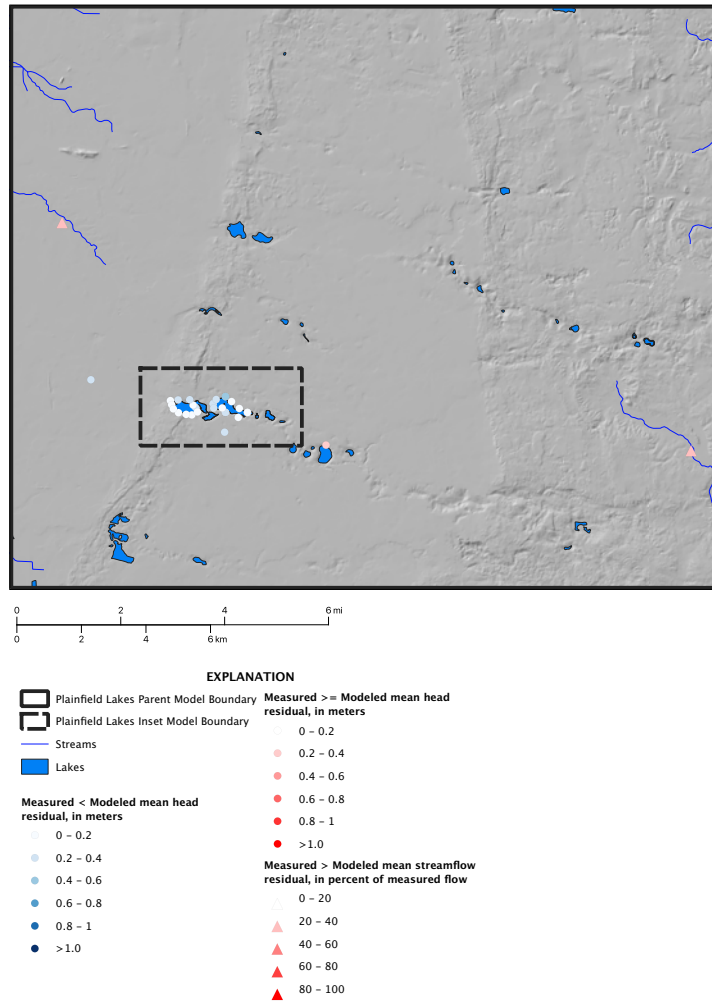


Figure 41: Spatial pattern of mean fit between measured and modeled observations for Plainfield Tunnel Channel Lakes inset model.

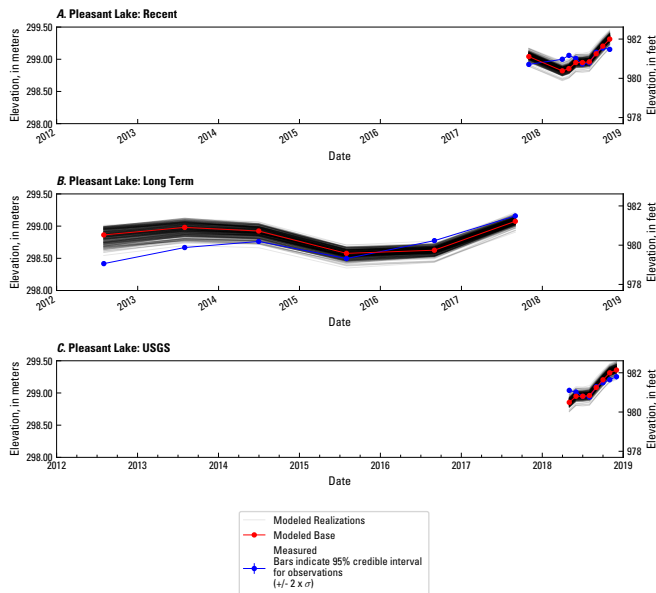


Figure 42: Time series of measured and modeled results for lake level observations in the Pleasant Lake inset model. Panel A is observation group wdnrlks_mon_tr, Panel B is observation group wdnrlks_ann_tr, and Panel C is observation group usgs_stages_tr.

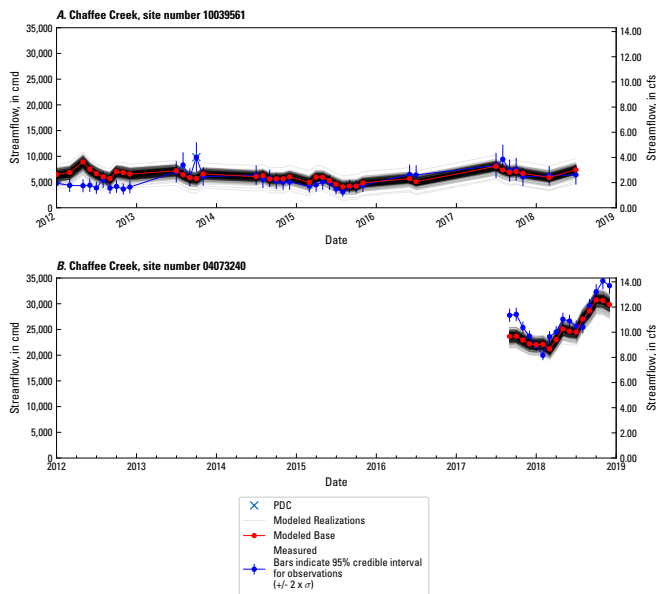


Figure 43: Time series of measured and modeled results for streamflow observations in Chaffee Creek sites 10039561 (panel A) and 4073240 (panel B) in the Pleasant Lake inset model.

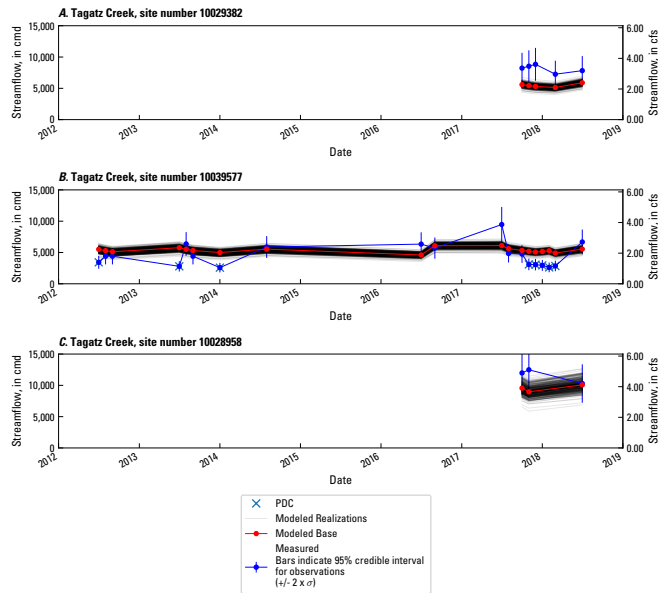


Figure 44: Time series of measured and modeled results for streamflow observations in Tagatz Creek sites 10029382 (panel A), 10039577 (panel B), and 10028958 (panel C) in the Pleasant Lake inset model.

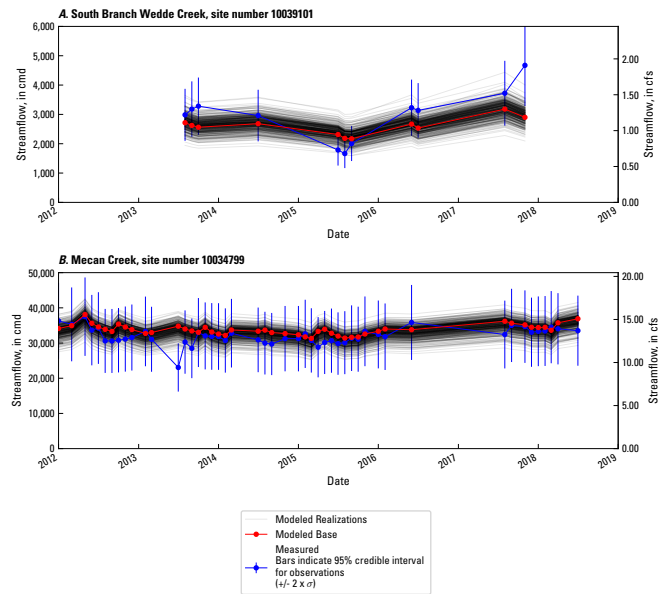


Figure 45: Time series of measured and modeled results over time for streamflow observations in South Branch Wedde Creek site 10039101 (panel A) and Mecan Creek site 10034799 (panel B).

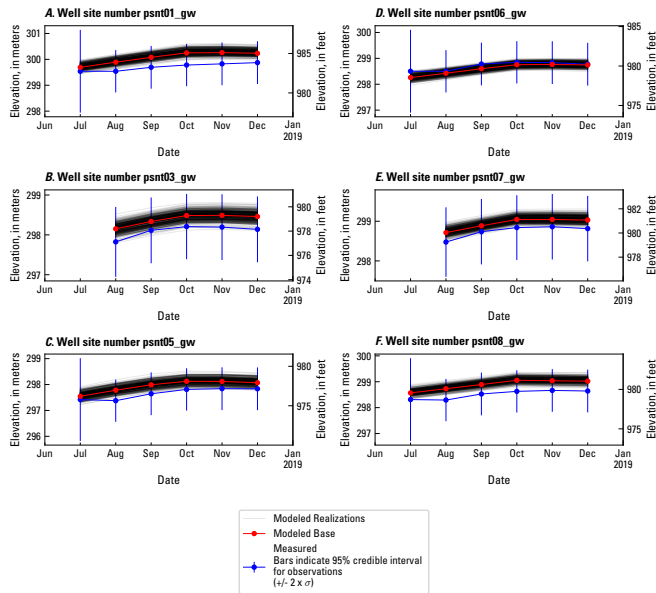


Figure 46: Time series of measured and modeled results for transient piezometers near Pleasant Lake in the group wdnrwells_tr, (part 1).

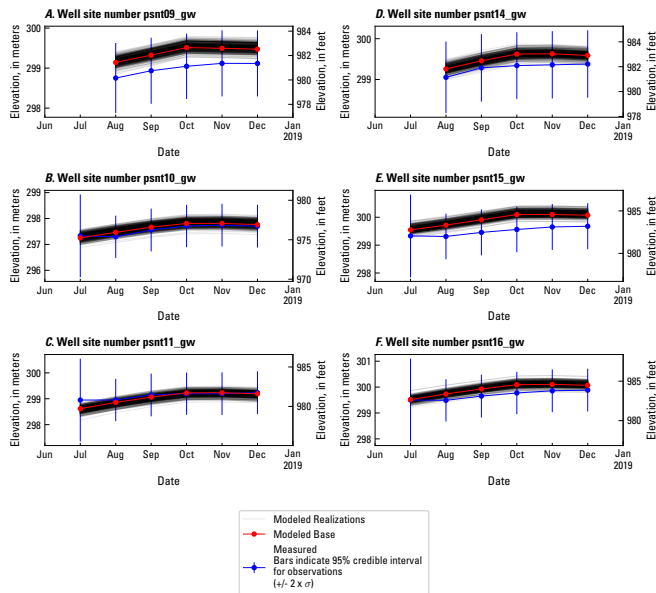


Figure 47: Time series of measured and modeled results for transient piezometers near Pleasant Lake in the group wdnrwells_tr, (part 2).

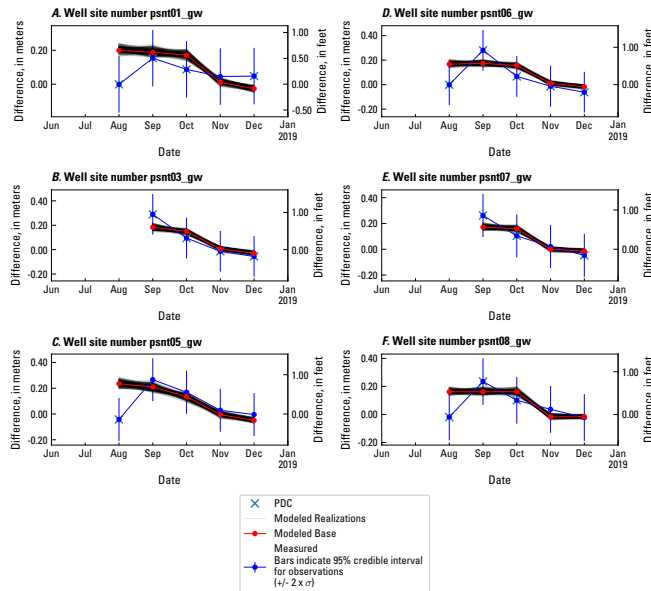


Figure 48: Time series of measured and modeled results for temporal differences in transient piezometers near Pleasant Lake in the group wdnrwwells_tr_tdiff, (part 1).

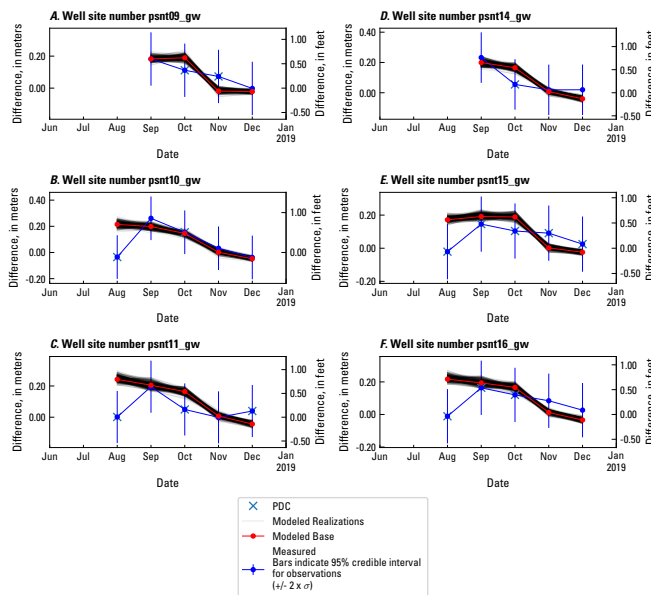


Figure 49: Time series of measured and modeled results for temporal differences in transient piezometers near Pleasant Lake in the group wdnrwwells_tr_tdiff, (part 2).

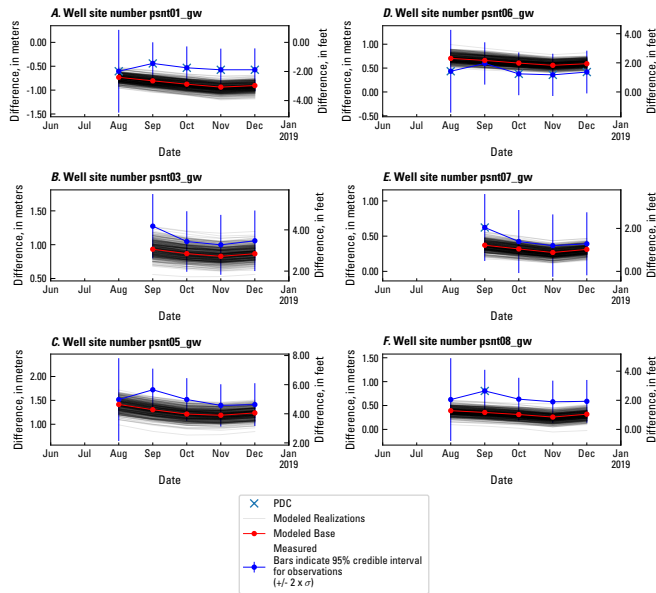


Figure 50: Time series of measured and modeled results for spatial differences in transient piezometers near Pleasant Lake in the group wdnr wells_tr_sdiff, (part 1).

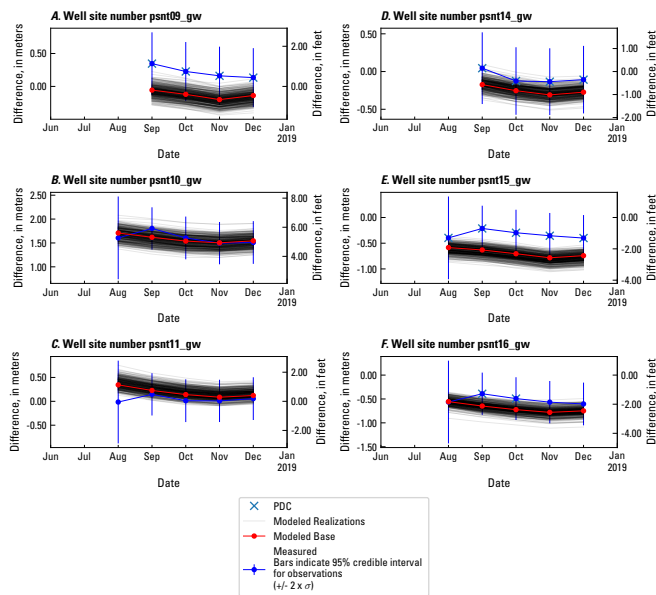


Figure 51: Time series of measured and modeled results for spatial differences in transient piezometers near Pleasant Lake in the group wdnr wells_tr_sdiff, (part 2).

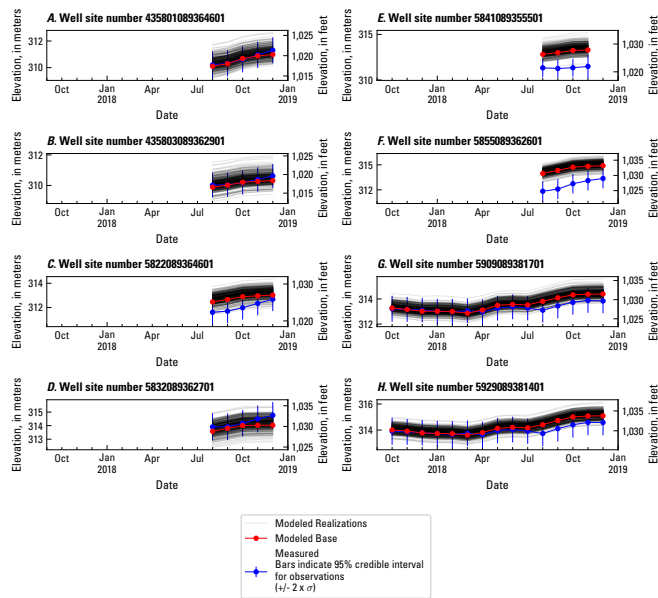


Figure 52: Time series of measured and modeled results for heads in wells with daily values in NWIS in the Pleasant Lake inset model in the group nwisdvs_tr (part 1).

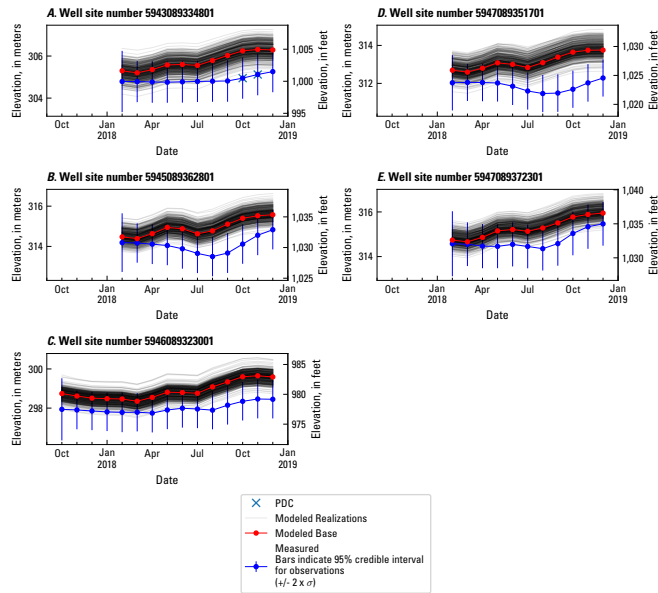


Figure 53: Time series of measured and modeled results for heads in wells with daily values in NWIS in the Pleasant Lake inset model in the group nwisdvs_tr (part 2).

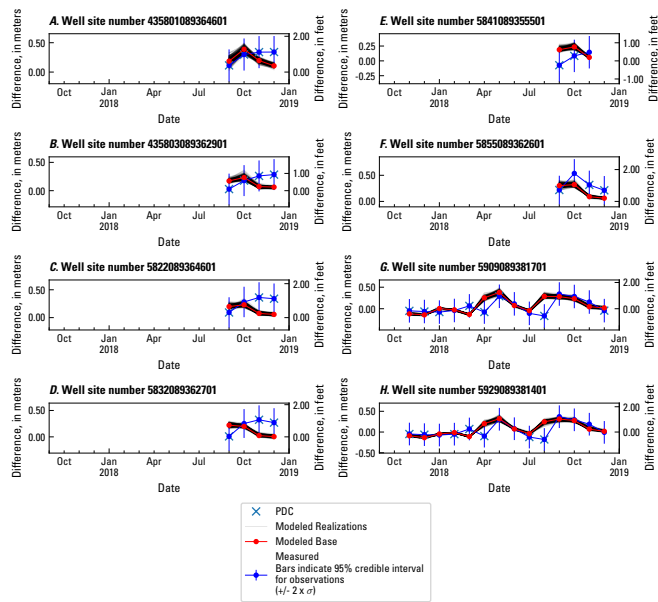


Figure 54: Time series of measured and modeled results for temporal difference of heads in wells with daily values in NWIS in the Pleasant Lake inset model in the group nwisdvs_tr_tdiff (part 1).

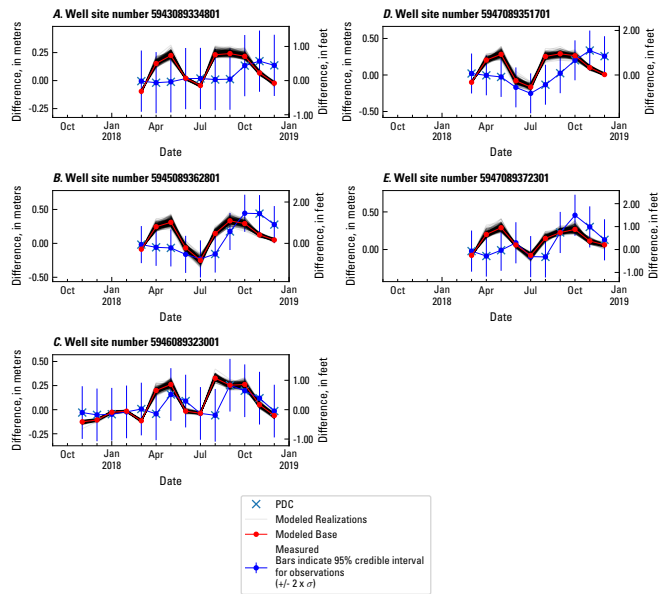


Figure 55: Time series of measured and modeled results for temporal difference of heads in wells with daily values in NWIS in the Pleasant Lake inset model in the group nwisdvs_tr_tdiff (part 2).

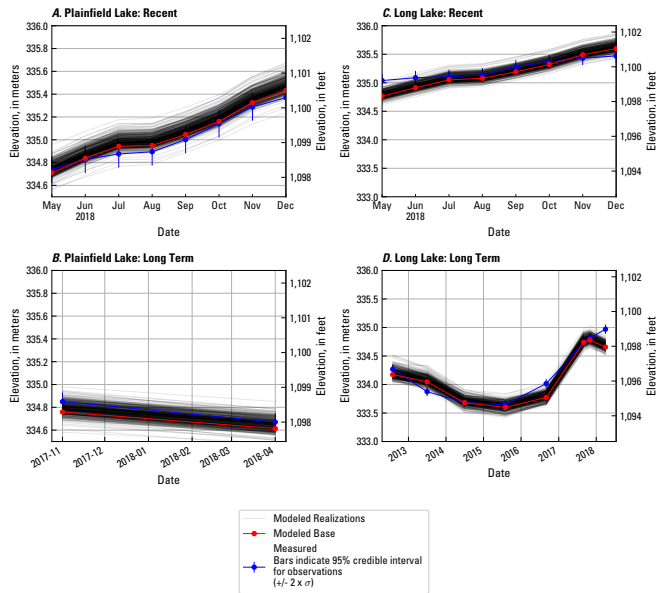


Figure 56: Time series of measured and modeled results for lake level observations in the Pleasant Lake inset model. Panel A is Plainfield Lake, observation group wdnrlks_mon_tr, Panel B is Plainfield Lake, observation group wdnrlks_ann_tr, Panel C is Long Lake, observation group wdnrlks_mon_tr, and Panel D is Long Lake, observation group wdnrlks_ann_tr.

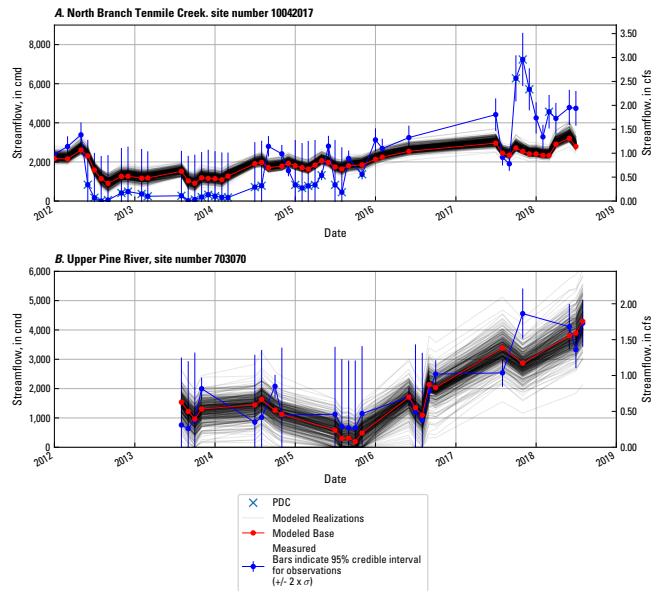


Figure 57: Time series of measured and modeled results for streamflow observations in North Branch Tenmile Creek site 10042017 (panel A) and Upper Pine River site 703070 (panel B) in the Plainfield Tunnel Channel Lakes inset model.

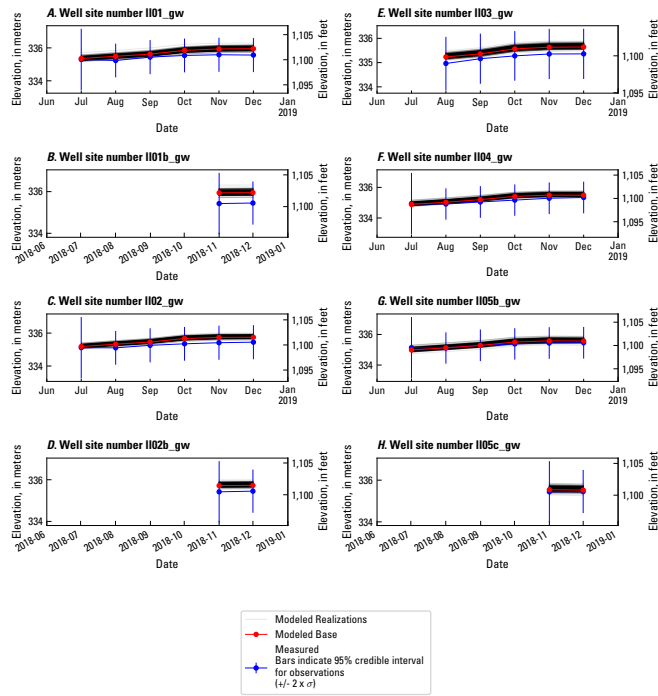


Figure 58: Time series of measured and modeled results for transient piezometers near Long Lake in the group wdnrwwells_tr, (part 1).

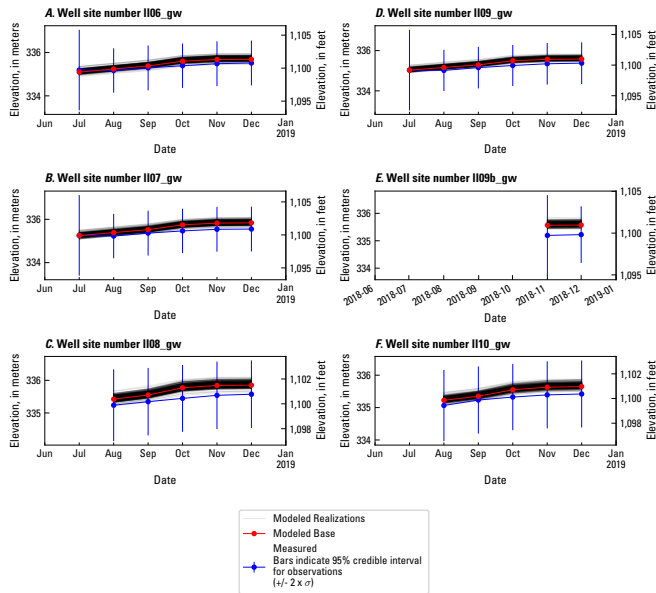


Figure 59: Time series of measured and modeled results for transient piezometers near Long Lake in the group wdnrwwells_tr, (part 2).

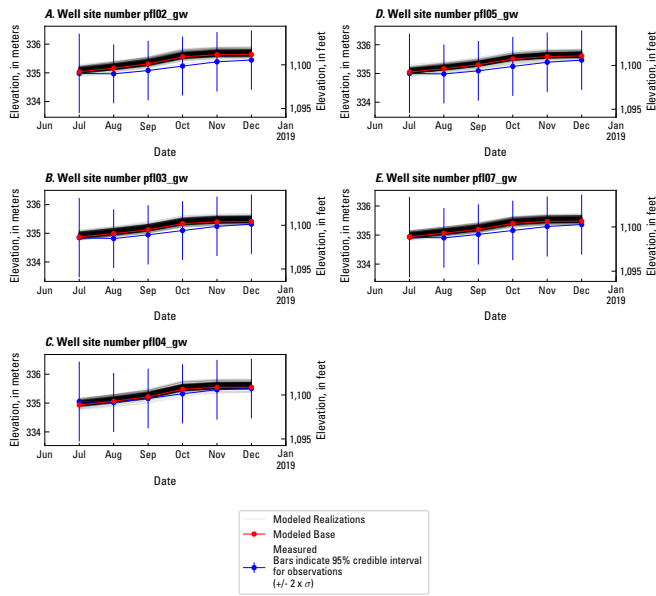


Figure 60: Time series of measured and modeled results for transient piezometers near Plainfield Lake in the group wdnrwwells_tr, (part 1).

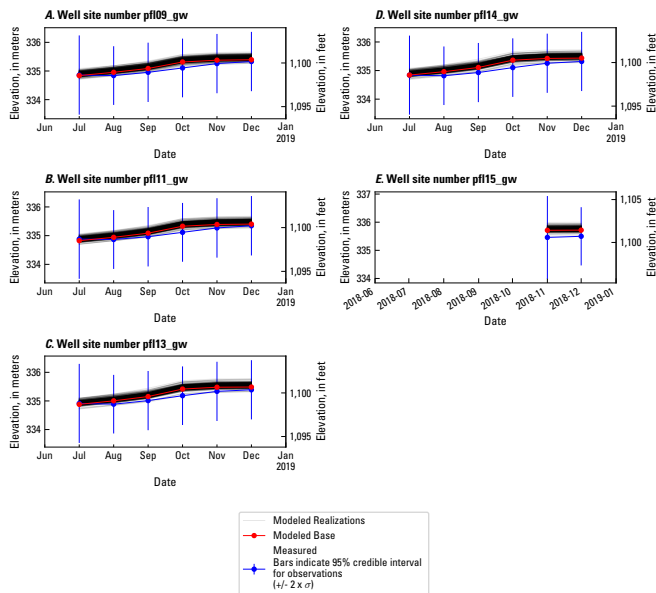


Figure 61: Time series of measured and modeled results for transient piezometers near Plainfield Lake in the group wdnr wells_tr, (part 2).

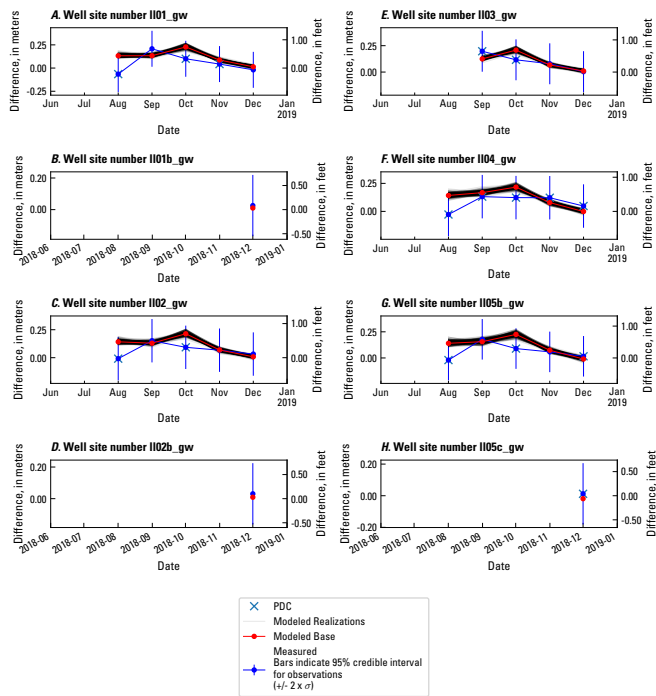


Figure 62: Time series of measured and modeled results for temporal differences in transient piezometers near Long Lake in the group wdnr wells_tr_tdiff, (part 1).

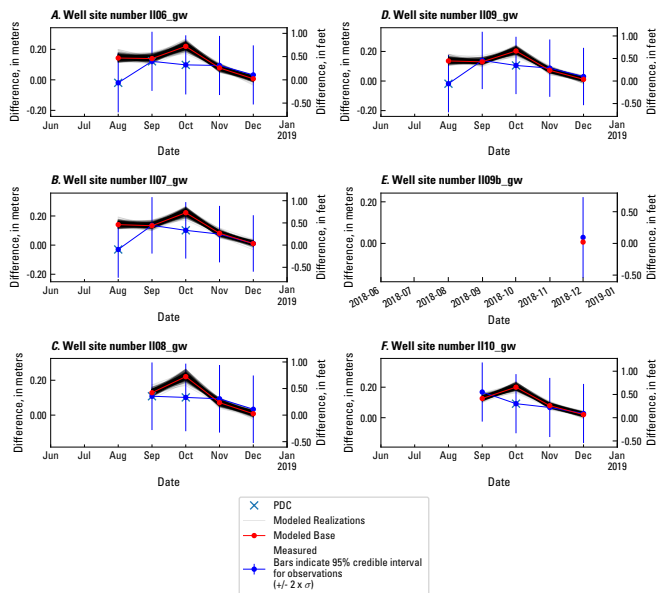


Figure 63: Time series of measured and modeled results for temporal differences in transient piezometers near Long Lake in the group wdnrwwells_tr_tdiff, (part 2).

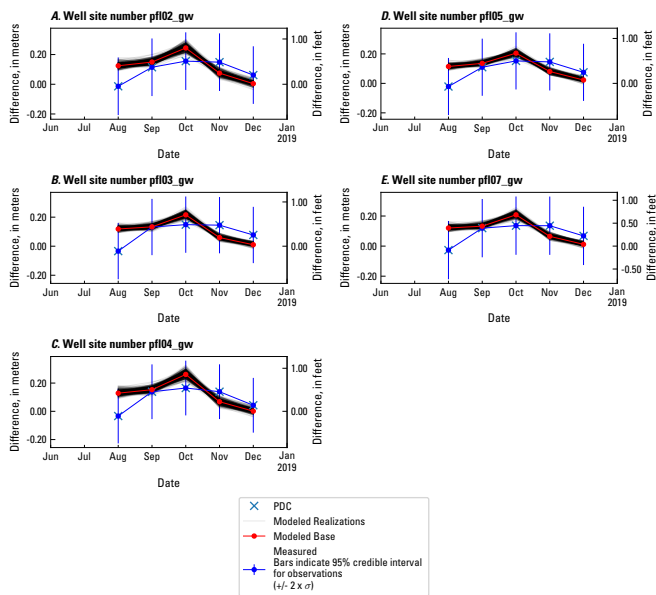


Figure 64: Time series of measured and modeled results for temporal differences in transient piezometers near Plainfield Lake in the group wdnrwwells_tr_tdiff, (part 1).

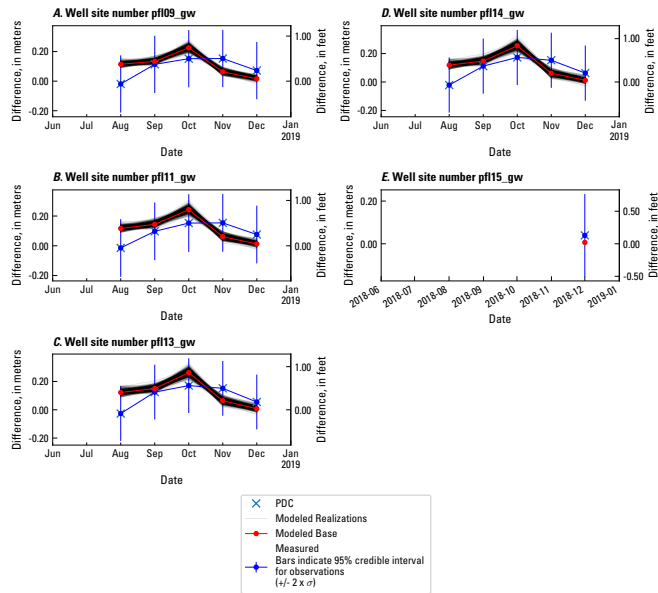


Figure 65: Time series of measured and modeled results for temporal differences in transient piezometers near Plainfield Lake in the group wdnrwwells_tr.tdiff, (part 2).

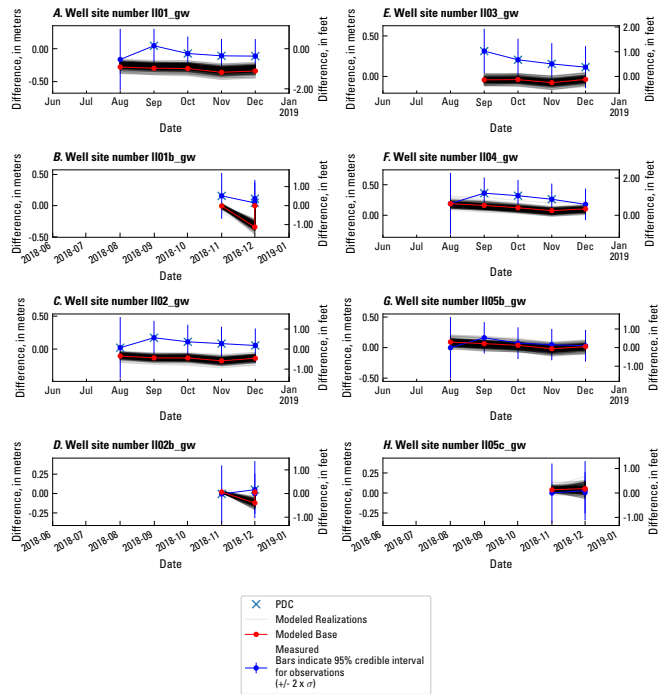


Figure 66: Time series of measured and modeled results for spatial differences in transient piezometers near Long Lake in the group wdnrwells_tr_sdiff, (part 1).

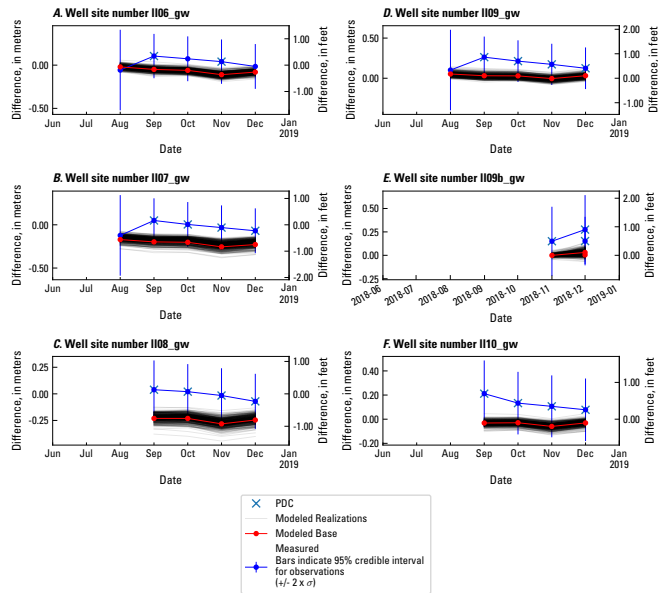


Figure 67: Time series of measured and modeled results for spatial differences in transient piezometers near Long Lake in the group wdnr wells_tr_sdiff, (part 2).

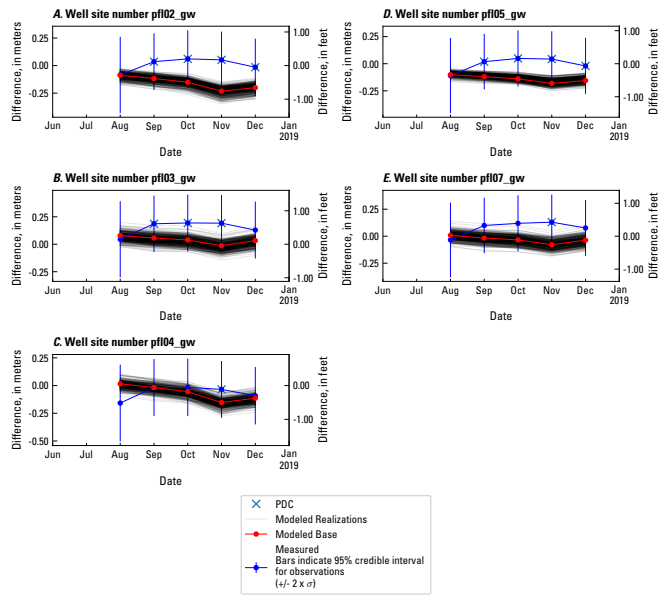


Figure 68: Time series of measured and modeled results for spatial differences in transient piezometers near Plainfield Lake in the group wdnr wells_tr_sdiff, (part 1).

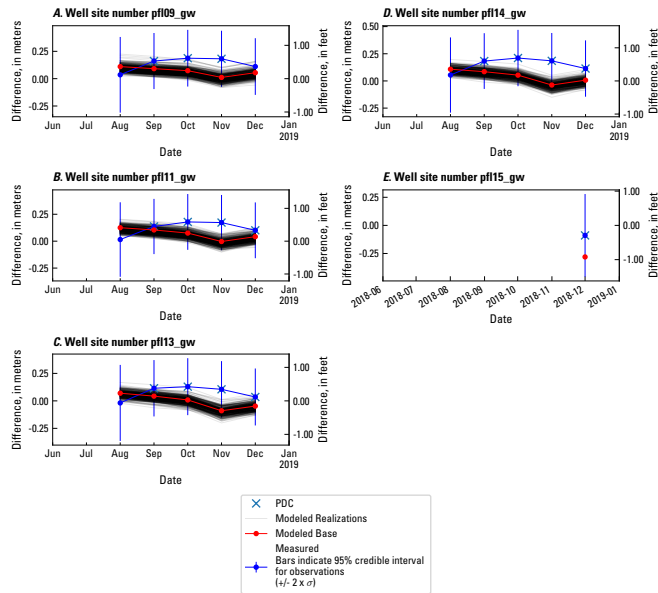


Figure 69: Time series of measured and modeled results for spatial differences in transient piezometers near Plainfield Lake in the group wdnrwwls_tr_sdifff, (part 2).

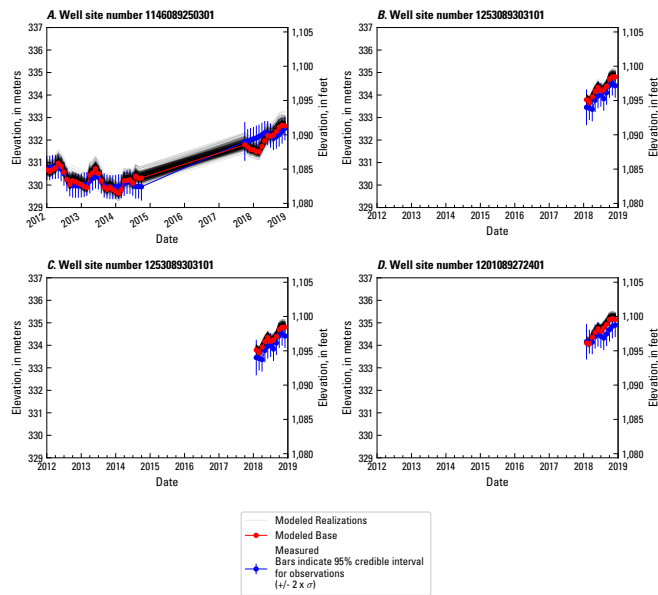


Figure 70: Time series of measured and modeled results for heads in wells with daily values in NWIS in the Plainfield Tunnel Channel Lakes inset model in the group nwis-dvs_tr.

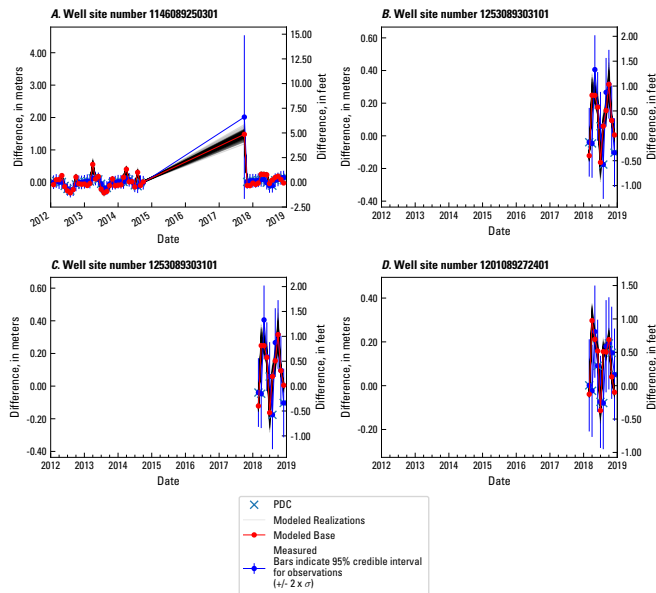


Figure 71: Time series of measured and modeled results for temporal difference of heads in wells with daily values in NWIS in the Plainfield Tunnel Channel Lakes inset model in the group nwisdvs_tr_tdiff.

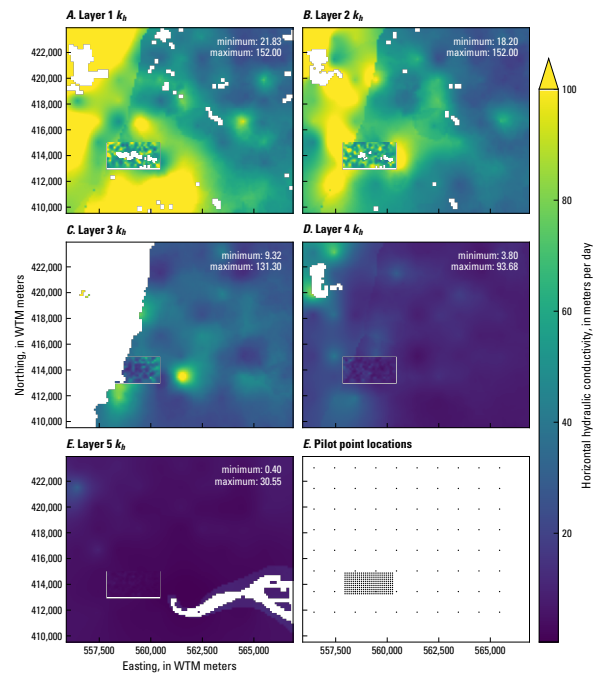


Figure 72: Horizontal hydraulic conductivity (K_h) estimates for the Plainfield Tunnel Channel Lakes model. White areas indicate locations where a layer is absent in the model ($idomain=0$). Pilot point locations apply to all layers.

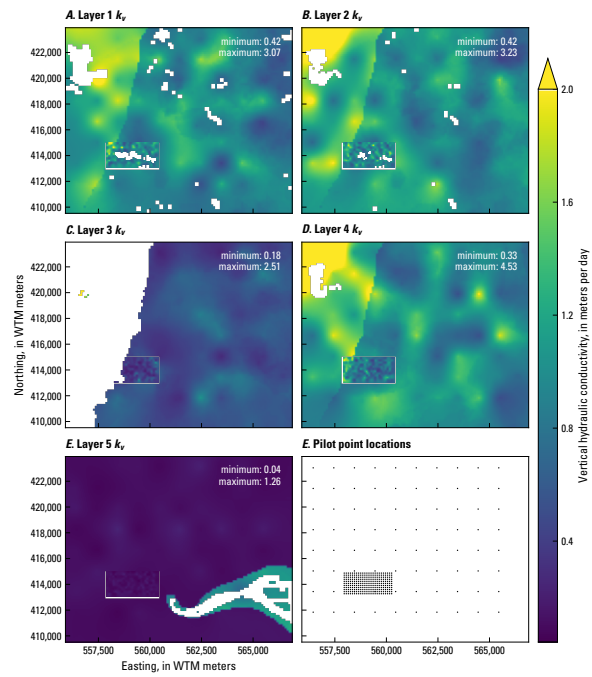


Figure 73: Vertical hydraulic conductivity (K_v) estimates for the Plainfield Tunnel Channel Lakes model. White areas indicate locations where a layer is absent in the model ($idomain=0$). Pilot point locations apply to all layers.

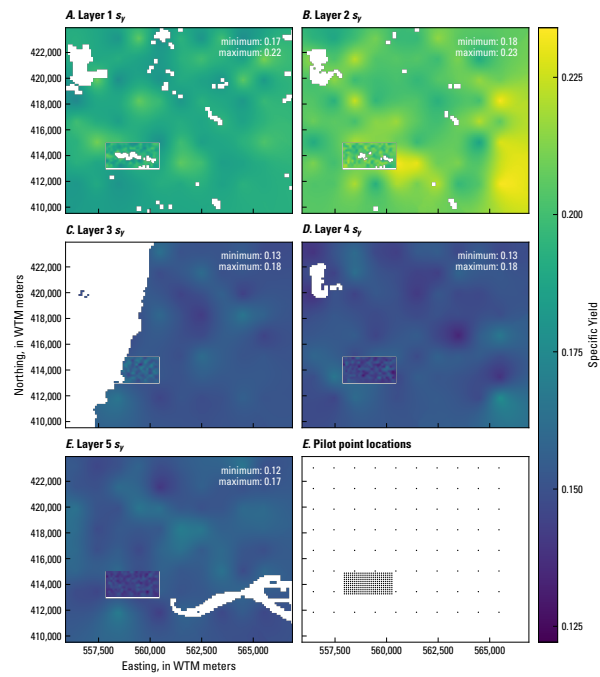


Figure 74: Specific Yield (s_y) estimates for the Plainfield Tunnel Channel Lakes model. White areas indicate locations where a layer is absent in the model ($i_{domain}=0$). Pilot point locations apply to all layers.

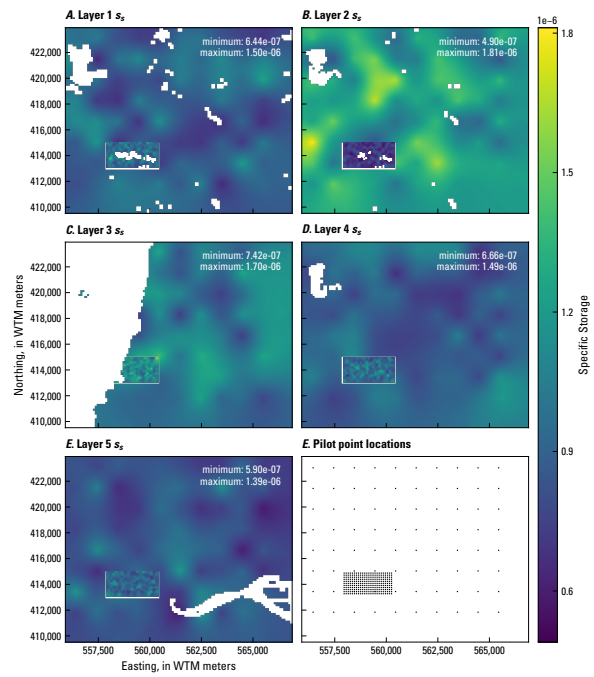


Figure 75: Specific Storage (S_s) estimates for the Plainfield Tunnel Channel Lakes model. White areas indicate locations where a layer is absent in the model ($idomain=0$). Pilot point locations apply to all layers.

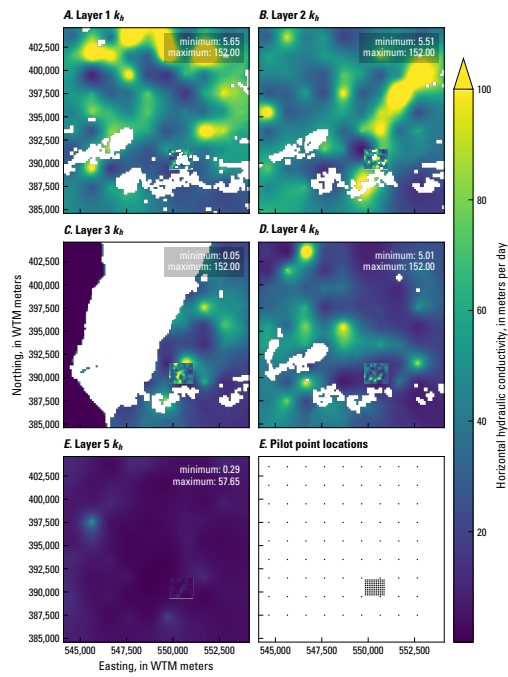


Figure 76: Horizontal hydraulic conductivity (K_h) estimates for the Pleasant Lake model. White areas indicate locations where a layer is absent in the model ($idomain=0$). Pilot point locations apply to all layers.

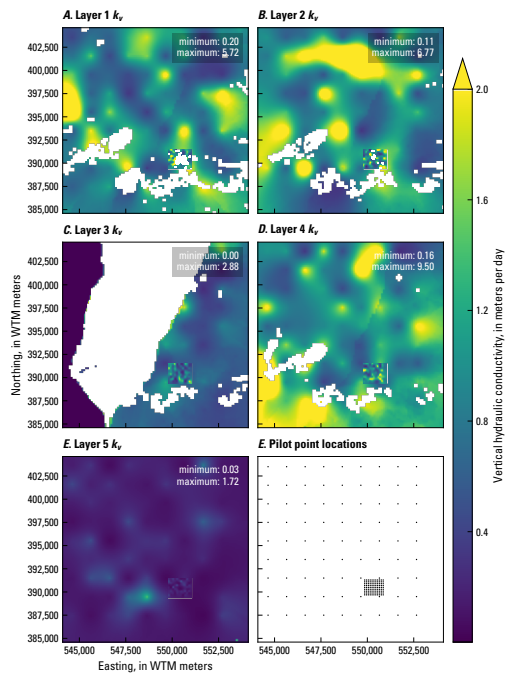


Figure 77: Vertical hydraulic conductivity (K_v) estimates for Pleasant Lake model. White areas indicate locations where a layer is absent in the model ($idomain=0$). Pilot point locations apply to all layers.

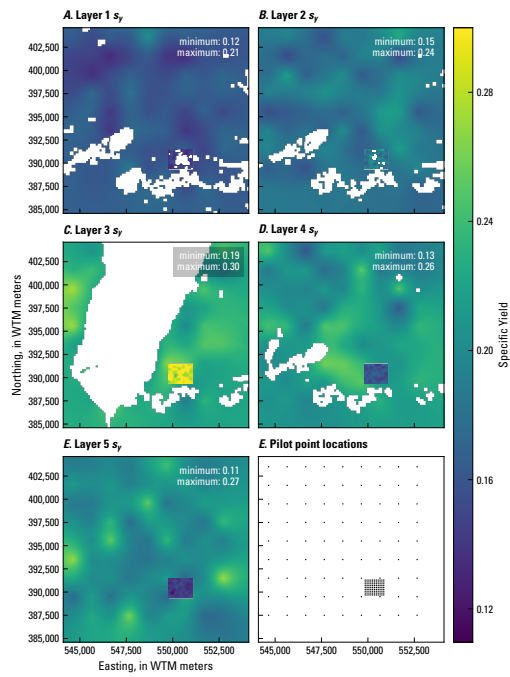


Figure 78: Specific Yield (S_y) estimates for the Pleasant Lake model. White areas indicate locations where a layer is absent in the model ($idomain=0$). Pilot point locations apply to all layers.

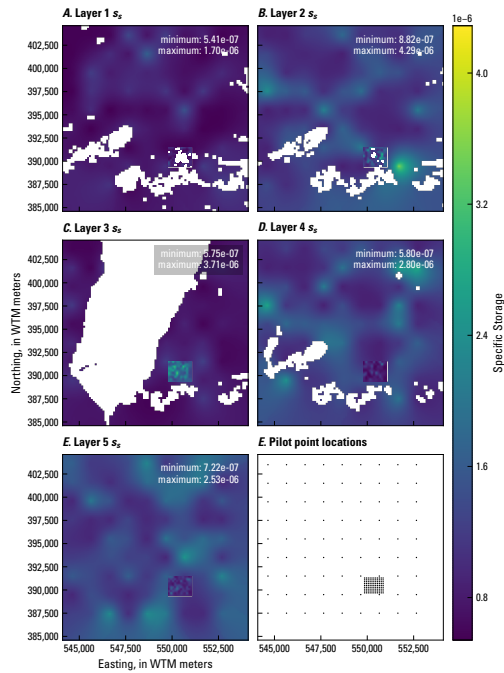


Figure 79: Specific Storage (S_s) estimates for the Pleasant Lake model. White areas indicate locations where a layer is absent in the model ($idomain=0$). Pilot point locations apply to all layers.

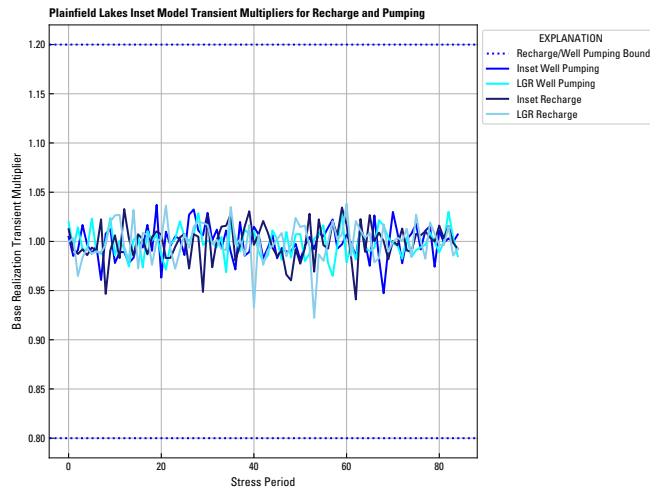


Figure 80: Recharge and well pumping multiplier estimates for the Plainfield Tunnel Channel Lakes Inset model.

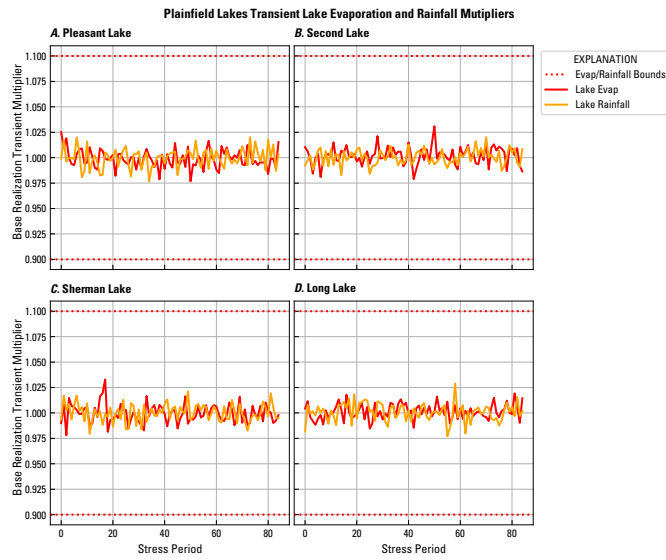


Figure 81: Lake package evaporation and rainfall multiplier estimates for Plainfield (A), Second(B), Sherman (C), and Long (D) Lakes in the Plainfield Tunnel Channel Lakes Inset model.

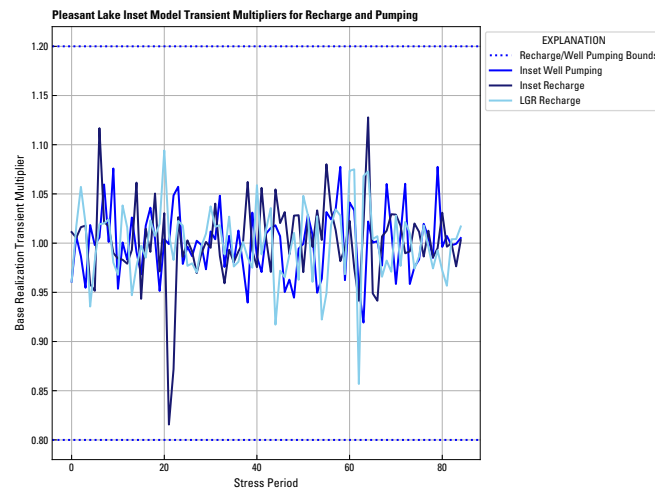


Figure 82: Recharge and well pumping multiplier estimates for the Pleasant Lakes Inset model.

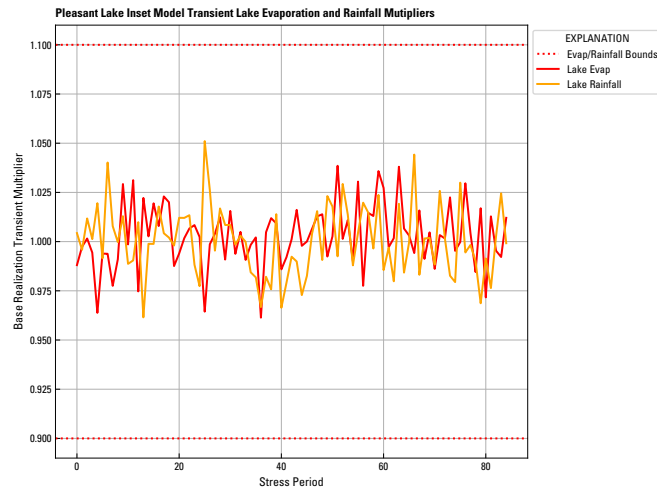


Figure 83: Lake package evaporation and rainfall multiplier estimates for Pleasant Lake in the Pleasant Lake Inset model.

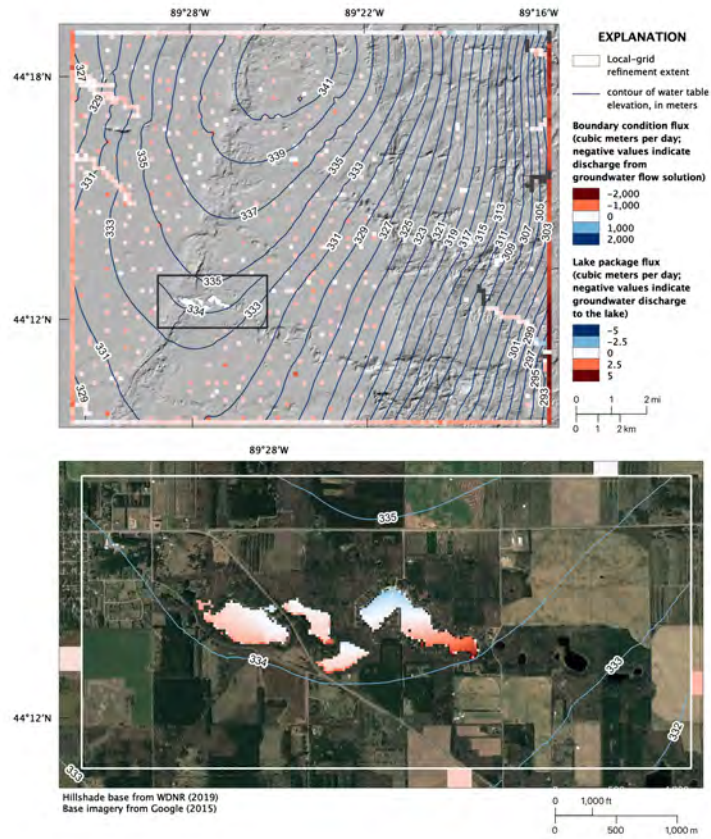


Figure 84: Plainfield Tunnel Channel Lakes model steady-state water table and boundary fluxes.

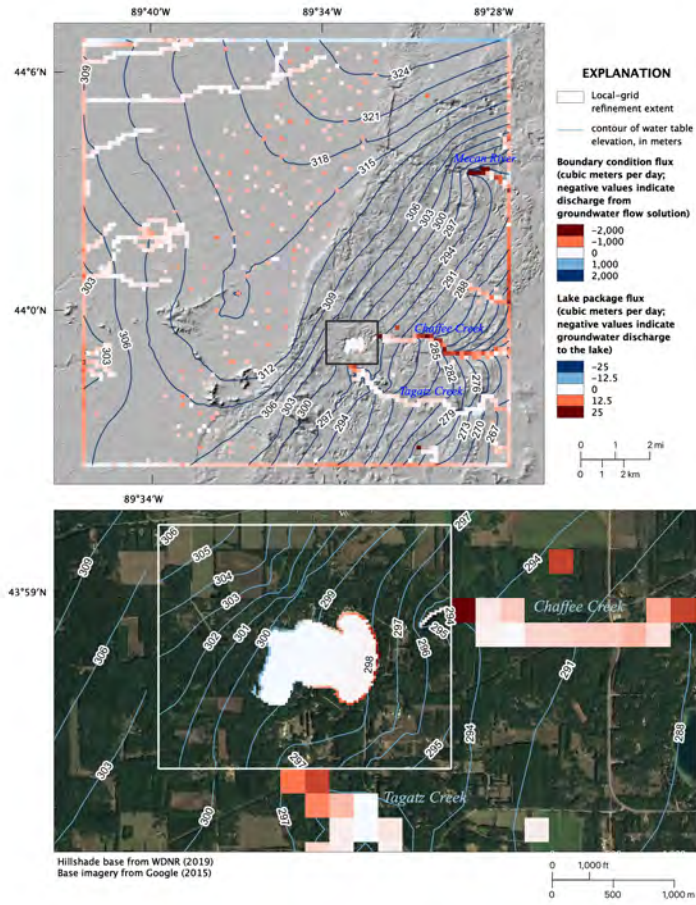


Figure 85: Pleasant Lake model steady-state water table and boundary fluxes.

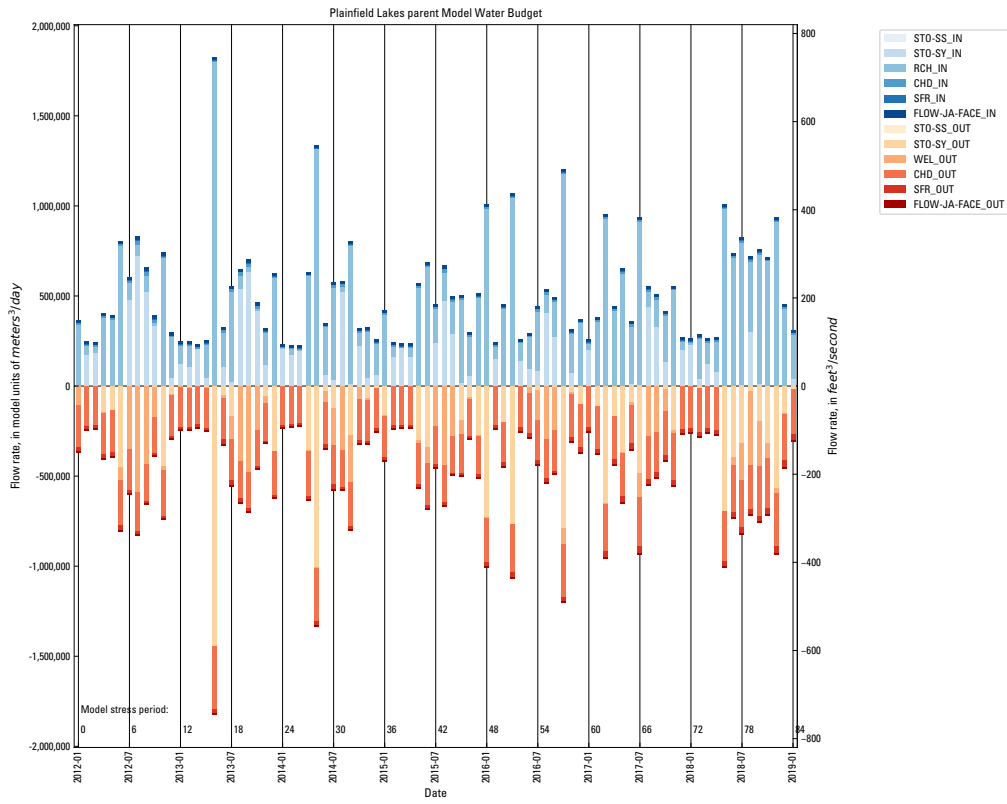


Figure 86: Plainfield Tunnel Channel Lakes inset model water budget.

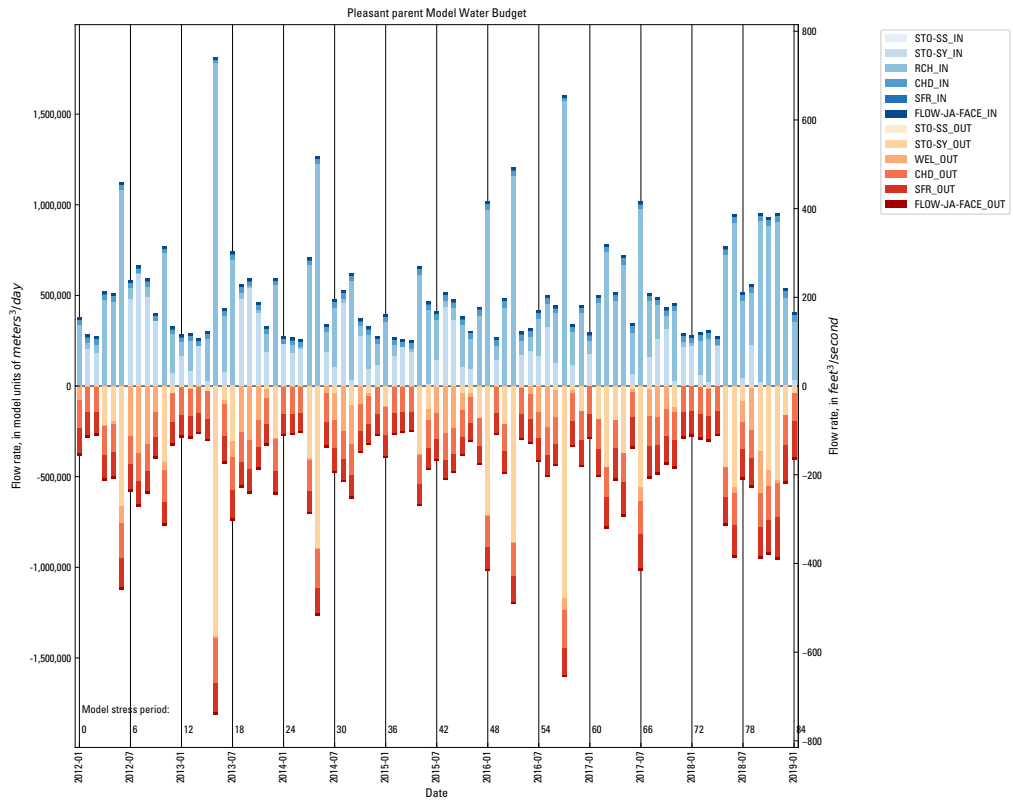


Figure 87: Pleasant Lake inset model water budget.

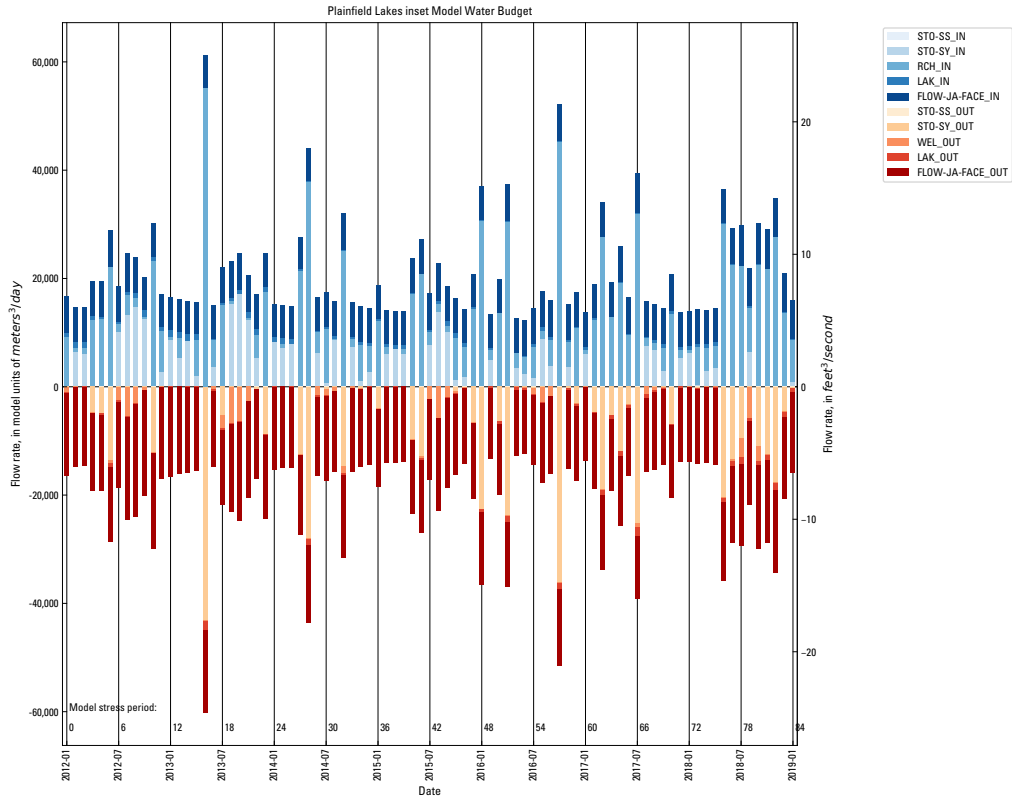


Figure 88: Plainfield Tunnel Channel Lakes LGR sub-model water budget.

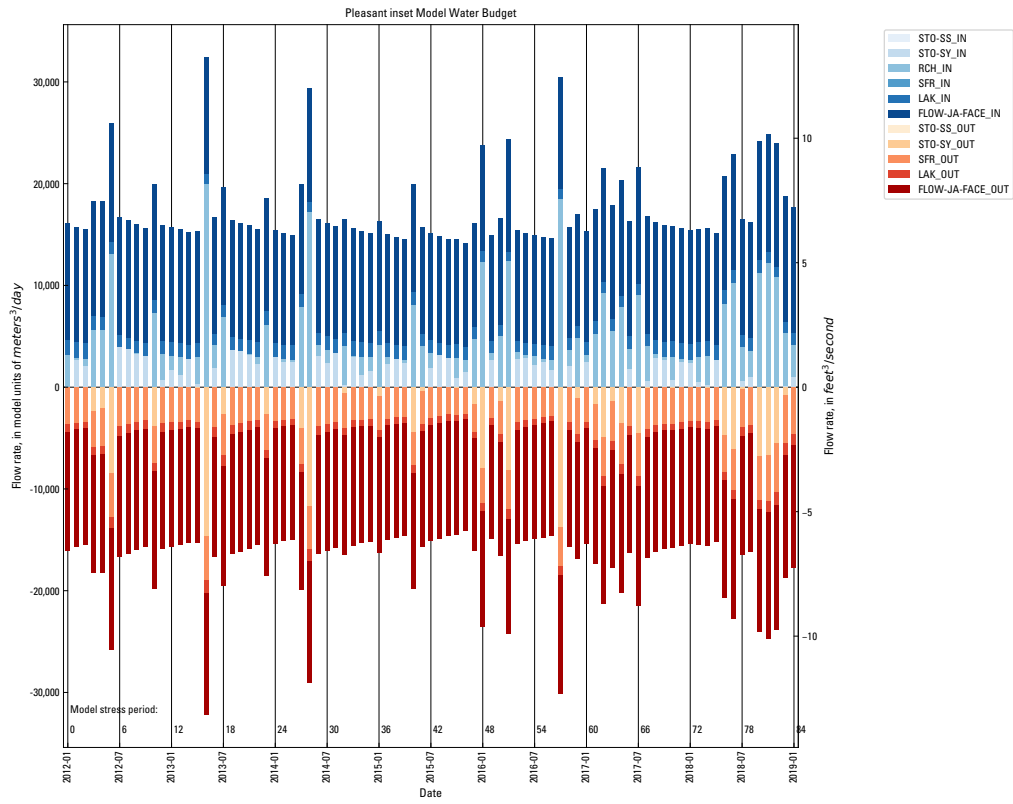


Figure 89: Pleasant Lake LGR sub-model water budget.

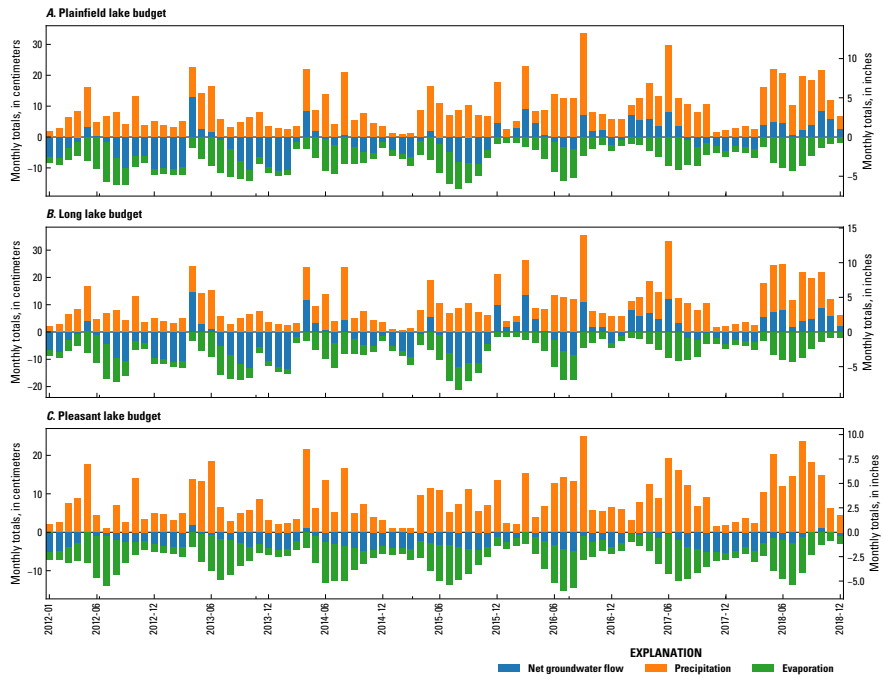


Figure 90: Lake water budgets.

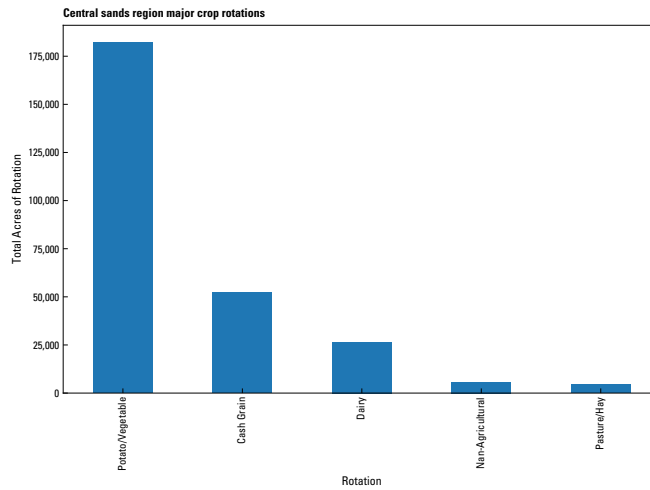


Figure 91: Total acres of each major crop rotation in the regional model domain.

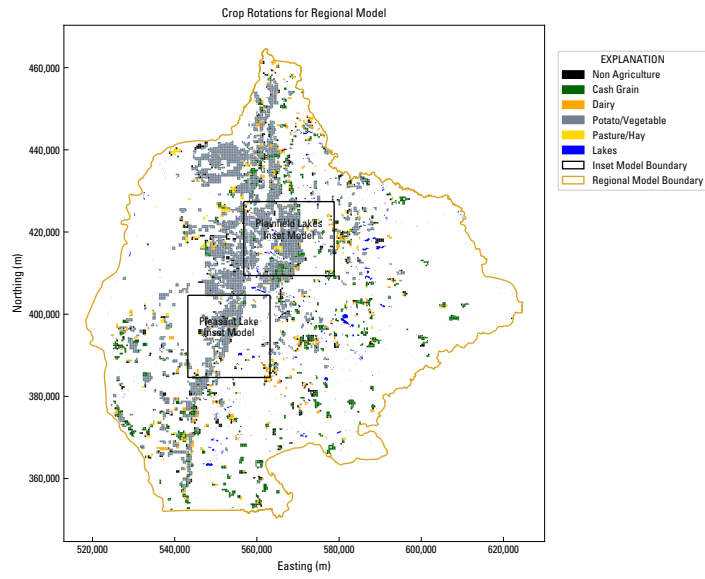


Figure 92: Spatial distribution of the major crop rotations in the regional model domain.

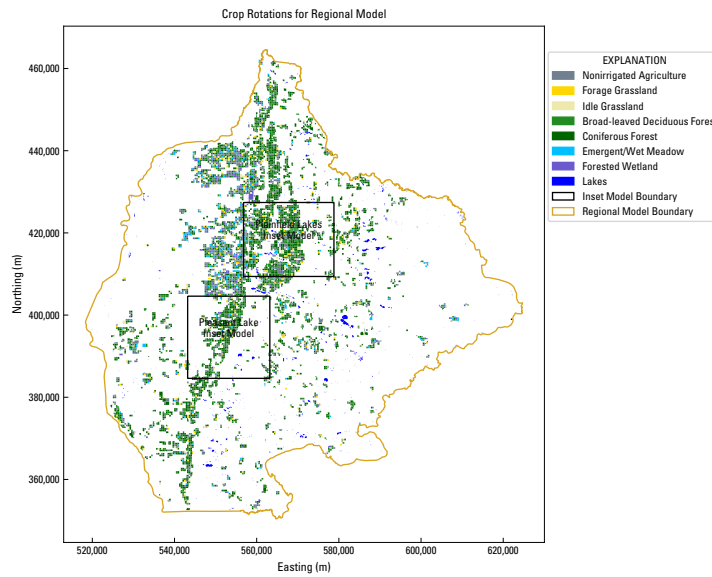


Figure 93: Spatial distribution of alternative land use assumed for the no irrigated agriculture scenario in the regional model domain.

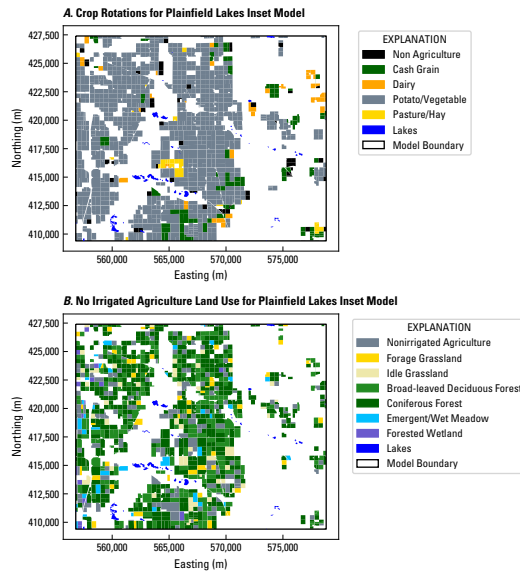


Figure 94: Spatial distribution of the major crop rotations (A) and the alternative land use assumed for the no irrigated agriculture scenario (B) in the Plainfield Tunnel Channel Lakes inset model.

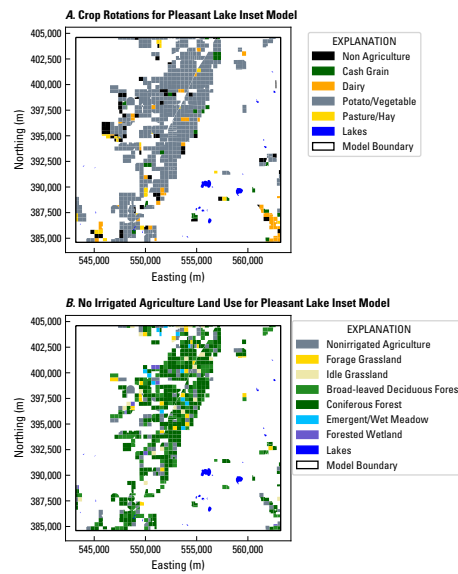


Figure 95: Spatial distribution of the major crop rotations (A) and the alternative land use assumed for the no irrigated agriculture scenario (B) in the Pleasant Lake inset model.

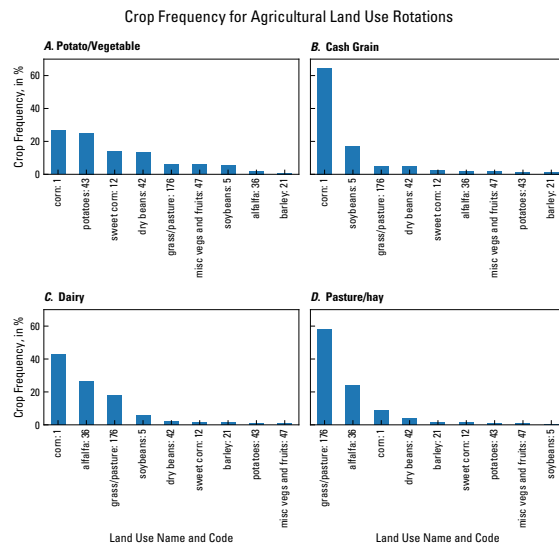


Figure 96: Frequency of each land-use code/crop within the four crop rotations as a percent of area.

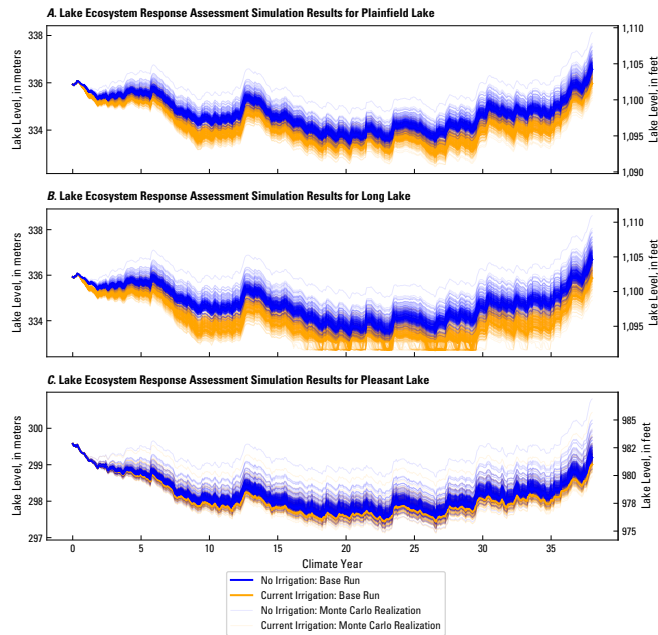


Figure 97: Lake stages for the three study lakes, Plainfield, Long, and Pleasant, in panels A, B, and C, respectively over the Lake Ecosystem Response Assessment (LERA) representative climate. Blue lines indicate Monte Carlo ensemble members for the non-irrigation scenario, and orange lines indicate ensemble members for the current irrigation scenario.

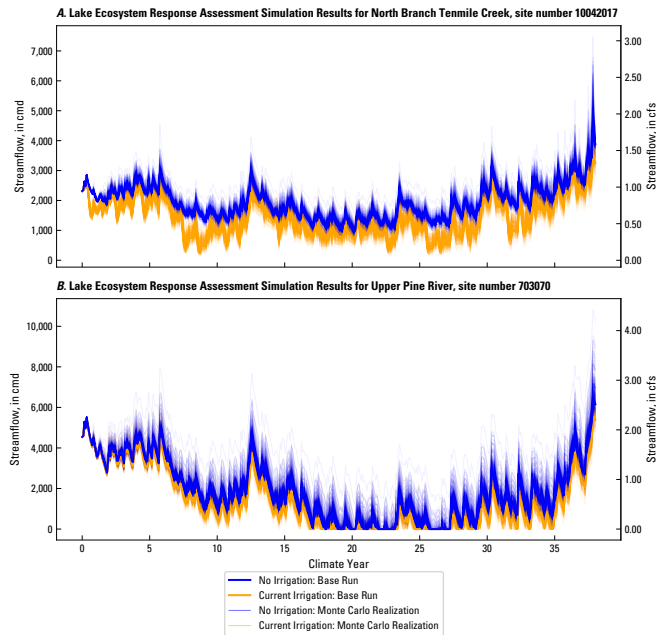


Figure 98: Streamflow in selected streams in the Plainfield inset model respectively over the Lake Ecosystem Response Assessment (LERA) representative climate. Blue lines indicate Monte Carlo ensemble members for the non-irrigation scenario, and orange lines indicate ensemble members for the current irrigation scenario. Panel A is North Branch of Tenmile Creek, and panel B is Upper Pine River.

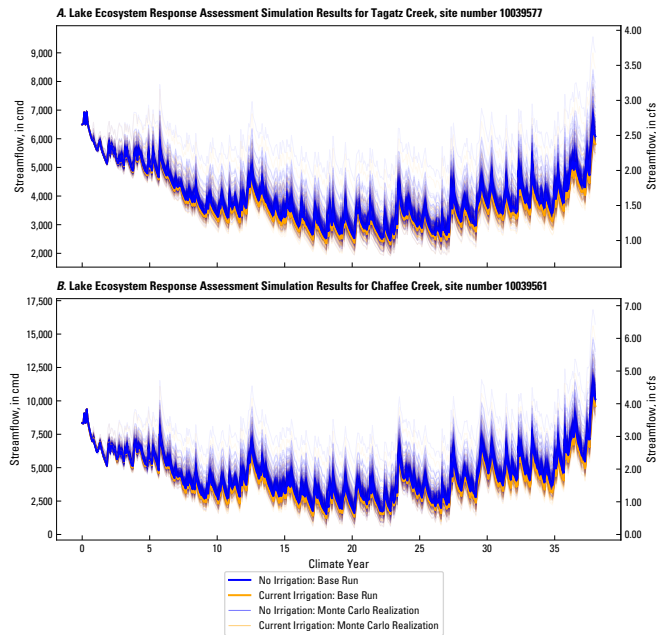


Figure 99: Streamflow in selected streams in the Pleasant inset model respectively over the Lake Ecosystem Response Assessment (LERA) representative climate. Blue lines indicate Monte Carlo ensemble members for the non-irrigation scenario, and orange lines indicate ensemble members for the current irrigation scenario. Panel A is Tagatz Creek, and panel B is Chaffee Creek.

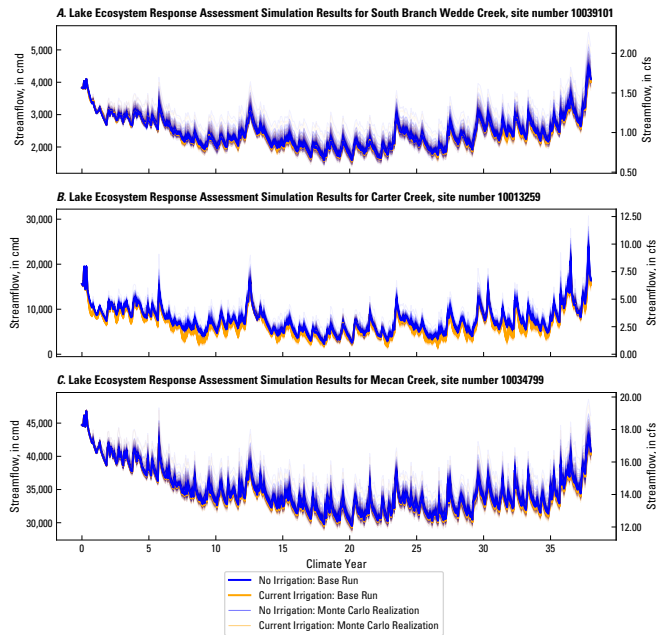


Figure 100: Streamflow in selected streams in the Pleasant inset model respectively over the Lake Ecosystem Response Assessment (LERA) representative climate. Blue lines indicate Monte Carlo ensemble members for the non-irrigation scenario, and orange lines indicate ensemble members for the current irrigation scenario. Panel A is South Branch Wedde Creek, panel B is Carter Creek, and panel C is Mecan Creek.

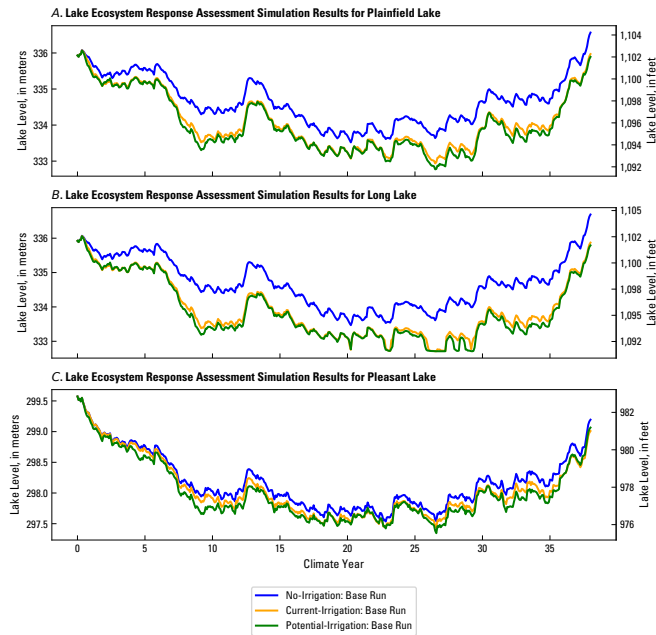


Figure 101: Lake stages for the three study lakes, Plainfield, Long, and Pleasant, in panels A, B, and C, respectively, over the Lake Ecosystem Response Assessment (LERA) representative climate for the base SWB parameters. In each panel, the blue line depicts the no-irrigated-agriculture scenario, the orange line depicts the current-irrigated agriculture scenario, and the green line depicts the potential-irrigated-agriculture scenario.

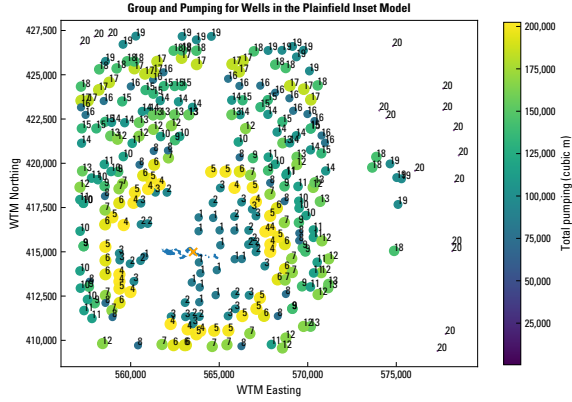


Figure 102: Group identification, based on distance from the center of Long Lake for irrigation wells in the Plainfield inset model and total pumping over the LERA simulation time. Orange 'x' indicates the center of Long Lake.

Long Lake Stage Difference Converting Each Group from Current to No Irrigated Agriculture

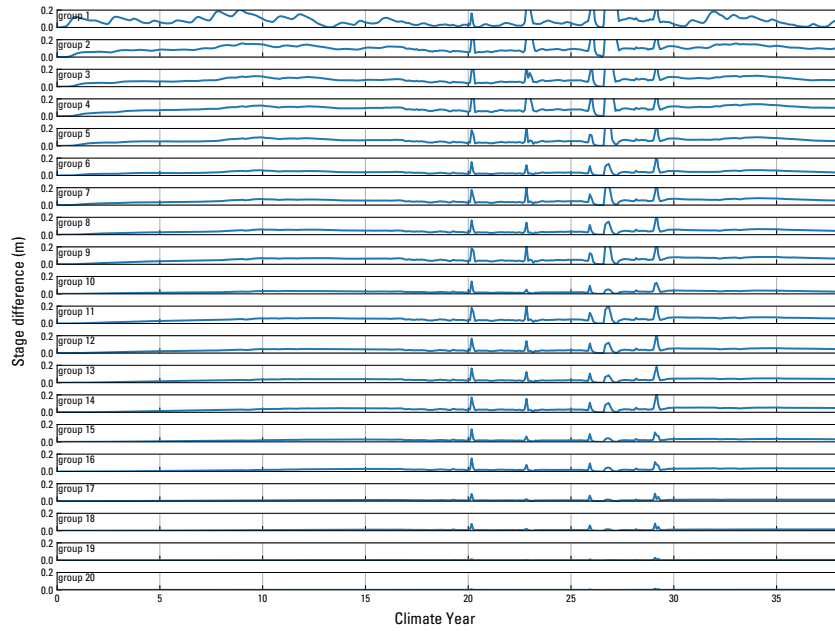


Figure 103: Stage changes in Long Lake resulting from each well group simulated as converted from current irrigation to no irrigation recharge and water use. Positive responses indicate an increase in lake stage due to the conversion.